Development of Microfluidic Devices to Accelerate Clinical Application of Lipid-Based Nanomedicines

脂質ナノ粒子製剤の臨床応用を加速化するマイクロ流路デバイスの開発

Yuka Matsuura-Sawada

Graduate School of Chemical Sciences Engineering

Hokkaido University

Title: Development of Microfluidic Devices to Accelerate Clinical Application of Lipid-Based Nanomedicines

Author: Yuka Matsuura-Sawada

Degree: Doctor of Philosophy (Engineering)

Supervisor: Professor Manabu Tokeshi

Table of Contents:

CHAPTER 1

General Introduction

1.1 Lipid-based nanoparticles and their application to commercial products

Liposomes are closed spherical vesicles composed of lipid bilayers. Since Bangham et al. first discovered and reported on them in 1964 [1], liposomes have been actively investigated [2]. As a result, numerous liposomal products are commercially available in various fields [2,3].

Liposomes have unique physicochemical properties, making them an important subject of investigation. They are composed mainly of amphiphilic phospholipids, which allow the encapsulation of hydrophilic compounds in the internal aqueous phase and hydrophobic compounds in the lipid bilayers depending on their chemical properties. In addition, liposomes have high biocompatibility and biodegradability because phospholipids are the main components of cell membranes. These characteristics are among the reasons that liposomes are applied in a wide range of fields.

Various types of lipid-based nanoparticles (Lb-NPs) have been developed, beginning with liposomes (Figure 1.1). The development of liposomes was followed by that of solid lipid nanoparticles (SLNs), nanostructured lipid carriers (NLCs), and, most recently, RNA carrying lipid nanoparticles (LNPs), which have come of age with the development of mRNA vaccines against COVID-19 [4–6]. SLNs were introduced in 1991 by Müller [7,8]. They consist of a solid lipid core surrounded by a surfactant shell. Triglycerides and fatty acids are widely used as components of SLNs because of their high melting points (above body temperature) [7]. NLCs consist of solid and liquid crystalline lipids and reportedly have the potential for higher drug-loading capacity and physicochemical storage stability compared to SLNs [8,9] and liposomes [10].

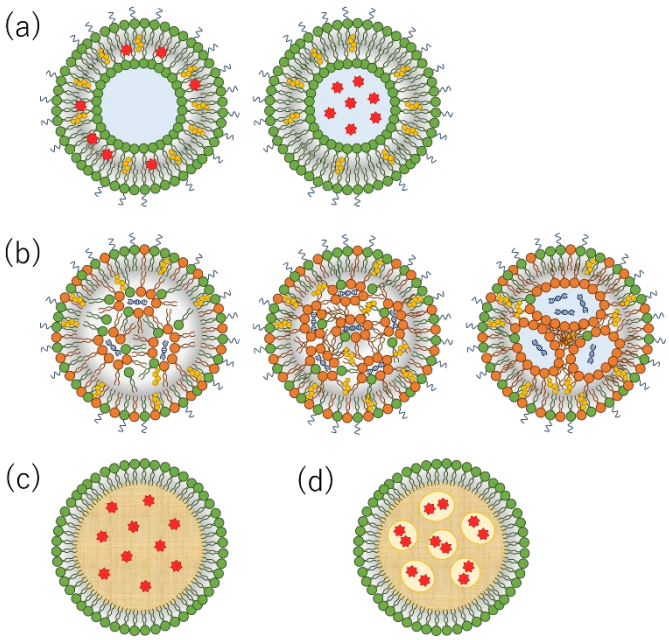

Figure 1.1 Diverse lipid-based nanoparticles (Lb-NPs). Schematic representation of (a) liposomes encapsulating hydrophobic and hydrophilic drugs, (b) lipid nanoparticles (LNPs) in which nucleic acids are organized in inverse lipid micelles, (c) solid lipid nanoparticle (SLN), and (d) nanostructured lipid carrier (NLC).

The following subsection focuses on liposomes and LNPs, which are the most versatile Lb-NPs, and gives an overview of their physicochemical properties and clinical applications.

1.1.1 Physicochemical properties of liposomes and their clinical applications and products

The term “liposome” was coined shortly after the discovery of closed lipid bilayer vesicles that form spontaneously in the aqueous phase. Liposomes are classified into several categories according to their size and internal structure (Figure 1.2). The size range of liposomes is very broad, and particles with sizes ranging from tens of nanometers to micro-order size can be prepared and observed. Unilamellar liposomes smaller than approximately 100 nm are called small unilamellar vesicles (SUVs). By contrast, unilamellar liposomes with sizes of approximately 200 to 500 nm are referred to as large unilamellar vesicles (LUVs), whereas microscopic liposomes larger than 1000 nm are called giant unilamellar vesicles (GUVs). In terms of structure, liposomes with several to several dozen lamellae and an onion-like structure are called multilamellar vesicles (MLVs), and liposomes

containing multiple small vesicles are called multivesicular vesicles (MVVs).

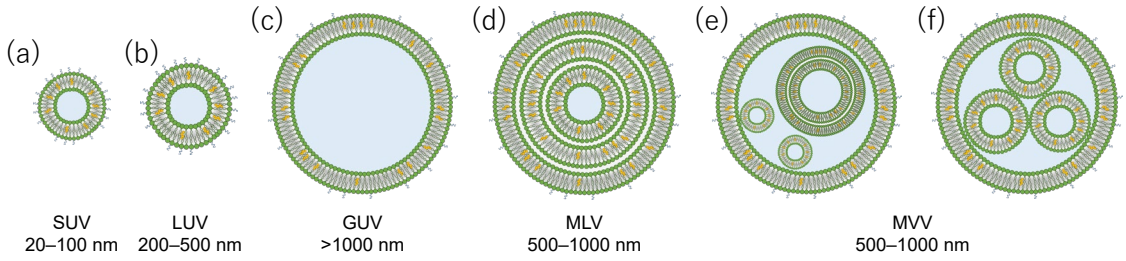

Figure 1.2 Classification of liposomes according to size and lamellarity: (a) small unilamellar vesicle (SUV), (b) large unilamellar vesicle (LUV), (c) giant unilamellar vesicle (GUV), (d) multilamellar vesicles (MLV), and (e) and (f) multivesicular vesicles (MVV).

The size of liposomes can be adjusted according to their purposes and applications. For parenteral drug delivery carriers, especially those for intravenous injection, liposomes with sizes of 10–200 nm are preferable because larger liposomes tend to be phagocytosed and eliminated from blood. In addition, larger liposomes with broader size distributions are difficult to sterilize by filtration (0.2 μm filters are commonly used for non-thermal pharmaceutical sterilization). Moreover, liposome size also affects the cellular uptake and biodistribution of liposomes and encapsulated drugs [11,12]. However, slightly larger liposomes can also be applied in topical products such as transdermal formulations and cosmetics because topical administration does not depend on stable blood circulation and sterilization in principle. By contrast, microsized giant liposomes have been used as models of cells for the functional analysis of membrane proteins and intracellular phenomena [13–15].

The internal structure of liposomes affects the drug release profile and drug concentration in blood and thus can contribute to more extended release of drugs in blood and at the application site and can reduce the potential adverse effect of drugs [16,17].

Liposomes are essentially composed of phospholipids (for example, phosphatidylcholine, phosphatidylglycerol, and phosphatidylserine) and cholesterol. These components also make up the cell membrane. The physicochemical properties of liposomes can be modulated by selecting the type of phosphatidylcholine and amount of cholesterol. It is also possible to modify the surface of liposomes to obtain additional functions and characteristics. Polyethylene glycol (PEG) is often used

to achieve stealth in blood circulation. Target-specific ligands are also applied to obtain the ability to deliver the liposomes to target organs and cells.

The potential of liposomes as drug delivery carriers was recognized shortly after their discovery because of their stability and ability to encapsulate both hydrophilic and hydrophobic drugs. As a result, more than 10 liposomal nanomedicines have been approved. In addition to pharmaceutical products, numerous liposomal cosmetic products are on the market. Clinically approved liposomal medicines and commercially available liposomal cosmetics are listed in Tables 1.1 and 1.2, respectively.

Table 1.1 Clinically approved liposome-based medicines

Trade name (Administration)	Active ingredient	Composition	Carrier	Indication for use	Manufacturer
AmBisome (i.v.)	Amphotericin B	HSPC/DSPG/cholesterol (52.6:26.3:21.1)	Liposomes	Fungal infections	Sumitomo Pharma
DaunoXome (i.v.)	Daunorubicin	DSPC/cholesterol (2:1)	Liposomes	AIDS-related Kaposi's sarcoma	Galen
Depocyt (Spinal)	Cytarabine/Ara-C	DOPC/DPPG/cholesterol/ triolein (7:1:11:1)	Liposomes (Multivesicle)	Neoplastic meningitis	DepoTech Corporation/ Pacira Pharmaceuticals
DepoDur (Epidural)	Morphine sulfate	DOPC/DPPG/cholesterol/ triolein (7:1:11:1)	Liposomes (Multivesicle)	Pain management	Pacira Pharmaceuticals, Inc.
Doxil/Caelyx (i.v.)	Doxorubicin	HSPC/cholesterol/DSPE-PEG2000 (56.3:38.4:5.3)	PEGylated liposomes	Breast and ovarian cancer, HIV-related Kaposi's sarcoma, myeloma	Janssen Pharmaceutical K.K.
Epaxal (i.m.)	Inactivated hepatitis A virus (stain RGSB)	DOPC/DOPE (75:25)	Liposomes (Virosome)	Hepatitis A	Crucell
Exparel (s.c.)	Bupivacaine	DEPC/DPPG/cholesterol/ tricaprylin (43.2:4.5:45.4:15.9)	Liposomes (Multivesicle)	Pain management	Pacira Pharmaceuticals, Inc.
Fungizone (i.v.)	Amphotericin B	DMPC/DMPG	Liposomes	Systemic fungal infections	Apothecon Pharmaceuticals
Inflexal V (i.m.)	Inactivated hemagglutinin of influenza virus strains A and B	DOPC/DOPE (75:25)	Liposomes (Virosome)	Influenza	Crucell, Berna Biotech
Lipusu (i.v.)	Paclitaxel	EPC/cholesterol (8:2)	Liposomes	Squamous non-small-cell lung cancer, esophageal cancer	Luye Pharmaceuticals
Marqibo (i.v.)	Vincristine	ESM/cholesterol (60:40)	Liposomes	Acute lymphoblastic leukemia	Acrotech Biopharma, Inc.

Table 1.1 (continued) Clinically approved liposome-based medicines

Trade name (Administration)	Active ingredient	Composition	Carrier	Indication for use	Manufacturer
Metpact (i.v.)	Mifamurtide	DOPS/POPC (3:7)	Liposomes	High-grade, resectable, nonmetastatic osteosarcoma	Takeda France SAS
Myocet (i.v.)	Doxorubicin	EPC/cholesterol (55:45)	Liposomes	Combination therapy with cyclophosphamide in metastatic breast cancer	Teva B.V.
Onivyde (i.v.)	Irinotecan	DSPC/cholesterol/DSPE-PEG2000 (59.8:39.9:0.3)	PEGylated liposomes	Combination therapy with fluorouracil and leucovorin in metastatic pancreatic adenocarcinoma	Ipsen Pharma
Visudyne (i.v.)	Verteporphin	DMPC/EPG (62.5:37.5)	Liposomes	Choroidal neovascularization	Clinigen Limited
Vyxeos (i.v.)	Daunorubicin/Cytarabine (1:5)	DSPC/DSPG/cholesterol (7:2:1)	Liposomes	Acute myeloid leukemia	Celator Pharmaceuticals Inc.
Lipo-Dox (i.v.)	Doxorubicin	DSPC/cholesterol/DSPE-PEG2000 (56.3:38.4:5.3)	PEGylated liposomes	Breast and ovarian cancer, HIV-related Kaposi's sarcoma, myeloma.	Sun Pharmaceutical Industries Ltd.

DEPC (dierucoyl phosphatidylcholine); DMPC (dimyristoyl phosphatidylcholine); DOPC (dioleoyl phosphatidylcholine); DOPE (dioleoly phosphatidylethanolamine); DOPS (dioleoyl phosphatidylserine); DPPA (dipalmitoyl-phosphatidic acid); DPPC (dipalmitoyl phosphatidylcholine); DPPG (dipalmitoyl phosphatidylglycerol); DSPC (distearoyl phosphatidylcholine); DSPE (distearoyl phosphatidylethanolamine); DSPG (distearoyl phosphatidylglycerol); DSPE-PEG2000 (distearoyl phosphatidylethanolamine-N-[amino(polyethylene glycol)-2000); EPC (egg phosphatidylcholine); ESM (egg sphingomyelin); HSPC (hydrogenated soy phosphatidylcholine); POPC (palmitoyl-oleoyl phosphatidylcholine). i.v. (intravenous); i.m. (intramuscular); s.c. (subcutaneous). References: [3,6,18,19]

Table 1.2 Marketed liposomal cosmetic products

Product name	Producer	Activity
Celadrin® Topical Liposome Lotion	NOW Solutions	Topical liposome lotion
Capture Totale	Christian Dior	Antiaging and skin repair
Eye Perfector	Avon	Soothing cream for eye irritation
Everyday Skin® Penetrating Lotion	Kara Vita	Skin moisturizer
Moisture Liposome Face Cream	Decorte	Skin moisturizer
Moisture Liposome Eye Cream	Decorte	Skin moisturizer, conditioner
Liposome Advanced Repair Serum Time Released Multilamellar Liposomes	Decorte	Skin moisturizer, conditioner
Liposome Treatment Liquid	Decorte	Skin moisturizer, conditioner
Moisture Liposome	Decorte	Skin moisturizer, conditioner
Moisture Liposome Mask	Decorte	Skin moisturizer, conditioner
Natural Progesterone Liposomal Skin Cream	NOW Solutions	Skin conditioner
C-Vit Liposomal Serum	Sesderma	Skin moisturizer, conditioner
Fillderma Lips Lip Volumizer	Sesderma	Lip volumizer, wrinkle repair, skin moisturizer
Lumessence Eye Cream	Aubrey Organics	Anti-wrinkle & firming
Russell Organics Liposome Concentrate	Russell Organics	Skin moisturizer & rejuvenator
Clinicians Complex Liposome Face & Neck Lotion	Clinicians Complex	Skin conditioner, sunscreen
Rehydrating Liposome Day Crème	Kerstin Florian	Skin moisturizer
Liposomal Vitamin C	California Gold Nutrition	Supplement

Reference: [6]

1.1.2 Physicochemical properties of lipid nanoparticles and their clinical applications and products

LNPs are the latest generation of Lb-NPs. The term “LNP” has been applied to oligonucleotide-encapsulated Lb-NPs with an electron-dense core inside the particles instead of a hollow inner aqueous phase [20].

Oligonucleotides can be used to modulate gene expression through a wide range of processes, including RNAi, target protein generation, target degradation by RNase H-mediated cleavage, splicing modulation, non-coding RNA inhibition, gene activation, and programmed gene editing. For example, siRNAs and miRNAs down-regulate the generation of target proteins by binding the antisense strand of these RNAs to form the RNA-induced silencing complex and thus degrade the target mRNAs. These mRNAs are translated into proteins; therefore, mRNA medicines can generate the target proteins in the patient’s body. Thus, these molecules have therapeutic potential for myriad diseases, and several oligonucleotide medicines have recently been approved [21] and are undergoing clinical trials [22]. These technologies have the potential to meet medical needs that could not be met using conventional small molecules.

However, oligonucleotides interact with biomolecules or work inside the cell, especially in the cytosol or nucleus. Therefore, they must be delivered to target organs and cells and released into target organelles [20]. However, oligonucleotides are easily degraded during storage and also in the body [5]. Therefore, the development of nanoparticle technologies to deliver intact oligonucleotides to target cells and organs has attracted much attention. LNPs are among the most promising nanoparticle technologies for pharmaceutical applications because of their high biocompatibility and high potential to deliver RNAs into cytosol. Consequently, a number of RNA encapsulated LNP-based nanomedicines have been clinically approved in recent years, as shown in Table 1.3.

LNPs are essentially composed of several types of lipids, including cationic/ionizable lipids, helper lipids, cholesterol, and surface modifiers such as PEG or target ligands [18,20,23]. Cationic or ionizable lipids are important components that interact with negatively charged RNAs to encapsulate the RNAs into LNPs. Cationic lipids can also interact with cell membranes and introduce LNPs into cells because of their positive charge. Ionizable lipids can have pKa values in the acidic pH range, which gives them neutral charge at physiological pH and prevents them from interacting with blood cells and serum proteins and from being excluded from blood circulation [24,25]. The structure and

chemical properties of cationic or ionizable lipids reportedly affect RNA activity and efficacy [26–28]. It has also been reported that these types of helper lipids affect RNA activity and efficacy [26,29]. Recent papers have introduced the concept of selective organ targeting delivery by simply changing the composition ratio of cationic and helper lipids [30,31]. Thus, the precise optimization of the LNP formulation has attracted much attention. In addition to the main components of LNPs, the type and amount of surface modifiers also affect the efficient targeting of organs and tissues, RNA efficacy, and intracellular fate [32,33]. The size and polydispersity index of LNPs, like those of liposomes, affect their activity, for example, the efficiency of LNP and RNA delivery, and the endosomal escape rate inside cells [34,35].

Table 1.3 Clinically approved LNP-based nanomedicines

Active ingredient	Patisiran	Tozinameran	Elasomeran
Trade name	Onpattro	Comirnaty	Spikevax
Company	Alnylam	Pfizer/BioNTech	Moderna
LNP-formulated RNA	siRNA	mRNA	mRNA
Indication	hATTR amyloidosis	Prevention of COVID-19	Prevention of COVID-19
mRNA/siRNA dose; administration route	0.3 mg/kg; intravenous	30 µg; intramuscular	100 µg; intramuscular
Components	DLin-MC3-DMA/DSPC/cholesterol/ PEG2000-C-DMG	ALC-0315/DSPC/cholesterol/ALC-0159	SM-102/DSPC/cholesterol/PEG2000-DMG
Molar lipid ratio of components (%)	50:10:38.5:1.5	46.3:9.4:42.7:1.6	50:10:38.5:1.5
Molar N/P ratio[a]	3	6	6[b]
Buffer	・Potassium phosphate, monobasic, anhydrous ・Sodium phosphate, dibasic, heptahydrate ・pH ~ 7	・Potassium dihydrogen phosphate ・Disodium hydrogen phosphate dihydrate ・Potassium chloride ・pH 7–8	・Tris (tromethamine) ・pH 7–8
Other excipients	・Sodium chloride ・Water for injection	・Sodium chloride ・Sucrose ・Water for injection	・Sodium acetate ・Sucrose ・Water for injection
Storage conditions	2 °C–8 °C	−90 °C to −60 °C	−50 °C to −15 °C

[a] N = ionizable cationic lipid (nitrogen), P = nucleotide (phosphate). [b] Estimate. DLin-MC3-DMA ((6Z,9Z,28Z,31Z)heptatriaconta-6,9,28,31-tetraen19-yl-4-(dimethylamino) butanoate), PEG2000-C-DMG (Alpha-(3′-{[1,2di(myristyloxy)propanoxy] carbonylamino}propyl)ω-methoxy, polyoxyethylene), DSPC (1,2-Distearoyl-sn-glycero-3-phosphocholine), ALC-0315 ((4hydroxybutyl) azanediyl)bis (hexane-6,1-diyl)bis(2hexyldecanoate)), ALC-0159 (2-[(polyethylene glycol)-2000]-N,N ditetradecylacetamide), SM-102 ((heptadecan-9-yl 8-{(2-hydroxyethyl)[6oxo-6-(undecyloxy) hexyl] amino} octanoate)), PEG2000-DMG (1,2-Dimyristoyl-rac-glycero-3-methoxypolyethylene glycol-2000) Reference: [5,36]

1.2 Drug development pathway and flow

The development of a new therapeutic product is a long, complex, and expensive process. The drug development pathway from the identification of seeds to commercialization typically takes 10–12 years or longer. This development flow and drug development lifecycle usually consists of five stages, as shown in Figure 1.3.

In the discovery and development (basic research) stage, one or several new therapeutic seeds are identified from among thousands or tens of thousands of candidates. In small-molecule drug development, the focus is on promising compound discovery because excipients in the drug product are unlikely to affect the activity of candidate compounds. For nucleic-acid-loaded nanoparticulate medicines, however, the components of the nanomedicine reportedly have a significant impact on the overall quality of the product and the pharmacokinetics of the nucleic acids and the nanoparticles carrying them [30,31,33]. Therefore, when nanoparticle-based medicines are developed, it is necessary to optimize the composition and formulation at this stage [37].

The next stage is preclinical research. In preclinical research, the efficacy and toxicology/safety of a candidate product are examined by using cell lines (in vitro) and animals (in vivo) before testing the candidate compound/product in people.

After the efficacy and safety of a candidate compound are confirmed in preclinical research, the development process moves to clinical research. In this stage, the candidate compound/product is administered to humans. Here, the efficacy, safety/toxicity, and quality in humans are examined. Clinical research is divided into three phases. In Phase 1 study, the candidate compounds/products are administered to relatively few healthy volunteers or people with the disease/condition (generally, 20–100 people). The purpose of Phase 1 study is to confirm the appropriate dose strength, pharmacokinetics, and drug safety in humans. In Phase 2 study, a higher number of people with the disease/condition (typically up to several hundred people) are enrolled for participation. This study evaluates the concept of the mode of action and therapeutic effect of the candidate product at therapeutic dosing levels. Finally, after proof of concept of the candidate is confirmed, a Phase 3 trial is conducted. Numerous volunteers who have the disease or condition (approximately 300 to 3000 people) are studied at this stage to confirm the efficacy and monitor adverse reactions.

The pharmaceutical company files an application to market the candidate product if it has evidence from its basic research, preclinical research, and clinical research that the drug is safe and

effective for its intended use. The company prepares a new drug application (NDA), which outlines the full history of candidate product development, and submits it to the appropriate authority, which is the Ministry of Health, Labor, and Welfare (MHLW) in Japan (in the United States, it is the Food and Drug Administration, and in Europe, it is the European Medicines Agency). The NDA is then reviewed by the Pharmaceuticals and Medical Devices Agency and approved by the Minister of the MHLW for marketing.

After approval, the company manufactures and markets the product to patients. Production is performed stably under management to maintain good manufacturing practices. Once it is on the market, the pharmaceutical company is responsible for monitoring adverse events and providing information on the medicine to promote its proper use. The need and demand for medicines vary according to changes in the number of patients, the potential efficacy of the medicine, and the post-approval addition of new indications. Therefore, it is necessary to supply medicines stably in accordance with the needs of the market.

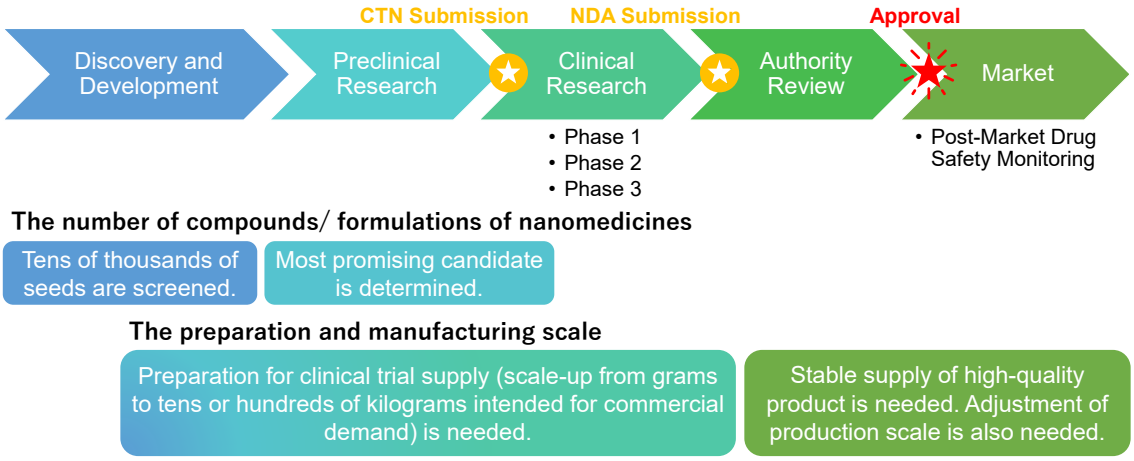

Figure 1.3 Basic drug development process and flow

CTN: clinical trial notification, NDA: new drug application

1.3 Preparation methods for lipid-based nanoparticles

Lb-NPs can be prepared by several methods. The most conventional and widely used method is thin-film hydration (the Bangham method) [2,20]. In this method, the lipid components are dissolved

in an organic solvent and dried under reduced pressure to form a thin lipid film on the inner surface of a flask. The aqueous solution is then poured into the flask to prepare the liposomes. This method is easy to implement, but a sizing process such as ultrasonication or extrusion is needed to prepare small liposomes with a narrow size distribution [38]. In addition, the method is difficult and time-consuming to scale up because the surface area and thickness of the lipid thin film affect the physicochemical properties of the Lb-NPs. In addition, it is necessary to change the manufacturing machine/equipment during scaling up or when adjusting the production scale according to the needs of patients. Therefore, this manufacturing process is not preferred and requires considerable effort.

The other popular and conventional method is solvent injection, where ethanol is commonly used as an organic solvent because of its safety [2,38]. In this method, lipids in organic solvent solution are poured dropwise into the aqueous phase to prepare Lb-NPs. Batzri et al. first described this method in 1973 [39]. This method is also easy to implement and enables the preparation of nanosized Lb-NPs; however, the Lb-NP size cannot be adjusted very precisely. The poor controllability of the organic solvent/aqueous solution interface and inhomogeneous dilution of the organic solvent promote the preparation of lipid bilayer intermediates of different sizes and produces Lb-NPs with low homogeneity and a narrow size range. Because this preparation method is also a batch-scale process, it has the same difficulties as the thin-film hydration method with scaling up and adjusting the production scale.

The microfluidic-device-assisted solvent dilution method has become the most promising and attractive method. Ethanol is also the most commonly used organic solvent in this method owing to its safety [2,38]. An organic solvent solution containing lipid components and the aqueous solution is introduced into the microfluidic device to prepare Lb-NPs. This method can be used for the continuous preparation of Lb-NPs simply by introducing the two solutions and diluting the ethanol rapidly and homogeneously in a microchannel. Therefore, this method makes it possible to prepare homogeneous Lb-NPs with fine tuning in a wider size range and also to prepare Lb-NPs on scales ranging from laboratory scale to mass production scale using the same concept and platforms.

This preparation method has been studied recently, and some channel structures suitable for preparing Lb-NPs have been proposed. T- or Y-shaped microfluidic channels were the first-generation channel structures for preparing Lb-NPs via microfluidic technology [40]. They produce a laminar flow in the channel, and the Lb-NPs are precipitated on the liquid/liquid interface. Then, a hydrodynamic flow-focusing channel was developed to increase the area of the liquid/liquid interface

between the aqueous and organic solvent phases [41–43]. The organic solvent phase is sandwiched between the aqueous phases, forming a sheath of fluid on both sides of the aqueous phase in the microfluidic device, which promotes more rapid dilution of ethanol [44]. In the second-generation structure, a microfluidic channel equipped with mixer structures was developed to allow for rapid ethanol dilution by inducing chaotic mixing or secondary flow in the channel [45]. The staggered herringbone mixer is among the widely used microfluidic devices that enable the rapid mixing of the aqueous and organic solvent phases by inducing chaotic mixing flow in the channel. The concept of this device was proposed by Stroock et al. in 2002 [46]. This microfluidic structure was commercialized by Precision Nanosystems Inc. Another microfluidic device, which was commercialized by Blacktrace Holdings Ltd., incorporates branched mixer structures in the channel. More recently, Precision Nanosystems Inc. developed a toroidal mixer microfluidic device that allows increasing flow rates to be used, enabling mass production [47].

Kimura et al. developed a microfluidic device equipped with baffle structures. This device, the invasive lipid nanoparticle production (iLiNP) device [48], induces secondary flow in the channel at high flow rates and can dilute the ethanol phase rapidly, which enables the preparation of Lb-NPs in a considerably wider size range compared to other microfluidic devices, including commercially available microfluidic devices such as the staggered herringbone mixer [48,49].

As mentioned above, microfluidic-device-assisted solvent dilution has potential for use as an alternative method for preparing Lb-NPs and might solve the problems of conventional batch-scale preparation methods. However, this microfluidic-device-assisted solvent dilution method has several problems that must be solved to extend its application for drug development and manufacturing. In the following section, I describe the problem with the optimization process of Lb-NP formulations and the mass production of Lb-NPs in the context of Lb-NP preparation using microfluidic devices.

1.3.1 Formulation screening of lipid nanoparticles via microfluidic technology

As mentioned in subsection 1.1.2, LNPs are composed of several types of functional lipids [50]. It is widely known that the types of lipids and composition ratios of lipids and also RNAs are directly related to the encapsulation efficiency of RNAs, the size and polydispersity of LNPs, and the gene silencing/expression efficiency of RNAs [20]. Thus, it is crucial to explore and discover the most promising LNP compositions and formulations by evaluating numerous types of LNPs in the non-

clinical phase, especially in the basic research (discovery and development) stage. LNPs are currently prepared by diluting an ethanol phase containing all the components of LNPs with an aqueous phase in the flow channel of a microfluidic device. It is extremely time-consuming and labor-intensive to prepare numerous types of LNPs using this conventional method because ethanol solutions for each lipid composition of the LNPs must be prepared, placed in syringes, and injected into pumps. In addition, when the solution is replaced, a cleaning solution must be prepared to clean the microfluidic device and tubes, and the cleaning solution and previously used solution must be discarded. All syringes used for the preparation of LNPs must be washed. Thus, as more LNP compositions are tested, the preparation process takes longer both before and after solutions are introduced into the microfluidic device.

1.3.2 Mass production for lipid-based nanoparticles via microfluidic technology

One drawback of Lb-NP preparation using a microfluidic device is the low production throughput. To overcome this difficulty, several solutions have been proposed and investigated: (1) the parallelization/integration of microfluidic devices, (2) increasing the flow rate, and (3) increasing the lipid concentration in the ethanol phase.

The parallelization/integration of microfluidic devices is a simple method of increasing the production rate of Lb-NPs. However, Lb-NPs prepared in this way must be carefully evaluated because they might have low homogeneity, and the physicochemical properties and efficacy of the encapsulated drugs might vary. Several pumps and devices must be used in the parallelization and integration of microfluidic devices; in fact, Pfizer uses eight pairs of pumps to prepare its COVID-19 vaccine [51]. When several pumps and devices are used, the process control and management of each pump and device during manufacturing, which is labor-intensive and undesirable [51], must be considered.

To increase the flow rate, it is necessary to change the microfluidic device and flow rate between the initial development and later stages. This change might affect the physicochemical properties of the Lb-NPs and the activity of the encapsulated drug.

By contrast, concentrated Lb-NPs can be obtained in a single short run time by using a highly concentrated lipid solution. The concentration of Lb-NPs is critical for the efficient delivery and release of the loaded drug. In addition, concentration steps using ultracentrifugation or tangential flow

filtration can be omitted, eliminating the possibility of changes in the particle properties of Lb-NPs during the concentration process.

There are many reports on the mass production of Lb-NPs by the parallelization and integration of microfluidic devices and by increasing the flow rate, and there are few reports on the preparation of Lb-NPs using highly concentrated lipid solutions in the ethanol phase. The reason is that the use of high-concentration lipid solutions in microfluidic devices is thought to produce larger and less homogeneous Lb-NPs [52–54], making it difficult to control the particle properties. Therefore, knowledge of and evidence for the use of highly concentrated lipid solutions is extremely scarce, and the effects of a highly concentrated lipid solution on the structure and physicochemical properties of Lb-NPs are still not clearly understood.

1.4 Outline of thesis

As described in subsection 1.3, microfluidic-device-assisted Lb-NP preparation methods have excellent potential as a promising Lb-NP preparation method. Nevertheless, challenges remain for the broad application of microfluidic devices from the research phase to the practical mass production phase.

A major challenge for the microfluidic preparation of Lb-NPs is the lack of an LNP preparation platform suitable for the high-throughput formulation screening of LNPs. As mentioned in subsection 1.3.1, the preparation of LNPs using microfluidic devices is simple and easy to control; however, the conventional platform is unsuitable and inefficient for preparing numerous types of LNPs simultaneously.

The other major challenge involving microfluidic preparation platforms is the production throughput. The production rate of a hydrodynamic flow-focusing device is <10 mL/h, and that of a staggered herringbone micromixer is <100 mL/h [55]. More efficient mass production methodologies have been investigated recently by using a toroidal mixer [47] and parallelized and integrated microfluidic devices; however, the production rate is <20 L/h [38,55,56]. The parallelization and integration of microfluidic devices is currently the most promising mass production method. However, it may affect quality control; for example, the uniformity of Lb-NPs may be reduced if each microfluidic device prepares Lb-NPs with slightly different particle sizes. It is necessary to consider and evaluate other combinable options for further increasing the production throughput or for mass

production without the parallelization and integration of microfluidic equipment. The use of highly concentrated lipid solutions can increase the throughput of Lb-NPs. As mentioned in subsection 1.3.2, although the potential for using highly concentrated lipid solutions is high, the applicability of highly concentrated lipid solutions in the microfluidic-based production of Lb-NPs has rarely been reported. Thus, the effect of using highly concentrated lipid solution in microfluidic devices on the physicochemical properties of Lb-NPs has not been elucidated.

To address these challenges and accelerate the development and clinical application of lipid-based nanomedicines, I conducted the investigations described in this thesis. Chapter 2 describes the development of a microfluidic platform for the on-device formulation screening of LNPs. A novel microfluidic platform for on-device formulation screening is proposed and evaluated to provide a proof of concept. In chapter 3, to address the challenges for mass production, I investigate the applicability of a highly concentrated lipid solution for the microfluidic-based preparation of Lb-NPs with a placebo formulation to clarify the fundamental effect of lipid concentration. In chapter 4, I investigate the detailed physicochemical properties of drug-loaded liposomes prepared using high-concentration lipid solutions. Liposomes loaded with the model compound paclitaxel were prepared using low- and high-concentration lipid solutions. Then, the differences in physicochemical properties and drug activity were evaluated.

1.5 References

[1] A.D. Bangham, R.W. Horne, Negative staining of phospholipids and their structural modification by surface-active agents as observed in the electron microscope, J Mol Biol. 8 (1964) 660-IN10.

[2] P. Liu, G. Chen, J. Zhang, A Review of Liposomes as a Drug Delivery System: Current Status of Approved Products, Regulatory Environments, and Future Perspectives, Molecules. 27 (2022) 1372.

[3] E. Beltrán-Gracia, A. López-Camacho, I. Higuera-Ciapara, J.B. Velázquez-Fernández, A.A. Vallejo-Cardona, Nanomedicine review: clinical developments in liposomal applications, Cancer Nanotechnol. 10 (2019) 11.

[4] T. Wang, Y. Luo, Biological fate of ingested lipid-based nanoparticles: current understanding and future directions, Nanoscale. 11 (2019) 11048–11063.

[5] L. Schoenmaker, D. Witzigmann, J.A. Kulkarni, R. Verbeke, G. Kersten, W. Jiskoot, D. Crommelin, mRNA-lipid nanoparticle COVID-19 vaccines: structure and stability, Int J Pharmaceut. 601 (2021) 120586.

[6] R. Tenchov, R. Bird, A.E. Curtze, Q. Zhou, Lipid Nanoparticles-From Liposomes to mRNA Vaccine Delivery, a Landscape of Research Diversity and Advancement, Acs Nano. 15 (2021) 16982–17015.

[7] Y. Mirchandani, V.B. Patravale, S. Brijesh, Solid lipid nanoparticles for hydrophilic drugs, J Control Release. 335 (2021) 457–464.

[8] J. Pardeike, A. Hommoss, R.H. Müller, Lipid nanoparticles (SLN, NLC) in cosmetic and pharmaceutical dermal products, Int J Pharmaceut. 366 (2009) 170–184.

[9] R. Chutoprapat, P. Kopongpanich, L.W. Chan, A Mini-Review on Solid Lipid Nanoparticles and Nanostructured Lipid Carriers: Topical Delivery of Phytochemicals for the Treatment of Acne Vulgaris, Molecules. 27 (2022) 3460.

[10] N. Mennini, M. Cirri, F. Maestrelli, P. Mura, Comparison of liposomal and NLC (nanostructured lipid carrier) formulations for improving the transdermal delivery of oxaprozin: Effect of cyclodextrin complexation, Int J Pharmaceut. 515 (2016) 684–691.

[11] A.U. Andar, R.R. Hood, W.N. Vreeland, D.L. DeVoe, P.W. Swaan, Microfluidic Preparation of Liposomes to Determine Particle Size Influence on Cellular Uptake Mechanisms, Pharmaceut Res. 31 (2014) 401–413.

[12] S. Dadpour, A. Mehrabian, M. Arabsalmani, E. Mirhadi, A. Askarizadeh, M. Mashreghi, M.R. Jaafari, The role of size in PEGylated liposomal doxorubicin biodistribution and anti-tumour activity, Iet Nanobiotechnol. 16 (2022) 259–272.

[13] I.L. Jørgensen, G.C. Kemmer, T.G. Pomorski, Membrane protein reconstitution into giant unilamellar vesicles: a review on current techniques, Eur Biophys J. 46 (2017) 103–119.

[14] S. Tanaka, K. Takiguchi, M. Hayashi, Repetitive stretching of giant liposomes utilizing the nematic alignment of confined actin, Commun Phys. 1 (2018) 18.

[15] T. Shimanouchi, H. Ishii, N. Yoshimoto, H. Umakoshi, R. Kuboi, Calcein permeation across phosphatidylcholine bilayer membrane: Effects of membrane fluidity, liposome size, and immobilization, Colloids Surfaces B Biointerfaces. 73 (2009) 156–160.

[16] K.-I. Joo, L. Xiao, S. Liu, Y. Liu, C.-L. Lee, P.S. Conti, M.K. Wong, Z. Li, P. Wang, Crosslinked multilamellar liposomes for controlled delivery of anticancer drugs, Biomaterials. 34 (2013) 3098–3109.

[17] Saujanya.L. Gosangari, K.L. Watkin, Effect of preparation techniques on the properties of curcumin liposomes: Characterization of size, release and cytotoxicity on a squamous oral carcinoma cell line, Pharm Dev Technol. 17 (2010) 103–109.

[18] L.M. Ickenstein, P. Garidel, Lipid-based nanoparticle formulations for small molecules and RNA drugs, Expert Opin Drug Del. 16 (2019) 1205–1226.

[19] N.A. Mohamed, I. Marei, S. Crovella, H. Abou-Saleh, Recent Developments in Nanomaterials-Based Drug Delivery and Upgrading Treatment of Cardiovascular Diseases, Int J Mol Sci. 23 (2022) 1404.

[20] M.J.W. Evers, J.A. Kulkarni, R. der Meel, P.R. Cullis, P. Vader, R.M. Schiffelers, State-of-the-Art Design and Rapid-Mixing Production Techniques of Lipid Nanoparticles for Nucleic Acid Delivery, Small Methods. 2 (2018) 1700375.

[21] Y.-K. Kim, RNA therapy: rich history, various applications and unlimited future prospects, Exp Mol Medicine. 54 (2022) 455–465.

[22] J.M. Sasso, B.J.B. Ambrose, R. Tenchov, R.S. Datta, M.T. Basel, R.K. DeLong, Q.A. Zhou, The Progress and Promise of RNA Medicine–An Arsenal of Targeted Treatments, J Med Chem. 65 (2022) 6975–7015.

[23] Y. Eygeris, M. Gupta, J. Kim, G. Sahay, Chemistry of Lipid Nanoparticles for RNA Delivery, Accounts Chem Res. 55 (2022) 2–12.

[24] J.A. Kulkarni, P.R. Cullis, R. van der Meel, Lipid Nanoparticles Enabling Gene Therapies: From Concepts to Clinical Utility, Nucleic Acid Ther. 28 (2018) 146–157.

[25] X. Hou, T. Zaks, R. Langer, Y. Dong, Lipid nanoparticles for mRNA delivery, Nat Rev Mater. (2021) 1–17.

[26] J.A. Kulkarni, J.L. Myhre, S. Chen, Y.Y.C. Tam, A. Danescu, J.M. Richman, P.R. Cullis, Design of lipid nanoparticles for in vitro and in vivo delivery of plasmid DNA, Nanomed Nanotechnol Biology Medicine. 13 (2017) 1377–1387.

[27] Y. Sato, K. Hashiba, K. Sasaki, M. Maeki, M. Tokeshi, H. Harashima, Understanding structure-activity relationships of pH-sensitive cationic lipids facilitates the rational identification of promising lipid nanoparticles for delivering siRNAs in vivo, J Control Release. 295 (2019) 140–152.

[28] X. Han, H. Zhang, K. Butowska, K.L. Swingle, M.-G. Alameh, D. Weissman, M.J. Mitchell, An ionizable lipid toolbox for RNA delivery, Nat Commun. 12 (2021) 7233.

[29] R. Zhang, R. El-Mayta, T.J. Murdoch, C.C. Warzecha, M.M. Billingsley, S.J. Shepherd, N. Gong, L. Wang, J.M. Wilson, D. Lee, M.J. Mitchell, Helper lipid structure influences protein adsorption and delivery of lipid nanoparticles to spleen and liver, Biomater Sci-Uk. 9 (2020) 1449–1463.

[30] Q. Cheng, T. Wei, L. Farbiak, L.T. Johnson, S.A. Dilliard, D.J. Siegwart, Selective organ targeting (SORT) nanoparticles for tissue-specific mRNA delivery and CRISPR–Cas gene editing, Nat Nanotechnol. 15 (2020) 313–320.

[31] S.T. LoPresti, M.L. Arral, N. Chaudhary, K.A. Whitehead, The replacement of helper lipids with charged alternatives in lipid nanoparticles facilitates targeted mRNA delivery to the spleen and lungs, J Control Release. 345 (2022) 819–831.

[32] R. Ran, H. Wang, Y. Liu, Y. Hui, Q. Sun, A. Seth, D. Wibowo, D. Chen, C.-X. Zhao, Microfluidic self-assembly of a combinatorial library of single- and dual-ligand liposomes for in vitro and in vivo tumor targeting, Eur J Pharm Biopharm. 130 (2018) 1–10.

[33] Y. Sato, Y. Note, M. Maeki, N. Kaji, Y. Baba, M. Tokeshi, H. Harashima, Elucidation of the physicochemical properties and potency of siRNA-loaded small-sized lipid nanoparticles for siRNA delivery, J Control Release. 229 (2016) 48–57.

[34] S. Chen, Y.Y.C. Tam, P.J.C. Lin, A.K.K. Leung, Y.K. Tam, P.R. Cullis, Development of lipid nanoparticle formulations of siRNA for hepatocyte gene silencing following subcutaneous administration, J Control Release. 196 (2014) 106–112.

[35] A. Hashiba, M. Toyooka, Y. Sato, M. Maeki, M. Tokeshi, H. Harashima, The use of design of experiments with multiple responses to determine optimal formulations for in vivo hepatic mRNA delivery, J Control Release. 327 (2020) 467–476.

[36] Y. Suzuki, H. Ishihara, Difference in the lipid nanoparticle technology employed in three approved siRNA (Patisiran) and mRNA (COVID-19 vaccine) drugs, Drug Metab Pharmacok. 41 (2021) 100424.

[37] Reflection paper on nucleic acids (siRNA)-loaded nanotechnology-based drug products, (2016). https://www.nihs.go.jp/drug/section4/nanomedicine_j/20160328_jim_siRNA.pdf. (accessed 27th October 2022).

[38] C. Webb, S. Ip, N.V. Bathula, P. Popova, S.K.V. Soriano, H.H. Ly, B. Eryilmaz, V.A.N. Huu, R. Broadhead, M. Rabel, I. Villamagna, S. Abraham, V. Raeesi, A. Thomas, S. Clarke, E.C. Ramsay, Y. Perrie, A.K. Blakney, Current Status and Future Perspectives on MRNA Drug Manufacturing, Mol Pharmaceut. 19 (2022) 1047–1058.

[39] S. Batzri, E.D. Korn, Single bilayer liposomes prepared without sonication, Biochimica Et Biophysica Acta Bba - Biomembr. 298 (1973) 1015–1019.

[40] J.A. Kulkarni, Y.Y.C. Tam, S. Chen, Y.K. Tam, J. Zaifman, P.R. Cullis, S. Biswas, Rapid synthesis of lipid nanoparticles containing hydrophobic inorganic nanoparticles, Nanoscale. 9 (2017) 13600–13609.

[41] A. Jahn, W.N. Vreeland, M. Gaitan, L.E. Locascio, Controlled Vesicle Self-Assembly in Microfluidic Channels with Hydrodynamic Focusing, J Am Chem Soc. 126 (2004) 2674–2675.

[42] A. Jahn, W.N. Vreeland, D.L. DeVoe, L.E. Locascio, M. Gaitan, Microfluidic Directed Formation of Liposomes of Controlled Size, Langmuir. 23 (2007) 6289–6293.

[43] A. Jahn, S.M. Stavis, J.S. Hong, W.N. Vreeland, D.L. DeVoe, M. Gaitan, Microfluidic Mixing and the Formation of Nanoscale Lipid Vesicles, Acs Nano. 4 (2010) 2077–2087.

[44] S. Garg, G. Heuck, S. Ip, E. Ramsay, Microfluidics: a transformational tool for nanomedicine development and production, J Drug Target. 24 (2016) 1–15.

[45] M. Maeki, S. Uno, A. Niwa, Y. Okada, M. Tokeshi, Microfluidic technologies and devices for lipid nanoparticle-based RNA delivery, J Control Release. 344 (2022) 80–96.

[46] A.D. Stroock, S.K.W. Dertinger, A. Ajdari, I. Mezić, H.A. Stone, G.M. Whitesides, Chaotic Mixer for Microchannels, Science. 295 (2002) 647–651.

[47] C. Webb, N. Forbes, C.B. Roces, G. Anderluzzi, G. Lou, S. Abraham, L. Ingalls, K. Marshall, T.J. Leaver, J.A. Watts, J.W. Aylott, Y. Perrie, Using microfluidics for scalable manufacturing of nanomedicines from bench to GMP: A case study using protein-loaded liposomes, Int J Pharmaceut. 582 (2020) 119266.

[48] N. Kimura, M. Maeki, Y. Sato, Y. Note, A. Ishida, H. Tani, H. Harashima, M. Tokeshi, Development of the iLiNP Device: Fine Tuning the Lipid Nanoparticle Size within 10 nm for Drug Delivery, Acs Omega. 3 (2018) 5044–5051.

[49] N. Kimura, M. Maeki, K. Sasaki, Y. Sato, A. Ishida, H. Tani, H. Harashima, M. Tokeshi, Three-dimensional, symmetrically assembled microfluidic device for lipid nanoparticle production, Rsc Adv. 11 (2021) 1430–1439.

[50] K. Paunovska, D. Loughrey, J.E. Dahlman, Drug delivery systems for RNA therapeutics, Nat Rev Genet. 23 (2022) 265–280.

[51] B.E. Cott, E. deBruyn and J. Corum, J. Corum, How Pfizer Makes Its Covid-19 Vaccine, The NewYork Times, (2021). https://www.nytimes.com/interactive/2021/health/pfizer-coronavirus-vaccine.html. (accessed 27th October 2022).

[52] R.R. Hood, D.L. DeVoe, High-Throughput Continuous Flow Production of Nanoscale Liposomes by Microfluidic Vertical Flow Focusing, Small. 11 (2015) 5790–5799.

[53] T.A. Balbino, N.T. Aoki, A.A.M. Gasperini, C.L.P. Oliveira, A.R. Azzoni, L.P. Cavalcanti, L.G. de la Torre, Continuous flow production of cationic liposomes at high lipid concentration in microfluidic devices for gene delivery applications, Chem Eng J. 226 (2013) 423–433.

[54] F. Yanar, A. Mosayyebi, C. Nastruzzi, D. Carugo, X. Zhang, Continuous-Flow Production of Liposomes with a Millireactor under Varying Fluidic Conditions, Pharm. 12 (2020) 1001.

[55] S.J. Shepherd, C.C. Warzecha, S. Yadavali, R. El-Mayta, M.-G. Alameh, L. Wang, D. Weissman, J.M. Wilson, D. Issadore, M.J. Mitchell, Scalable mRNA and siRNA Lipid Nanoparticle Production Using a Parallelized Microfluidic Device, Nano Lett. 21 (2021) 5671–5680.

[56] S.J. Shepherd, D. Issadore, M.J. Mitchell, Microfluidic formulation of nanoparticles for biomedical applications, Biomaterials. 274 (2021) 120826.

CHAPTER 2

Microfluidic Platform Enabling Efficient On-Device Preparation of Lipid Nanoparticles for Formulation Screening

2.1 Introduction

RNAs, including aptamer, antisense oligonucleotide, small interfering RNA (siRNA), microRNA, messenger RNA, self-amplifying RNA, and CRISPR RNA, have great potential for accessing undruggable targets and addressing complex medical needs [1,2]. RNAs are unstable and easily decomposed in the body and blood [3,4]; thus RNA-based medicines must be combined with drug carriers for delivery to target organs and cells [5,6]. Among the numerous nanoparticle technologies available, lipid nanoparticles (LNPs) are the most promising RNA carriers, demonstrating great efficacy and biocompatibility [7–11]. LNPs are composed of several functional lipids. For RNA delivery, LNPs are designed with cationic or ionizable lipids, helper lipids, cholesterol, and surface modifiers; the lipid composition has a considerable impact on the efficacy and stability of RNA-loaded LNPs [12–15].

Microfluidic devices are established tools for LNP production [16,17], including RNA medications [18,19]. This technology allows for greater control of LNP size and dispersion than conventional manufacturing processes. Although this technology is user friendly, it requires the solution to be changed and flow channel to be cleaned after each round of preparation. This can be particularly time-consuming and labor-intensive when producing LNPs under various preparation conditions.

Several studies have attempted to overcome the limitations of microfluidic technologies [20–23]. These studies employed robotic liquid handling systems to explore optimal lipid compositions but neglected to assess the potential of a continuous screening system based on a microfluidic platform. Valencia et al. [24] developed a microfluidic platform for polymeric nanoparticle synthesis; however, the flow rate was not sufficiently high (~60 μL/min) for rapid condition screening, and the microchannel structure of the particle-formation region was not suitable to feed sample solutions at high flow rates [24].

This study proposes a novel microfluidic platform for continuous screening of LNP formation that fully integrates lipid composition adjustment and LNP formation sections into a single device. I investigated the flow stability of the microfluidic platform to continuously adjust the lipid composition to the flow conditions and compared the physicochemical properties of generated LNPs, including their size and polydispersity index (PDI). Following proof-of-concept experiments, siRNA-loaded LNPs with different lipid compositions and surface modifier ratios were prepared, and their

physicochemical properties and gene-silencing activity were evaluated via in vitro experiments. I found that the proposed platform allows for the effective adjustment of lipid composition by controlling the flow conditions of the lipid solutions and does not require a large number of individual syringes with distinct lipid compositions for LNP optimization screening. Further, the platform allows for continuous flow of the lipid solution through the microchannel, circumventing the need for the microchannel to be cleaned and, therefore, the use of cleaning solutions.

2.2 Experimental

2.2.1 Materials

POPC, DSPC, DOTAP, and DMG-PEG2000 were purchased from the NOF America Corporation (White Plains, NY, USA). Cholesterol and ethanol (≥ 99.5% for HPLC) were purchased from Sigma-Aldrich (St. Louis, MO, USA). siGL4 was purchased from Hokkaido System Science (Sapporo, Japan). The sense and antisense strand sequences of siGL4 were 5′-CCGUCGUCUUCGUGAGCAATT-3′ and 5′-UUGCUCACGAAUACGGTT-3′, respectively. Monohydrate, phosphate-buffered saline (PBS) and acetic acid were purchased from FUJIFILM Wako Pure Chemical Corporation (Osaka, Japan). N-(2-hydroxyethyl)piperazine-N'-2-ethanesulfonic acid (HEPES) was purchased from Nacalai Tesque (Kyoto, Japan). Quant-iT RiboGreen RNA reagent was purchased from Thermo Fisher Scientific (Waltham, MA, USA). Sodium acetate was purchased from KANTO CHEMICAL (Tokyo, Japan).

2.2.2 Fabrication of microfluidic device with baffle structures

The microfluidic device was purchased from Shin-Etsu Chemical (Chiyoda City, Japan). The microfluidic device was fabricated by a typical wet etching method using 10% hydrofluoric acid, the glass substrate with the microchannel was covered with a planar glass substrate, and a pair of glass substrates was bonded using thermal fusion bonding. The microchannel structure and dimensions of the microchannel are summarized in Figure 2.1. The microfluidic device has three inlets and two mixing regions. The baffle structures were applied to the mixing regions of the channel.

2.2.3 Evaluation of flow rate stability

The stability of the flow rate was evaluated by the weight of the solution collected from the outlet of the microfluidic device (see Figure 2.1). I used milli Q water prepared by the Milli-Q Advantage system (Millipore, Milford, MA, USA) as the aqueous phase and ethanol as an organic phase. I introduced ethanol through separate inlets and changed the FRR from “50 to 50” to “10 to 90”. I applied a TFR of 500 and 600 μL/min, and the FRR of the aqueous phase and the two ethanol phases were set to 3. The recovery rate (%) was calculated as the weight of the solution collected from the outlet, per unit time, divided by the theoretical mass of the mixture of water and ethanol.

2.2.4 Preparation of POPC/cholesterol LNPs by off- and on-device mixing

To prepare the POPC/cholesterol LNPs by off-device mixing, a 14 mM POPC and 6 mM cholesterol mixture solution was dissolved in ethanol. The lipid/ethanol solution was introduced from two inlets, and PBS was introduced from one inlet into the microfluidic platform at a TFR of 500 μL/min by changing the FRR from 1 to 3. In comparison, when preparing the POPC/cholesterol LNPs by on-device mixing, a 28 mM POPC/ethanol and 12 mM cholesterol/ethanol solution were separately introduced into the microchannel. The investigated TFR and FRR were identical. After collecting the LNP solution from the outlet, it was dialyzed overnight with PBS using dialysis membrane tubing with a 12–14 kDa MWCO (Repligen Corporation, Waltham, MA, USA). The size of dialyzed LNPs was measured by dynamic light scattering (DLS) with a Zetasizer Ultra instrument (Malvern Instruments, Worcestershire, UK).

2.2.5 Preparation of DOTAP/DSPC/Cholesterol/DMG-PEG2000 LNPs

LNPs with different lipid compositions were prepared via on-device solution mixing. Two solutions composed of different lipids were prepared, one with 7.2 mM cholesterol, 0.8 mM DSPC, and 0.08 mM DMG-PEG2000, and the other with 7.2 mM DOTAP, 0.8 mM DSPC, and 0.08 mM DMG-PEG2000. The lipid solutions were introduced into the platform and mixed with 25 mM acetate buffer (pH 4.0) or 100 μg/mL siRNA in 25 mM acetate buffer (pH 4.0). The total flow rate (TFR) was 540 μL/min, and the flow rate ratio (FRR) of the aqueous and ethanol phases was 2. The composition of the LNPs was changed by adjusting the FRR of the two ethanol phases. After collecting the LNP solution from the outlet, it was dialyzed overnight with PBS. The size and zeta potential of the dialyzed LNPs were measured using DLS and ELS, respectively. The RiboGreen assay was used to measure

siRNA encapsulation efficiency [25].

2.2.6 Preparation of LNPs with different surface modification ratios of polymer

LNPs coated with different amounts of surface modifiers were prepared via on-device solution mixing. Two different lipid solutions were prepared, one with 2.4 mM DOTAP, 0.4 mM DSPC, 1.2 mM cholesterol, and 0.48 mM DMG-PEG2000, and the other with 2.4 mM DOTAP, 0.4 mM DSPC, and 1.2 mM cholesterol. These lipid solutions were introduced into the microfluidic platform and mixed with 50 μg/mL of siRNA in PBS. The investigated TFR was 600 μL/min, and the FRR of the aqueous and ethanol phases was 3. The composition of the LNPs was changed by adjusting the FRR of the two ethanol phases. When preparing 0% and 12% PEG modified LNPs, each valve which was placed between the pump and microfluidic platform was closed to prevent the reverse flow. After collecting the LNP solution from the outlet, it was dialyzed overnight with PBS. The size and zeta potential of the dialyzed LNPs were measured by DLS and ELS. The RiboGreen assay was used to measure siRNA encapsulation efficiency [25].

2.2.7 In vitro assay

HeLa cells stably expressing firefly and renilla luciferase (HeLa-dluc) were cultured as previously described [26]. Cells were seeded at a concentration of 6×10^3 cells per well in a 96 well-microplate for 24 h prior to LNP treatment for cell viability and gene expression assays. The cells were then treated with LNPs and incubated for 24 h. After incubation, cell viability was measured using a Cell Counting Kit-8 (Dojindo, Kumamoto, Japan) according to the manufacturer's protocol. For gene expression assays, firefly luciferase activity was measured using a One-Glo assay and a GloMax Explorer System (Promega, Madison, WI, USA) according to the manufacturer's protocol. The amount of protein in the cell lysate was measured using a BCA protein assay kit (Bio-Rad Laboratories, Hercules, CA, USA).

2.2.8 Statistical analysis

The results are expressed as mean ± standard deviation. For a one-to-one comparison, an

unpaired multiple t-test was performed. For multiple comparisons, I performed one-way ANOVA followed by Dunnett's multiple comparison test.

2.3 Results and discussion

2.3.1 On-device LNP-formulation screening using the proposed microfluidic platform

For on-device formulation screening, the microfluidic platform was equipped with three inlets and two mixing regions, which enabled the continuous adjustment of LNP composition. The LNP composition can be adjusted in the first mixing region by changing the FRR of the two ethanol phases. In the second mixing region, LNPs are formed by diluting the lipid-containing ethanol phase to an aqueous phase (Figure 2.1). The microfluidic platform consisted of ten sets of baffle structures as previously reported [27]. The baffle structure was 150 μm in width and 20 μm in length. The flow rate stability was investigated during continuous adjustment of the rates. The recovery rate of the solutions was ~100% with little variation, regardless of the TFR and FRR (Figure 2.2 (a) and (b)). These results indicate that the microfluidic platform allows for on-device lipid formulation screening by controlling flow conditions.

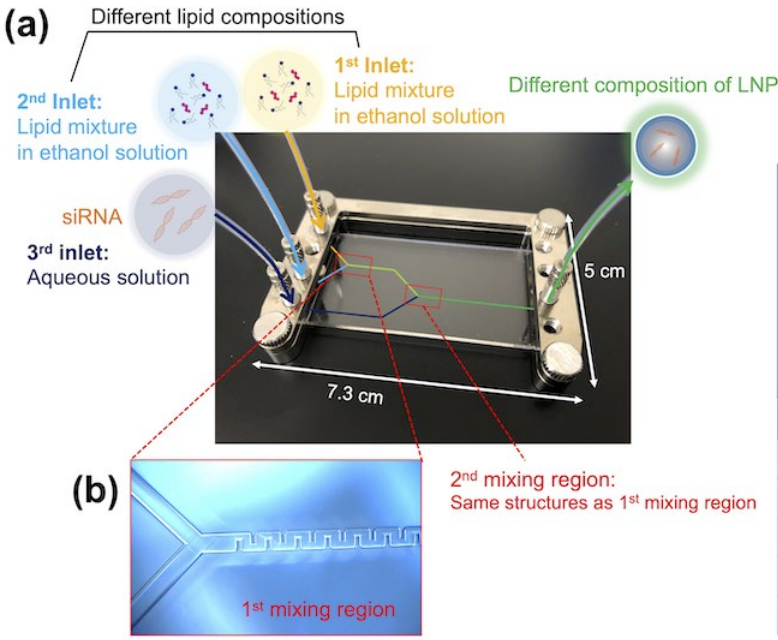

(c)

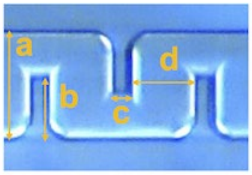

Position	Length (μm)
a	280
b	150
c	20
d	180
Depth	60

Figure 2.1 Microfluidic platform for on-device LNP formulation screening. (a) Overview of the platform showing three inlets and two baffle structure regions. From three of the two inlets (1st and 2nd inlet), a lipid-containing ethanol solution is introduced. By modulating the flow rate ratio (FRR) of these solutions and mixing them in the 1st mixing region, the mixture can be adjusted to meet the target composition. From the 3rd inlet, aqueous phases are introduced and mixed with the lipid mixture solution in the 2nd baffle region; LNPs, with user-determined compositions, are obtained from the outlet. (b) Photograph of mixing region with ten sets of baffle structures in the flow channel. (c) Photograph and dimensions of the flow channel and baffle structure.

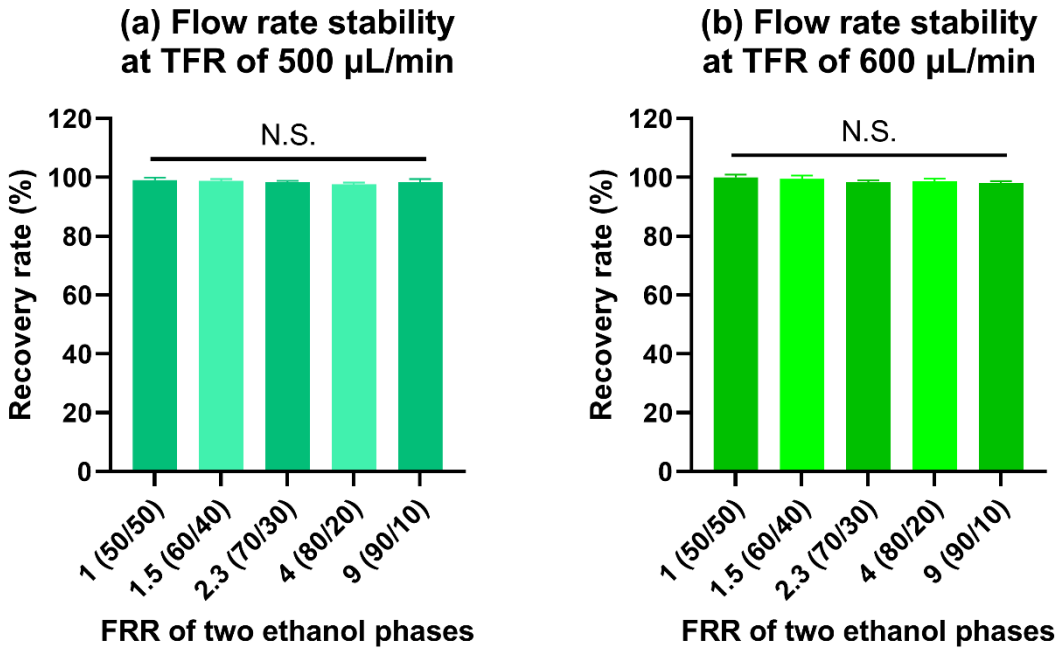

Figure 2.2 Recovery rates for flow rate ratios (FRRs) of two ethanol phases from 1–9 (flow percentages of 50/50 to 90/10). The total flow rate (TFR) was (a) 500 µL/min and (b) 600 µL/min. The FRR of the aqueous phase and the total for the two ethanol phases was 3. The error bars represent the standard deviation (SD) of at least three independent experiments. Not significant (N.S., $P > 0.05$) against the FRR (of two ethanol phases) of 1 was determined by one-way ANOVA followed by Dunnett's multiple comparison test.

2.3.2 Physicochemical properties of generated LNPs

The proposed platform can operate stably over a wide range of FRRs for the two ethanol phases (Figure 2.2). Next, I compared the size (hydrodynamic size, nm) and PDI of LNPs prepared using the microfluidic platform with those using ordinary off-device mixing of lipid components. For on-device mixing, 28 mM 1-palmitoyl-2-oleoyl-sn-glycero-3-phosphocholine (POPC)/ethanol and 12 mM cholesterol/ethanol solutions were separately introduced and mixed in the first mixing region. In off-device mixing, 14 mM POPC and 6 mM cholesterol were dissolved in ethanol and mixed in a tube. The FRR of the two inlets for the ethanol phase was fixed at 1, regardless of the on- and off-device mixing conditions.

LNP size exhibited a similar reduction trend for both on- and off-device mixing with little difference (Figure 2.3 (a)). The LNPs of on-device mixing had a PDI of ~0.2, which was almost comparable to that of off-device mixing (Figure 2.3 (b)). Therefore, my microfluidic platform can efficiently mix the lipid components in the microchannel and produce LNPs with physicochemical properties comparable to those of conventional off-device mixing processes.

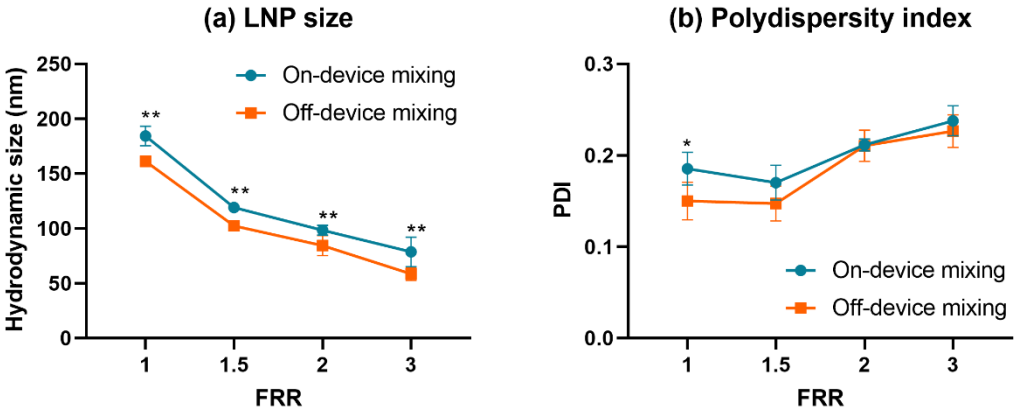

Figure 2.3 Physicochemical properties of POPC/cholesterol LNPs produced at various FRRs. (a) Hydrodynamic size and (b) polydispersity index (PDI) of LNPs produced by on-device and off-device mixing, respectively. In on-device mixing, one ethanol phase contained POPC and the other contained cholesterol. In off-device mixing, both ethanol phases were pre-mixed before being introduced through two inlets. The error bars represent the SD calculated from at least six independent experiments. Significant difference (*; $P < 0.05$, **; $P < 0.01$) against on-device mixing was calculated by unpaired multiple t-tests.

2.3.3 Application of on-device screening for LNP compositions

I investigated the feasibility of producing LNPs with different ratios of 1,2-dioleoyl-3-trimethylammonium-propane (DOTAP), a cationic lipid component. This has practical significance because cationic lipids are essential for the function of RNA-loaded LNPs. First, I prepared LNPs without siRNA (Figure 2.4 (a)–(c)). As the ratio of DOTAP in the LNP composition increased, LNP size decreased from 75 to 48 nm (Figure 2.4 (a)). PDI was almost constant (≤ 0.2) except for LNPs

with the highest ratio of DOTAP. My results are comparable with previous findings that 1,2-distearoyl-sn-glycero-3-phosphocholine (DSPC) and cholesterol promote the stability of LNPs and contribute to their structural integrity [28]. The zeta potential gradually increased as the ratio of DOTAP in LNP increased. This result was a reasonable consequence of incorporating an amount of DOTAP with cationic potential.

Next, I screened the lipid composition in the preparation of siRNA-loaded LNPs (Figure 2.4 (d)–(g)). LNP size was nearly constant (73–96 nm), independent of changes in lipid composition, which I assumed to be the effect of siRNA interacting electrostatically with DOTAP. This electrostatic interaction was reflected in the lower PDI values for LNPs with siRNA (Figure 2.4 (e)). In both LNPs with and without siRNA, the zeta potential increased with the increasing DOTAP ratio (Figure 2.4 (c) and (f)), but the zeta potential was higher in LNPs without siRNA. Mechanistically, the positive charge of DOTAP forms a complex with the negative charge of siRNA, and the complexes between DOTAP and siRNA are encapsulated into the LNP. Therefore, siRNA-loaded LNPs showed a lower zeta potential than LNPs without siRNA. The siRNA encapsulation efficiency was ~100% for all compositions, but significant differences were observed compared to the LNPs composed of DOTAP/ DSPC/ cholesterol = 2/1/7 (Figure 2.4 (g)). These results suggest that the microfluidic platform allows on-device lipid composition screening when incorporating commercial cationic lipids and siRNA.

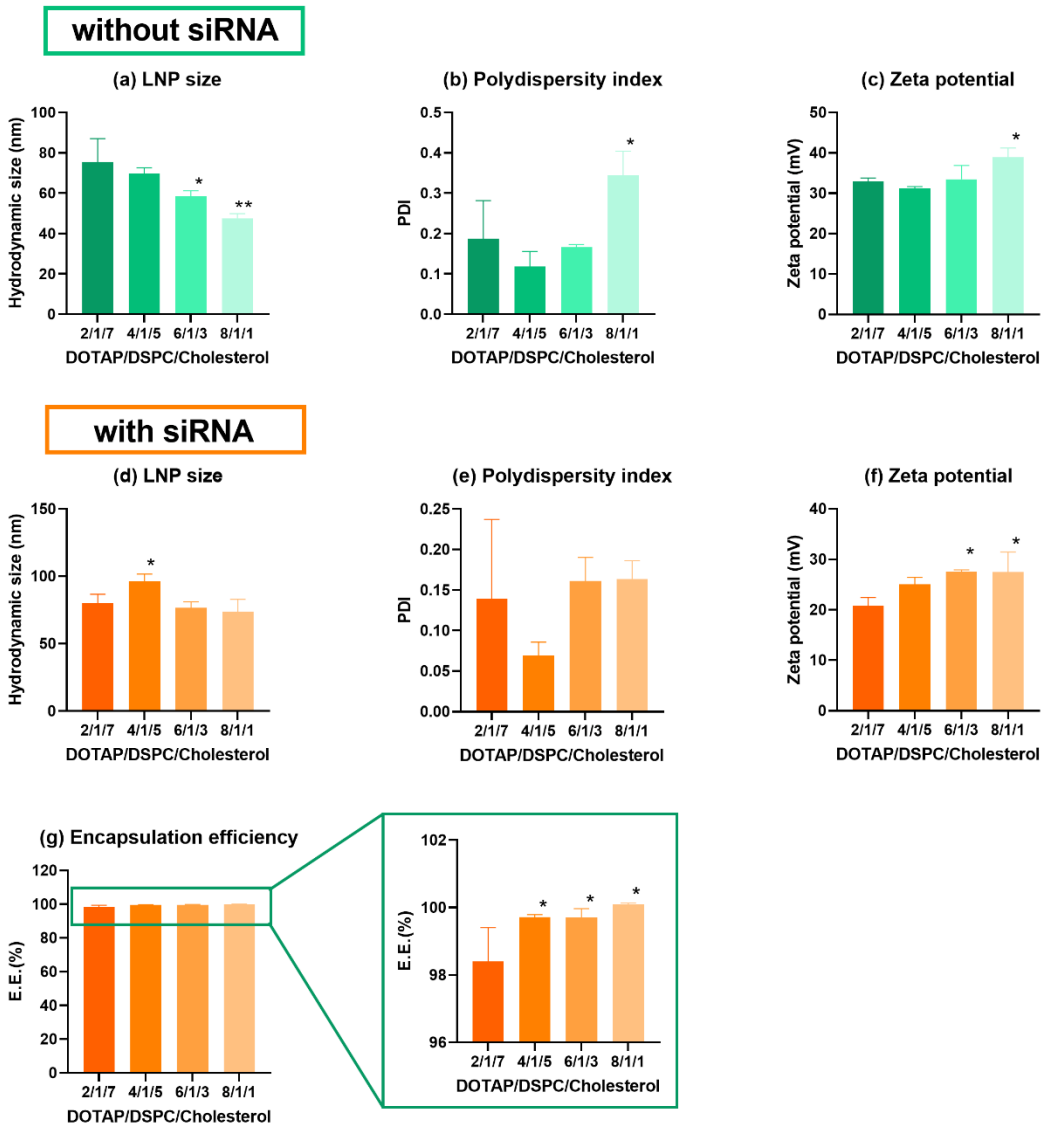

Figure 2.4 Preparation of DOTAP/DSPC/Cholesterol/DMG-PEG2000 LNPs at varying FRRs. (a–c) LNPs without siRNA; (d–g) LNPs with siRNA. The x-axis shows the lipid composition of LNPs, except for DMG-PEG2000, in the molar ratio as indicated in the x-axis title. All LNPs included 1% of DMG-PEG2000 in the molar ratio. The error bars represent the SD from at least three independent experiments. Significant difference (*; $P < 0.05$, **; $P < 0.01$) against the DOTAP/DSPC/Cholesterol/DMG-PEG2000 (2/1/7/0.1 in molar ratio) LNP was calculated by one-way ANOVA followed by Dunnett's multiple comparison test.

2.3.4 On-device screening for optimized surface modification of LNPs

I then applied the microfluidic device to screen for LNP surface modifications. It is widely accepted that the efficiency of gene silencing and delivery to target organs/tissues of siRNA is influenced by not only the size and composition of the LNPs, but also the amount of surface modifiers on the LNPs [12,23,25,29–31]. To validate the broader application of this device, I selected 1,2-dimyristoyl-rac-glycero-3-methoxypolyethylene glycol-2000 (DMG-PEG2000) as a model surface modifier and prepared LNPs with different surface modification ratios.

LNP size decreased with increasing amounts of DMG-PEG2000 (Figure 2.5 (a)). DMG-PEG2000 can generate a hydrate layer at the interface between the LNP and its intermediates in the outer aqueous phase, resulting in a decrease in the size of the LNPs [30,32]. PDI values were consistently below 0.2 from 0% to 7% DMG-PEG2000 (Figure 2.5 (b)). In contrast, LNPs modified with 9% and 12% DMG-PEG2000 showed slightly higher values. As the amount of DMG-PEG2000 increased, the LNPs exhibited a multimodal particle-size distribution (Figure 2.5 (c)). This may be due to the excess amount of DMG-PEG2000, which behaves like a surfactant, generating micelle-like particles and inducing LNP instability [33,34]. The zeta potential of the LNPs showed a decreasing trend, comparable to that of LNP size (Figure 2.5 (d)). LNPs without DMG-PEG2000 showed the highest zeta potential (~44 mV), which I attributed to the activity of DOTAP (as described in subsection 2.3.3). As the amount of DMG-PEG2000 increased, the thickness of the hydrate layer on the surface of the LNPs also increased until the cationic potential of the internal parent LNPs could no longer be detected using electrophoretic light scattering (ELS). The encapsulation efficiency was almost constant, and all LNPs encapsulated ~100% of siRNA (Figure 2.5 (e)).

After four weeks of storage at 4 °C, LNPs without DMG-PEG2000 tended to be larger than LNPs with the surface modifier (Figure 2.6). This can be explained by the absence of DMG-PEG2000 inducing interactions and agglomeration between LNPs. On the contrary, even if the DMG-PEG2000 amount was minimal (e.g., 1%), the steric stability of LNPs would be maintained for at least four weeks at 4 °C.

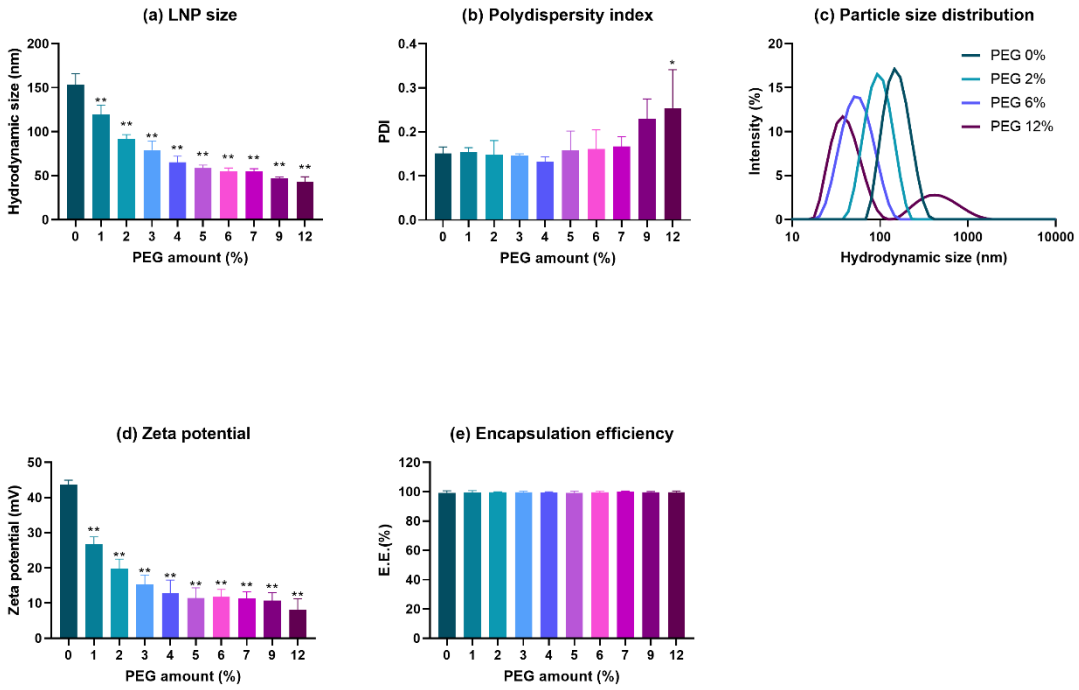

Figure 2.5 Properties of siRNA-loaded DOTAP/DSPC/Cholesterol/DMG-PEG2000 LNPs prepared at varying FRRs of two organic solvent phases. (a) LNP size, (b) PDI, (c) particle size distribution, (d) zeta potential, and (e) encapsulation efficiency of siRNA in LNPs. The error bars represent the SD calculated from at least three independent experiments. Significant difference (*; $P < 0.05$, **; $P < 0.01$) against the unmodified (0% DMG-PEG2000 modified) LNP was calculated by one-way ANOVA followed by Dunnett's multiple comparison test.

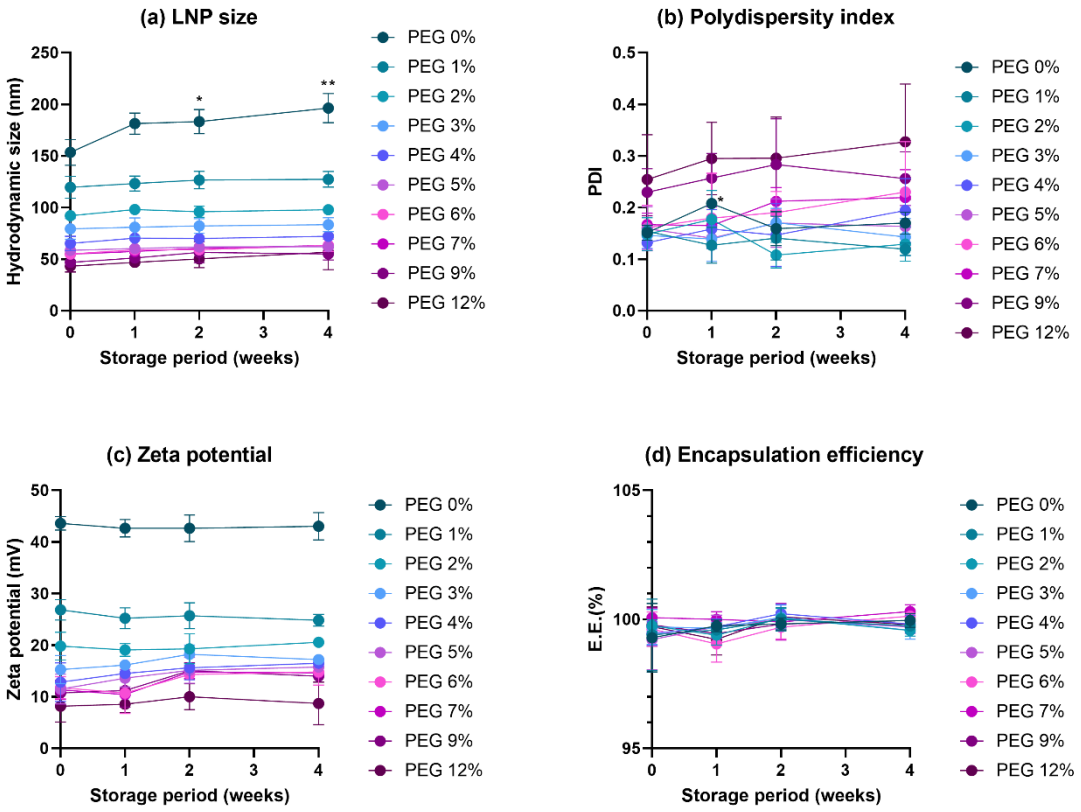

Figure 2.6 Stability of siRNA-loaded DOTAP/DSPC/Cholesterol/DMG-PEG2000 LNPs after 4 weeks at 4 °C. (a) LNP size, (b) PDI, (c) zeta potential, and (d) encapsulation efficiency of siRNA in LNPs. The error bars represent the SD calculated from at least three independent experiments. Significant difference (*; $P < 0.05$, **; $P < 0.01$) against each initial value was calculated by one-way ANOVA followed by Dunnett's multiple comparison test.

From a physicochemical perspective, I concluded that LNPs were successfully prepared using the microfluidic platform. I performed in vitro gene knockdown and cytotoxicity assays using representative LNPs to evaluate the effect of DMG-PEG2000 on the efficacy and safety of siRNA-loaded LNPs.

LNPs modified with 3% DMG-PEG2000 showed the highest luciferase knockdown activity among the six types of LNPs at siGL4 RNA doses of 100 and 60 nM (Figure 2.7 (a)). Although DMG-PEG2000 below a certain amount played a fundamental role in enhancing the dispersity of LNPs, excessive amounts of DMG-PEG2000 prevented the interaction of LNPs with HeLa cells even within that DMG-PEG2000 concentration range [35].

On the contrary, at 30 nM siGL4 RNA, I observed higher knockdown efficiency at PEG amounts of 12%. LNP size, rather than the DMG-PEG2000 modification amount, might have contributed to knockdown efficiency; it has also been reported that smaller particles exhibit higher intracellular uptake [36].

Regarding the cytotoxicity of siRNA-loaded LNPs at different DMG-PEG2000 compositions, I found that cell viability tended to be lower in LNPs modified with 9% and 12% DMG-PEG2000 than in the controls (Figure 2.7 (b)). Excessive amounts of DMG-PEG2000 are known to be cytotoxic [37]. In this case, I assumed that the cytotoxicity might be attributed to excess amounts of DMG-PEG2000 acting as a surfactant.

Based on these results, my microfluidic platform allowed me to easily evaluate slight physicochemical differences among more than ten different LNP compositions. Given this efficiency, my proposed method can save time, expenses, and resources (especially expensive ingredients including RNAs and other bioactive ingredients (functional lipids and surface modifiers)), making it cleaner/“greener” than the conventional technology.

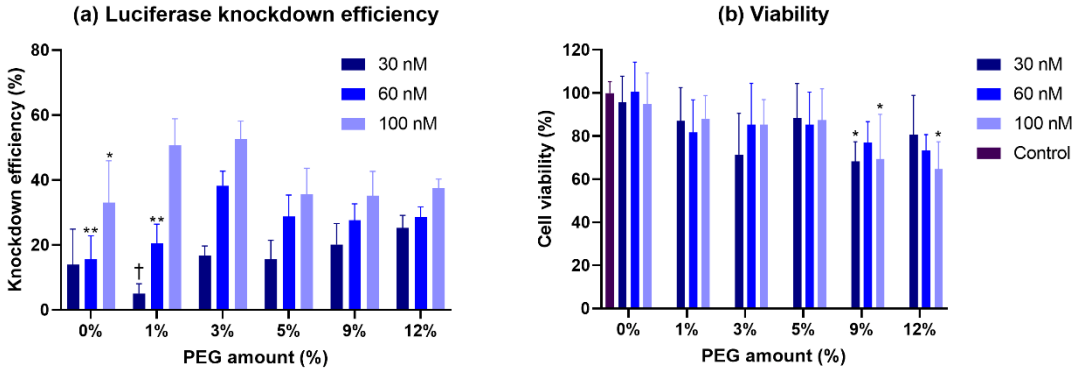

Figure 2.7 In vitro efficacy and cytotoxicity assays of siGL4 RNA-loaded DOTAP/DSPC/Cholesterol/DMG-PEG2000 LNPs. (a) Luciferase knockdown efficiency (%). The error bars represent the SD calculated from at least three independent experiments. Significant difference against 3% DMG-PEG2000 modified LNP (*; $P < 0.05$, **; $P < 0.01$) and 12% DMG-PEG2000 modified LNP (†; $P < 0.05$) was calculated by one-way ANOVA followed by Dunnett's multiple comparison test. (b) Cell viability (%). The error bars represent the SD calculated from at least three independent experiments. Significant difference against control (*; $P < 0.05$) was calculated by one-way ANOVA followed by Dunnett's multiple comparison test.

2.4 Conclusion

I developed a novel microfluidic platform for the continuous formulation of LNPs with varying lipid compositions. My microfluidic platform was capable of independent and stable flow of the three solutions. Lipid formulation screening and optimization of surface modifiers can easily be manipulated. This platform enables a more convenient and seamless design of LNPs, reduces the time and costs associated with screening, and minimizes the amount of active pharmaceutical ingredients and lipids disposed as waste. I propose that my microfluidic platform represents an optimized and more efficient alternative to the conventional technology, and that it could accelerate the development and application, both experimental and clinical, of LNP formulations.

2.5 References

[1] J.M. Sasso, B.J.B. Ambrose, R. Tenchov, R.S. Datta, M.T. Basel, R.K. DeLong, Q.A. Zhou, The Progress and Promise of RNA Medicine An Arsenal of Targeted Treatments, J Med Chem. 65 (2022) 6975–7015.

[2] Y.-K. Kim, RNA therapy: rich history, various applications and unlimited future prospects, Exp Mol Medicine. 54 (2022) 455–465.

[3] L.-H. Huang, P.-H. Lin, K.-W. Tsai, L.-J. Wang, Y.-H. Huang, H.-C. Kuo, S.-C. Li, The effects of storage temperature and duration of blood samples on DNA and RNA qualities, Plos One. 12 (2017) e0184692.

[4] C. Wang, H. Liu, Factors influencing degradation kinetics of mRNAs and half-lives of microRNAs, circRNAs, lncRNAs in blood in vitro using quantitative PCR, Sci Rep-Uk. 12 (2022) 7259.

[5] S.A. Lim, A. Cox, M. Tung, E.J. Chung, Clinical progress of nanomedicine-based RNA therapies, Bioact Mater. 12 (2021) 203–213.

[6] P.R. Cullis, M.J. Hope, Lipid Nanoparticle Systems for Enabling Gene Therapies, Mol Ther. 25 (2017) 1467–1475.

[7] L.M. Ickenstein, P. Garidel, Lipid-based nanoparticle formulations for small molecules and RNA drugs, Expert Opin Drug Del. 16 (2019) 1205–1226.

[8] X. Zhang, V. Goel, G.J. Robbie, Pharmacokinetics of Patisiran, the First Approved RNA Interference Therapy in Patients With Hereditary Transthyretin-Mediated Amyloidosis, J Clin Pharmacol. 60 (2019) 573–585.

[9] X. Zhang, V. Goel, H. Attarwala, M.T. Sweetser, V.A. Clausen, G.J. Robbie, Patisiran Pharmacokinetics, Pharmacodynamics, and Exposure-Response Analyses in the Phase 3 APOLLO Trial in Patients With Hereditary Transthyretin-Mediated (hATTR) Amyloidosis, J Clin Pharmacol. 60 (2020) 37–49.

[10] Y.N. Lamb, BNT162b2 mRNA COVID-19 Vaccine: First Approval, Drugs. 81 (2021) 495–501.

[11] L. Schoenmaker, D. Witzigmann, J.A. Kulkarni, R. Verbeke, G. Kersten, W. Jiskoot, D. Crommelin, mRNA-lipid nanoparticle COVID-19 vaccines: structure and stability, Int J Pharmaceut. 601 (2021) 120586.

[12] A. Hashiba, M. Toyooka, Y. Sato, M. Maeki, M. Tokeshi, H. Harashima, The use of design of experiments with multiple responses to determine optimal formulations for in vivo hepatic mRNA delivery, J Control Release. 327 (2020) 467–476.

[13] J.A. Kulkarni, J.L. Myhre, S. Chen, Y.Y.C. Tam, A. Danescu, J.M. Richman, P.R. Cullis, Design of lipid nanoparticles for in vitro and in vivo delivery of plasmid DNA, Nanomed Nanotechnol Biology Medicine. 13 (2017) 1377–1387.

[14] J.A. Kulkarni, D. Witzigmann, J. Leung, Y.Y.C. Tam, P.R. Cullis, On the role of helper lipids in lipid nanoparticle formulations of siRNA, Nanoscale. 11 (2019) 21733–21739.

[15] B.-K. Kim, G.-B. Hwang, Y.-B. Seu, J.-S. Choi, K.S. Jin, K.-O. Doh, DOTAP/DOPE ratio and cell type determine transfection efficiency with DOTAP-liposomes, Biochimica Et Biophysica Acta Bba - Biomembr. 1848 (2015) 1996–2001.

[16] Y. Matsuura-Sawada, M. Maeki, T. Nishioka, A. Niwa, J. Yamauchi, M. Mizoguchi, K. Wada, M. Tokeshi, Microfluidic Device-Enabled Mass Production of Lipid-Based Nanoparticles for Applications in Nanomedicine and Cosmetics, Acs Appl Nano Mater. 5 (2022) 7867–7876.

[17] M. Maeki, S. Uno, A. Niwa, Y. Okada, M. Tokeshi, Microfluidic technologies and devices for lipid nanoparticle-based RNA delivery, J Control Release. 344 (2022) 80–96.

[18] X. Hou, T. Zaks, R. Langer, Y. Dong, Lipid nanoparticles for mRNA delivery, Nat Rev Mater. (2021) 1–17.

[19] M. Maeki, Y. Okada, S. Uno, A. Niwa, A. Ishida, H. Tani, M. Tokeshi, Production of siRNA-Loaded Lipid Nanoparticles using a Microfluidic Device, J Vis Exp. No. 181 (2022) e62999.

[20] L. Cui, S. Pereira, S. Sonzini, S. van Pelt, S.M. Romanelli, L. Liang, D. Ulkoski, V.R. Krishnamurthy, E. Brannigan, C. Brankin, A.S. Desai, Development of a high-throughput platform for screening lipid nanoparticles for mRNA delivery, Nanoscale. 14 (2022) 1480–1491.

[21] Y. Fan, C.-W. Yen, H.-C. Lin, W. Hou, A. Estevez, A. Sarode, A. Goyon, J. Bian, J. Lin, S.G. Koenig, D. Leung, K. Nagapudi, K. Zhang, Automated high-throughput preparation and characterization of oligonucleotide-loaded lipid nanoparticles, Int J Pharmaceut. 599 (2021) 120392.

[22] L. Cui, M.R. Hunter, S. Sonzini, S. Pereira, S.M. Romanelli, K. Liu, W. Li, L. Liang, B. Yang, N. Mahmoudi, A.S. Desai, Mechanistic Studies of an Automated Lipid Nanoparticle Reveal Critical Pharmaceutical Properties Associated with Enhanced mRNA Functional Delivery In Vitro and In Vivo, Small. 18 (2022) 2105832.

[23] A. Sarode, Y. Fan, A.E. Byrnes, M. Hammel, G.L. Hura, Y. Fu, P. Kou, C. Hu, F.I. Hinz, J. Roberts, S.G. Koenig, K. Nagapudi, C.C. Hoogenraad, T. Chen, D. Leung, C.-W. Yen, Predictive high-throughput screening of PEGylated lipids in oligonucleotide-loaded lipid nanoparticles for neuronal gene silencing, Nanoscale Adv. 4 (2022) 2107–2123.

[24] P.M. Valencia, E.M. Pridgen, M. Rhee, R. Langer, O.C. Farokhzad, R. Karnik, Microfluidic Platform for Combinatorial Synthesis and Optimization of Targeted Nanoparticles for Cancer Therapy, Acs Nano. 7 (2013) 10671–10680.

[25] Y. Sato, Y. Note, M. Maeki, N. Kaji, Y. Baba, M. Tokeshi, H. Harashima, Elucidation of the physicochemical properties and potency of siRNA-loaded small-sized lipid nanoparticles for siRNA delivery, J Control Release. 229 (2016) 48–57.

[26] N. Kimura, M. Maeki, K. Sasaki, Y. Sato, A. Ishida, H. Tani, H. Harashima, M. Tokeshi, Three-dimensional, symmetrically assembled microfluidic device for lipid nanoparticle production, Rsc Adv. 11 (2021) 1430–1439.

[27] N. Kimura, M. Maeki, Y. Sato, Y. Note, A. Ishida, H. Tani, H. Harashima, M. Tokeshi, Development of the iLiNP Device: Fine Tuning the Lipid Nanoparticle Size within 10 nm for Drug Delivery, Acs Omega. 3 (2018) 5044–5051.

[28] C.B. Roces, G. Lou, N. Jain, S. Abraham, A. Thomas, G.W. Halbert, Y. Perrie, Manufacturing Considerations for the Development of Lipid Nanoparticles Using Microfluidics, Pharm. 12 (2020) 1095.

[29] S. Chen, Y.Y.C. Tam, P.J.C. Lin, M.M.H. Sung, Y.K. Tam, P.R. Cullis, Influence of particle size on the in vivo potency of lipid nanoparticle formulations of siRNA, J Control Release. 235 (2016) 236–244.

[30] S. Chen, Y.Y.C. Tam, P.J.C. Lin, A.K.K. Leung, Y.K. Tam, P.R. Cullis, Development of lipid nanoparticle formulations of siRNA for hepatocyte gene silencing following subcutaneous administration, J Control Release. 196 (2014) 106–112.

[31] I.A. Khalil, H. Harashima, An efficient PEGylated gene delivery system with improved targeting: Synergism between octaarginine and a fusogenic peptide, Int J Pharmaceut. 538 (2018) 179–187.

[32] E. Lallana, R. Donno, D. Magrì, K. Barker, Z. Nazir, K. Treacher, M.J. Lawrence, M. Ashford, N. Tirelli, Microfluidic-assisted nanoprecipitation of (PEGylated) poly (d,l-lactic acid-co-caprolactone): Effect of macromolecular and microfluidic parameters on particle size and paclitaxel encapsulation, Int J Pharmaceut. 548 (2018) 530–539.

[33] K. Edwards, M. Johnsson, G. Karlsson, M. Silvander, Effect of polyethyleneglycol-phospholipids on aggregate structure in preparations of small unilamellar liposomes, Biophys J. 73 (1997) 258–266.

[34] A.S. Nosova, O.O. Koloskova, A.A. Nikonova, V.A. Simonova, V.V. Smirnov, D. Kudlay, M.R. Khaitov, Diversity of PEGylation methods of liposomes and their influence on RNA delivery, Medchemcomm. 10 (2019) 369–377.

[35] S. Sieber, P. Grossen, P. Uhl, P. Detampel, W. Mier, D. Witzigmann, J. Huwyler, Zebrafish as a predictive screening model to assess macrophage clearance of liposomes in vivo, Nanomed Nanotechnol Biology Medicine. 17 (2019) 82–93.

[36] A.U. Andar, R.R. Hood, W.N. Vreeland, D.L. DeVoe, P.W. Swaan, Microfluidic Preparation of Liposomes to Determine Particle Size Influence on Cellular Uptake Mechanisms, Pharmaceut Res. 31 (2014) 401–413.

[37] Y. Hattori, K. Tamaki, S. Sakasai, K.-I. Ozaki, H. Onishi, Effects of PEG anchors in PEGylated siRNA lipoplexes on in vitro gene-silencing effects and siRNA biodistribution in mice, Mol Med Rep. 22 (2020) 4183–4196.

CHAPTER 3

Microfluidic Device-Enabled Mass Production of Lipid-Based Nanoparticles for Applications in Nanomedicine and Cosmetics

3.1. Introduction

Liposomes and lipid-based nanoparticles (Lb-NPs) are nanosized vesicles that mainly consist of one or several kinds of amphiphilic phospholipids, and usually include cholesterol. The application of Lb-NPs has been expanded from medical use to broader areas such as cosmetics and nutrition [1]. In particular, various liposomal cosmetics for skincare and anti-aging are on the market. In pharmaceutical fields, Lb-NPs are among the most reliable and successful drug delivery carriers that can encapsulate hydrophilic or hydrophobic drugs and ribonucleic acids. The use of more than 10 approved clinical products, including AmBisome [2,3], Doxil [3,4], Onpattro [3,5,6], Comirnaty [7,8], and Spikevax [8], has proven the safety and efficacy of delivering Lb-NPs. Although the potential of Lb-NPs has been widely confirmed, the number of approved clinical products has barely increased [3,9].

The major obstacles in the clinical and commercial application of Lb-NP technologies might be the difficulties associated with the mass production and scaling up as well as with the stability of Lb-NPs during manufacturing and storage. In the traditional batch process, the lipid thin-film hydration method is commonly used to produce Lb-NPs. Using this method, large and polydisperse particles are generated, and a subsequent size reduction process, such as extrusion, sonication, or homogenization, is essential to control the size of Lb-NPs for pharmaceutical applications. These size-tuning processes sometimes result in the breaking of the encapsulated molecules because of physical load [9]. Moreover, the execution of several processes in the production of Lb-NPs could be time-consuming, complicated, and difficult to control [10]. It is, therefore, difficult to precisely control the particle size [11].

Recently, microfluidics has received considerable attention as a novel process for manufacturing Lb-NPs and is expected to simplify production and reduce the barriers to scaling up [11,12]. Microfluidics can be used in the generation of Lb-NPs by introducing only the aqueous phase and lipids into the organic solvent phase. The process parameters affecting the control of Lb-NP size have been explored considerably [13–15]. The dilution rate of the organic solvent and lipid concentration in the organic solvent phase substantially affect the size of Lb-NPs. The dilution rate of the organic solvent is changed by the dimension and structure of the microfluidic channel, the total flow rate (TFR), the velocity of the aqueous and organic solvent phases, and the flow rate ratio (FRR) of the aqueous phase to the organic solvent phase. In general, smaller Lb-NPs are produced by rapid mixing of the lipid and aqueous solutions using microchannel or micromixer structures [15–17].

A microfluidic device equipped with baffle structures was recently developed in my laboratory to produce LNPs with precise size control [13,18]. The developed microfluidic device named iLiNP® showed better size controllability of Lb-NPs over a wide range compared with other devices. Previously, Kimura et al. characterized iLiNP® by changing the TFR and FRR using 10 mg/mL 1-palmitoyl-2-oleoyl-sn-glycero-3-phosphocholine (POPC) and approximately 50 mg/mL POPC as the highest concentration under a specific process condition [13,19].

The benefit of using a highly concentrated lipid solution is that concentrated Lb-NPs can be obtained in a short run time. A high concentration of colloidal nanoparticles is critical to the delivery efficiency and release of the loaded drug. In addition, a highly concentrated Lb-NP suspension allows the solution to be diluted as needed to obtain the desired sample concentration. The preparation of highly concentrated Lb-NPs is one of the major advantages for the mass production of Lb-NPs, which is easier than concentration by ultracentrifugation or tangential flow filtration. In addition, it can prevent changes in the particle properties of the Lb-NPs during concentration. However, the ability to control the Lb-NP size using microfluidic devices, including iLiNP®, at high lipid concentrations, has not been thoroughly investigated. Several investigations on the feasibility of applying a higher lipid concentration with microfluidic devices have been reported; however, larger or polydisperse Lb-NPs were prepared in such studies (Table 3.1 and 3.2).

This study was aimed at elucidating the controllability of Lb-NP size under conditions of low to high lipid concentration using iLiNP® and comparing it with those of three commercially available microchannel devices. The size and concentration (particles/mL) of Lb-NPs in the solution were evaluated to estimate the formation of Lb-NPs at a high lipid concentration.

Table 3.1 Previous reports on investigations to assess the application of extremely high lipid concentrations (> 50 mg/mL)

No.	Formulation	Lipid conc.	Device design	FRR	TFR or Flow velocity	Particle size	Dispersity	Ref.
1	HSPC/mPEG-DSPE/Chol. = 56.2/38.5/5.3	90 mg/mL	Flow-focusing microfluidics device (45° geometry-based microreactor)	5	110 µL/min	190 ± 255 nm (Two peaks: 153±57; 675±389)	Bimodal distribution	[20]
2		90 mg/mL		10	105 µL/min	347 ± 283 nm	Monodispersity	
3	SPC	100 mM	Millireactor 60 mm Straight channel	5	1 mL/min	171.9 ± 2.7 nm	PDI: 0.285	[21]
4		200 mM		5	1 mL/min	245.6 ± 4.0 nm	PDI: 0.469	
5	Soybean lecithin	100 mM	Flow-focusing microfluidics device	10	0.125 m/s	Ca. 180 nm	PDI: ca. 0.2	[22]
6	DMPC/DCP/Chol. = 5/1/4	80 mM	a microfluidic vertical flow focusing (VFF) device	30–50	4.5 mL/min	Ca.300 nm (> 250 nm)	PDI: > ca.0.25	[23]
7	EPC/DOPE/DOTAP =50/25/25	75 mM	Single hydrodynamic focusing device	16	95 mm/s	173.1	PDI: 0.23	[24]
8				16	143 mm/s	241.0	PDI: 0.29	
9		92 mM		13	120 mm/s	202.4	PDI: 0.25	
10		75 mM	Double hydrodynamic focusing device	16	95 mm/s	659.2	PDI: 0.64	
11				16	143 mm/s	266.4	PDI: 0.29	
12		92 mM		13	120 mm/s	202.4	PDI: 0.25	

Table 3.2 Previous reports on investigations to assess the application of slightly high lipid concentrations (< 50 mg/mL)

No.	Formulation	Lipid conc.	Device design	FRR	TFR	Particle size	Dispersity	Ref.
1	EPC/Chol. = 60/40	40 mM	Double flow-focusing microfluidics device	10	1.1 mL/min	108.2 ± 2.4 nm	Monodispersity	[25]
2	EPC/POPC/Chol. = 30/30/40	40 mM		10	1.1 mL/min	180.3 ± 2.5 nm	Monodispersity	
3	POPC/Chol. = 60/40	40 mM		10	1.1 mL/min	139.0 ± 2.7 nm	Monodispersity	
4	HSPC/Chol./DSPE-PEG2000 = 3/1/1	40 mg/mL	Staggered herringbone micromixer (SHM)	1.5	12 mL/min	Ca. 100 nm	PDI: <0.2	[26]
5	DSPC/Chol./DSPE-PEG2000 = 3/1/1	40 mg/mL		1.5	12 mL/min	Ca. 100 nm	PDI: <0.2	
6	POPC	20 mM	Flow-focusing microfluidics device	10	66 µL/min	Ca. 170 nm	N.A.	[27]
7	DMPC/Chol./DHP = 5/4/1	40 mM	Periodic disturbance mixer (PDM)	8.6	0.3 mL/min	Ca. 160 nm	PDI: <0.2	[28]
8	SPC	40 mM	Millireactor 60 mm Straight channel	5	1 mL/min	150.5 ± 5.4 nm	PDI: 0.240	[21]

3.2. Experimental

3.2.1. Materials

POPC was purchased from the NOF AMERICA Corporation (White Plains, NY, USA). Cholesterol and ethanol (≥ 99.5%, for HPLC) were purchased from Sigma-Aldrich (St. Louis, MO, USA). Dulbecco's phosphate-buffered saline (D-PBS) was purchased from FUJIFILM Wako Pure Chemical Corporation (Osaka, Japan).

3.2.2. Fabrication of microfluidic devices with baffle structures

iLiNP® was fabricated using standard photolithography [29]. The detailed protocol has been described previously [13,19,30]. In brief, the master molds were made from SU-8 3050 (Nippon Kayaku Co., Ltd., Tokyo, Japan) for applying the 100 μm thick layer onto silicon wafers and then were exposed to UV light with a mask aligner. Finally, replicated poly (dimethylsiloxane) (PDMS) pieces were bonded with PDMS replicas by the oxygen plasma treatment (CUTE-1MP/R, Femto Science, Gwangju, Korea). iLiNP® with three inlets was fabricated in the same manner.

3.2.3. Description and dimensions of the microfluidic devices

Figure 3.1 shows the structures of devices investigated in this study. The basic iLiNP® structure (Figure 3.1 (a)) was defined based on previous results [13]. The width and height of the microchannels were 200 and 100 μm, respectively. The width, length, and interval of each baffle were 150, 100, and 100 μm, respectively. Twenty baffles were placed in the microchannel immediately after the confluence point. The other three devices, suitable for nanoparticle preparation, were purchased from the Blacktrace Company. Two devices (Figure 3.1 (b) and (c)) had a straight channel without mixer structures; the differences between the two devices were in the length and arrangement of channels in the device. The straight device with a short channel (Figure 3.1 (b)) had three inlets (two of the five inlets located on both the outer sides were not used for preparation), and the width and height of the microchannel after the confluence point were 160 and 150 μm, respectively. The straight device with a long channel (Figure 3.1 (c)) also had three inlets, and the width and height of the microchannels were the same as those in the straight device with a short channel. The micromixer device (Figure 3.1 (d)) had three inlets and mixer structures divided into two parts [31]. The upper side of the mixer

structure had four channels (125 µm width and 50 µm height), and the lower side had one channel (350 µm width and 125 µm height). Twelve sets of branched mixer structures were located at points throughout the channel.

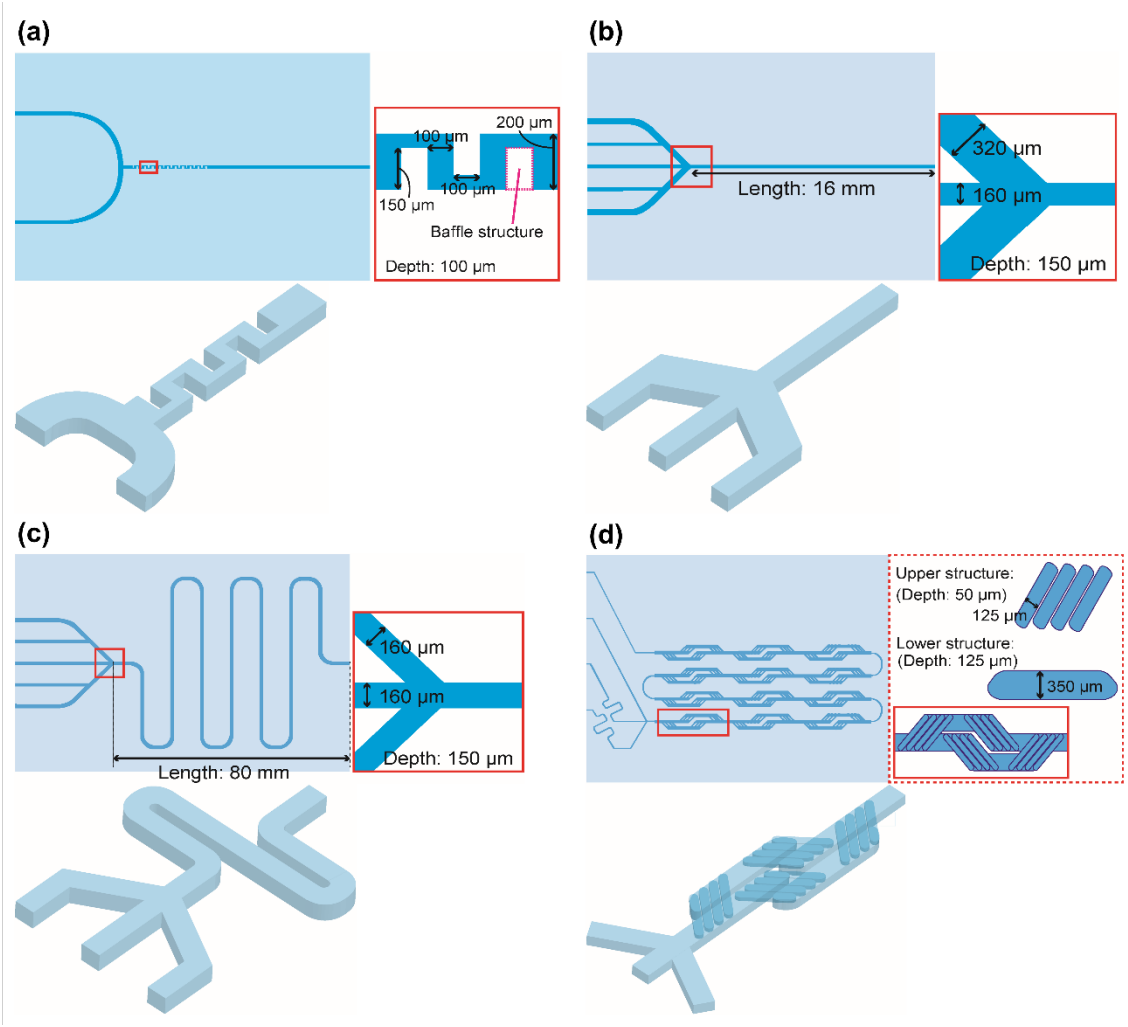

Figure 3.1 Structure of each device: (a) iLiNP® (2-inlets); the straight device with short (b) and long (c) channel; (d) the micromixer device

3.2.4. Preparation of POPC/cholesterol Lb-NPs

POPC/cholesterol (7/3 molar ratio) LNPs were prepared by mixing an aqueous phase and an organic phase in each microfluidic device. The entire system and equipment used is shown in Figure 3.2. An ethanol solution containing a certain amount of POPC and cholesterol was used as the organic

phase, and MilliQ water was used as the aqueous phase. These two solutions were placed in a liquid feeding pump (Mitos P-Pumps, Blacktrace Company, Royston, UK) and fed into each microfluidic device. The lipid solution was prepared with four POPC concentrations, viz., 10, 25, 50, and 100 mg/mL. The TFRs were 100, 500, and 1000 µL/min, and the FRR was fixed at 3. The collected LNP suspensions were dialyzed with 10,000 MWCO dialysis membrane tubing (RC membrane spectra/pro 6, Repligen Corporation, Waltham, MA, USA) overnight against D-PBS solution. The size of the LNPs was measured by dynamic light scattering (DLS) using a Zetasizer Ultra instrument (Malvern Instruments, Worcestershire, UK). The concentration (particles/mL) of the LNPs in the solution was evaluated using multi-angle dynamic light scattering (MADLS) with a Zetasizer Ultra instrument and nano tracking analysis (NTA) with Nanosight (Malvern Instruments).

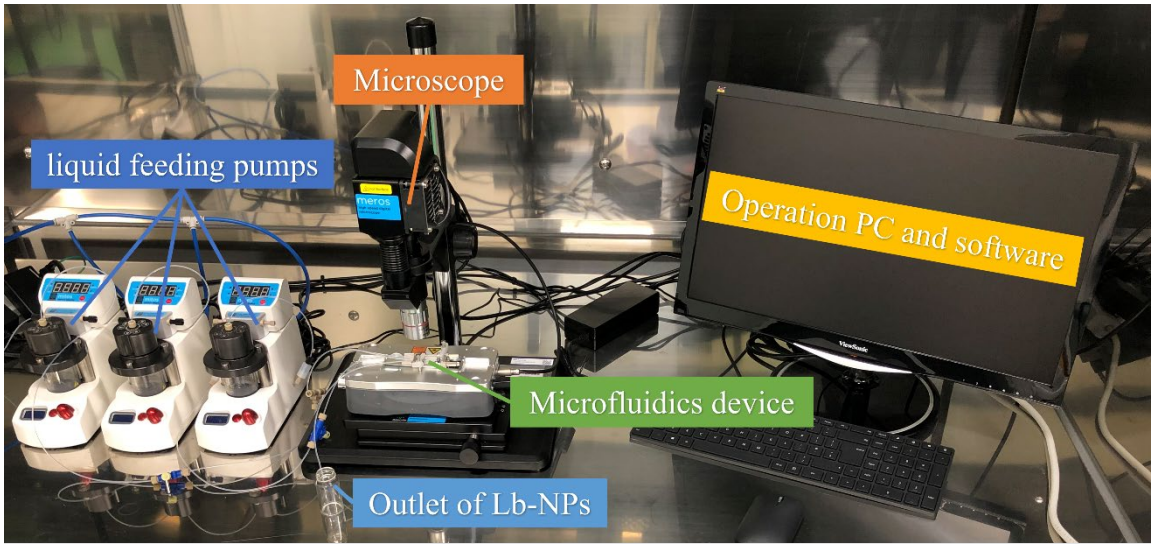

Figure 3.2 The whole preparation system and instruments. The Aqueous phase and organic phase with lipid components were fed from liquid feeding pumps to the microfluidics device located on the microscope. The feeding speed and ratio could be controlled by the PC through software.

3.2.5. Calculation of interparticle distance between Lb-NPs

The interparticle distance is defined as the distance between Lb-NPs. According to Hao et al. [32], the interparticle distance can be calculated as follows:

$$Interparticle\ distance = [(\sqrt{2\pi}/6\varphi)1/3\text{-}1]d$$

In this formula, "d" and "φ" are the diameter of particle and particle volume fraction, respectively.

Particle volume fraction, φ, is calculated as follows:

$$\varphi = \pi d3n/6v$$

where "v" and "n" are the unit volume and concentration of particles per unit volume, respectively.

3.2.6. Statistical analysis

The results are expressed as mean ± SD. For one-to-one comparison, unpaired t-test was performed. For multiple comparisons, I performed one-way ANOVA followed by Tukey's multiple comparison test.

3.3. Results and discussion

3.3.1. Comparison of the Lb-NP size controllability using the microfluidic devices

First, I evaluated the effect of the microchannel structure and lipid concentration on the Lb-NP size controllability. The FRR of the aqueous phase to the lipid phase was fixed at 3 to produce a highly concentrated Lb-NP solution to achieve high throughput. At a POPC concentration of 10 mg/mL, all the microfluidic devices produced homogeneous Lb-NPs smaller than 200 nm; in particular, the iLiNP® and micromixer devices generated Lb-NPs smaller than 100 nm (Figure 3.3 (a), (c) and (e)). At a POPC concentration of 100 mg/mL, the two straight channel devices could not produce Lb-NPs smaller than 200 nm, and a heterogeneous particle size distribution was observed (Figure 3.3 (b), (d) and (f)). On the contrary, iLiNP® and micromixer devices could produce 130 to 180 nm-sized Lb-NPs with a homogeneous size distribution depending on the flow conditions. Under high flow rate conditions, iLiNP® and micromixer devices formed homogeneous (polydispersity index (PDI) ≈ 0.2 or < 0.2) and small-sized (mean hydrodynamic size = 130–140 nm) Lb-NPs compared with those formed under low flow rate conditions (Figure 3.3 (d)). Generally, the rapid dilution of ethanol in the microchannels leads to the production of homogeneous and small-sized Lb-NPs. The high lipid concentration condition induces the aggregation of Lb-NPs or intermediates during Lb-NP formation and forms heterogeneous and large-sized Lb-NPs using microfluidic devices, such as the straight channel device. From these results, it is clear that iLiNP® and micromixer devices maintain good Lb-NP size controllability, even at a POPC concentration of 100 mg/mL. Previously, due to the slow

dilution of ethanol, large-sized and heterogeneous Lb-NPs were prepared at high lipid concentrations using a flow-focusing device, which has a similar channel structure as the straight short device I used where the lipid containing organic solvent phase was sandwiched in-between the aqueous phases [20,21,23,24]. These unfavorable results might be improved by increasing the FRR; however, the Lb-NP concentration in the product is also reduced by increasing the FRR. Therefore, I conclude that the flow-focusing device is not an appropriate structure for mass production of Lb-NPs using a highly concentrated lipid solution.

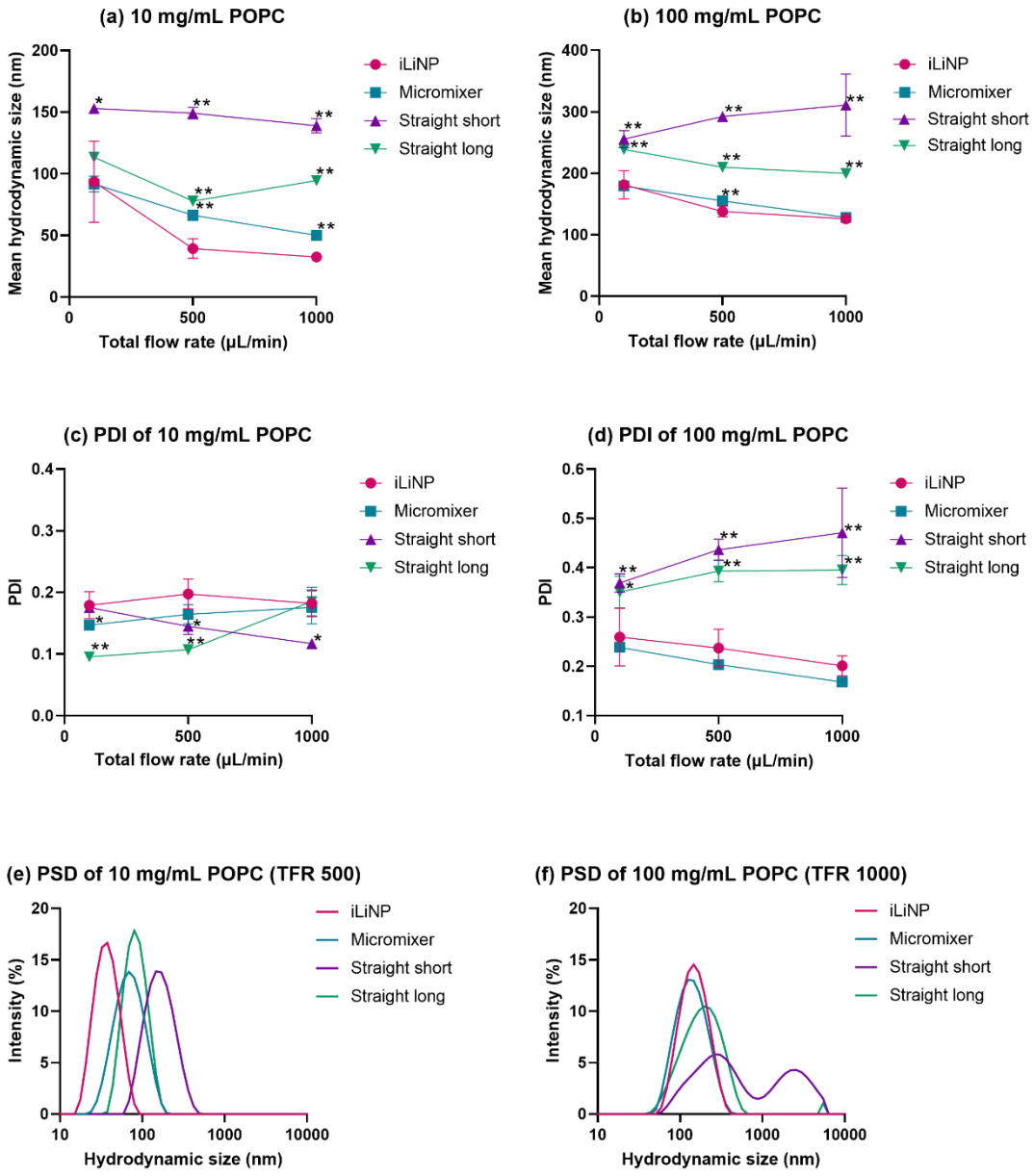

Figure 3.3 Transition of mean hydrodynamic size using (a) 10 mg/mL 1-palmitoyl-2-oleoyl-sn-glycero-3-phosphocholine (POPC) solution and (b) 100 mg/mL POPC solution. Transition of polydispersity index (PDI) using (c) 10 mg/mL POPC solution and (d) 100 mg/mL POPC solution. The error bars represent the standard deviation calculated from repeating each lipid-based nanoparticle (Lb-NP) formation experiment at least three times. Significant difference (*; $P < 0.05$, **; $P < 0.01$) against iLiNP® was calculated by one-way ANOVA followed by Tukey's multiple comparison test. (e–f): Particle size distribution (PSD) using (e) 10 mg/mL POPC at total flow rate (TFR) of 500 µL/min and (f) 100 mg/mL POPC solution at TFR of 1000.

3.3.2. Effect of lipid concentration on the size of Lb-NPs produced using iLiNP® and micromixer devices

I found a unique Lb-NP formation behavior of iLiNP® (Figure 3.3). iLiNP® produced the smallest Lb-NPs at a lipid concentration of 10 mg/mL and TFR of 1000 µL/min. However, I did not observe any size differences between iLiNP® and micromixer devices at 100 mg/mL POPC. For these reasons, I selected iLiNP® and micromixer devices and investigated the effect of lipid concentration on Lb-NP size. As shown in Figure 3.4, iLiNP® produced Lb-NPs smaller than 100 nm at a TFR of 1000 µL/min in the POPC concentration range of 10–50 mg/mL. Under the same conditions, the Lb-NP sizes produced by the micromixer device were at least 1.4-times larger than those produced by iLiNP® (Figure 3.4 (a)–(c)). Kimura et al. reported that iLiNP® could achieve a complete mixing state within 3 ms at a TFR of 500 and FRR of 3 and 9, and the Lb-NP sizes formed under the flow conditions were smaller than those prepared by a chaotic mixer device [13]. The micromixer device needs to achieve a complete mixing state for approximately 192 ms at a TFR of 500 and an FRR of 1 [31]. This was comparable to the differences in the size of Lb-NPs in the POPC concentration range of 10–50 mg/mL (Figure 3.4 (a)–(c)). At a POPC concentration of 100 mg/mL, the Lb-NPs produced by iLiNP® showed an almost similar trend of size reduction as those produced by the micromixer device. The size of Lb-NPs produced by iLiNP® was maintained at 130 nm when the TFR was increased from 500 to 1000 µL/min. However, the size of Lb-NPs prepared using the micromixer device decreased upon increasing the TFR from 100 to 1000 µL/min. From these results, I conclude that the threshold POPC concentration for different size reduction tendencies of iLiNP® and the micromixer devices is between 50 and 100 mg/mL.

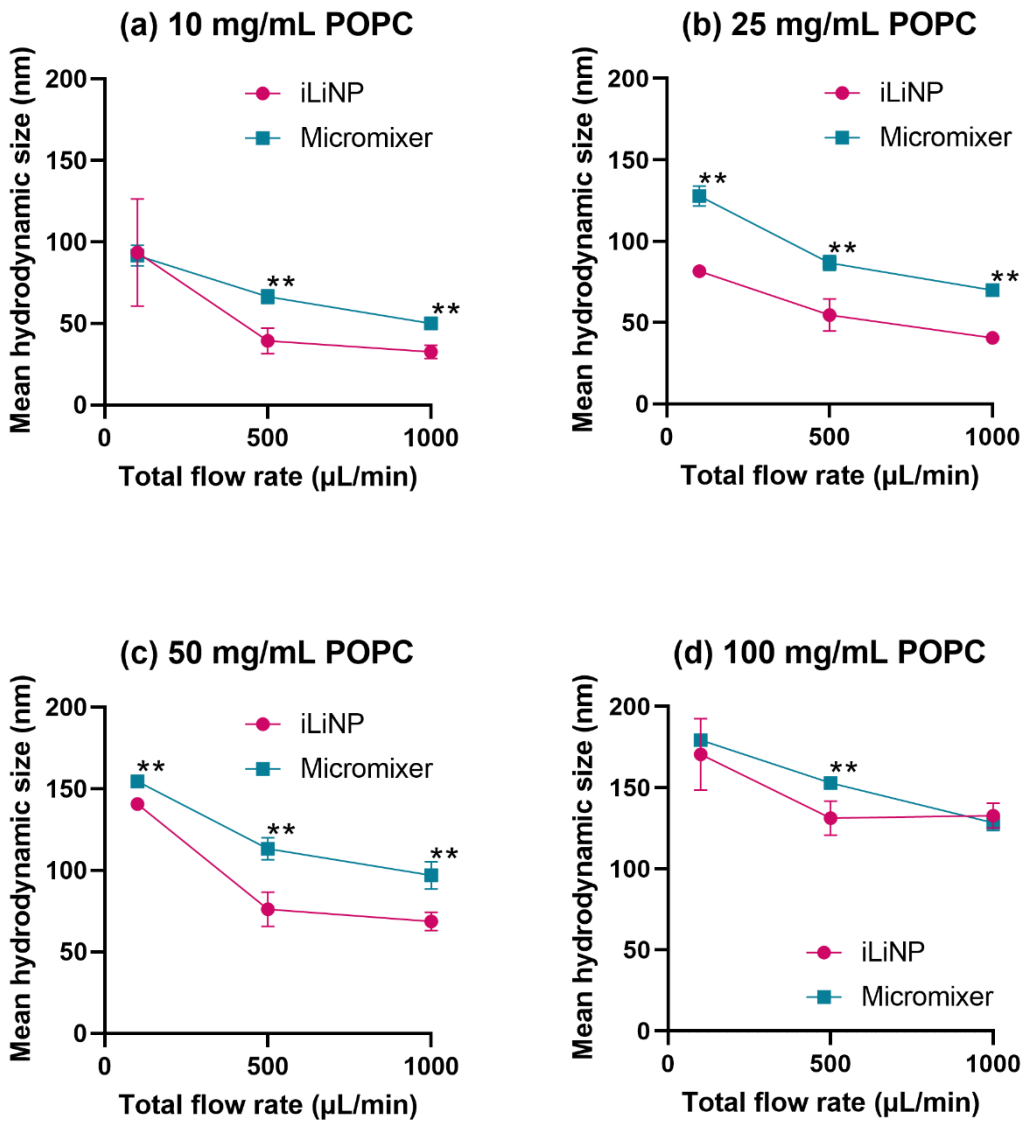

Figure 3.4 Transition of lipid-based nanoparticle (Lb-NP) size by changing the total flow rate of 1-palmitoyl-2-oleoyl-sn-glycero-3-phosphocholine (POPC) solution to (a) 10 mg/mL, (b) 25 mg/mL, (c) 50 mg/mL, and (d) 100 mg/mL. The error bars represent the standard deviation calculated from repeating each experiment at least three times. Significant difference (*; $P < 0.05$, **; $P < 0.01$) was calculated by unpaired t-test.

3.3.3. Effect of lipid concentration on the concentration and interparticle distance between Lb-NPs produced using iLiNP® and micromixer devices

I found that the size and formation of Lb-NPs change as the lipid concentration increases (Figure 3.4). It is assumed that Lb-NPs are formed from phospholipid molecules via lipid bilayer disk-like intermediates [33–35]. I, therefore, assumed that the concentration of Lb-NPs in the final product would reflect the concentration of Lb-NPs and intermediates immediately before forming Lb-NPs in the microchannel. I measured the concentration (particles/mL) of Lb-NPs in the final product to clarify the effect of lipid concentration (mg/mL) and Lb-NP size on Lb-NP formation.

The concentration of Lb-NPs was measured using two methods, NTA and MADLS. NTA is among the most standard measurement methods for counting the number of nanosized particles, such as extracellular vesicles, viruses, and proteins [36–38]. MADLS has a significant advantage over other measurement methods because it can be used to count the number of detectable particles with a wider range of size (from sub-nanometer to 10 μm diameter) [39]. Generally, NTA cannot measure Lb-NPs with diameter < 50 nm because of the weak scattering from small-sized particles. Therefore, small-sized Lb-NPs formed by iLiNP® at low lipid concentrations could not be measured by NTA (Figure 3.5 (a) and (b)). I mainly used MADLS to evaluate the Lb-NP concentration. NTA and MADLS were employed to evaluate the concentration of Lb-NPs with diameter > 50 nm.

As shown in Figure 3.6 (a), the concentration of Lb-NPs produced by the micromixer device was constant (1.3E+13–6.9E+13 particles/mL) at all POPC concentrations (10–100 mg/mL). Comparable results were observed in NTA measurements (Figure 3.5 (b)). In contrast, the concentration of LNPs prepared using iLiNP® decreased with the increasing lipid concentration. The maximum concentration of Lb-NPs (5.9E+14 particles/mL) was obtained at a POPC concentration of 25 mg/mL, and the minimum concentration of Lb-NPs (1.2E+13 particles/mL) was obtained at a POPC concentration of 100 mg/mL (Figure 3.6 (a)). As the POPC concentration increased from 10 mg/mL to 25 mg/mL, the concentration of Lb-NPs tended to increase. This upward trend may be attributed to the smaller ratio of increase in Lb-NP size obtained compared to the ratio of increase in lipid concentration. There was also a tendency for the concentration of Lb-NPs to decrease as the POPC concentration increased from 25 mg/mL to 100 mg/mL. Likewise, this decreasing trend can be explained by the larger ratio of the increase in Lb-NP size obtained compared to the ratio of increase in lipid concentration.

For practical applications, the ability to produce a highly concentrated Lb-NP suspension is essential for a manufacturing apparatus. Therefore, I compared the concentration of Lb-NPs produced by the micromixer and iLiNP® (Figure 3.6 (b)). When Lb-NPs with a diameter < 100 nm were produced in the microfluidic device, iLiNP® produced a higher concentration of Lb-NPs than the micromixer device.

As for the interparticle distance calculated from the Lb-NP concentration and size of Lb-NPs (Figure 3.6 (c)), the interparticle distance in the case of iLiNP® increased from 100 nm (at 10–50 mg/mL POPC) to 200–400 nm (at 100 mg/mL POPC), whereas the interparticle distance in the case of the micromixer device was constant. Assuming that intermediates individually become Lb-NPs, the interparticle distance should decrease as the number of intermediates and Lb-NPs increases with increasing lipid concentration. Conversely, the increase in interparticle distance is presumed to be due to the fact that intermediates are unable to individually become particles and fuse with each other during the particle formation process. This prediction is consistent with the results of increased Lb-NP size as well as with the possible changes in the internal structure of the Lb-NP with increasing lipid concentrations described in the Lb-NP concentration section. These findings suggest that although the formation of Lb-NPs in the micromixer device did not change at all lipid concentrations, it might change according to the lipid concentration in iLiNP®. The differences in the formation of Lb-NPs might be attributable to the elevation in the critical concentration of ethanol at which phospholipids generate and grow intermediates to form Lb-NPs. I previously reported the critical concentration of ethanol for forming the intermediates, and the concentration range of ethanol was 60%–80% when using a chaotic mixer device with a POPC concentration of 10 mg/mL [14]. This critical concentration of ethanol was changed depending on the concentration and chemical properties of the lipid species. At higher POPC concentrations, the critical concentration of ethanol might be increased; therefore, the rapid dilution rate in iLiNP® could not work as effectively as it did at lower POPC concentrations.

Based on the results presented in Figure 3.6, I inferred the LNP formation in the microchannel and have systematically illustrated it in Figure 3.7. At a high POPC concentration, the nucleation rate of intermediates is faster than the ethanol dilution rate in both microfluidic devices because of the high supersaturation in the solution. Therefore, intermediates can easily fuse to form large Lb-NPs rather than bending intermediates to form spherical LNPs. On the contrary, at low POPC concentrations, the dilution rate of ethanol dominates the size and concentration of Lb-NPs in both microfluidic devices. Therefore, iLiNP® allowed the production of small-sized Lb-NPs compared with the micromixer

device by rapid ethanol dilution.

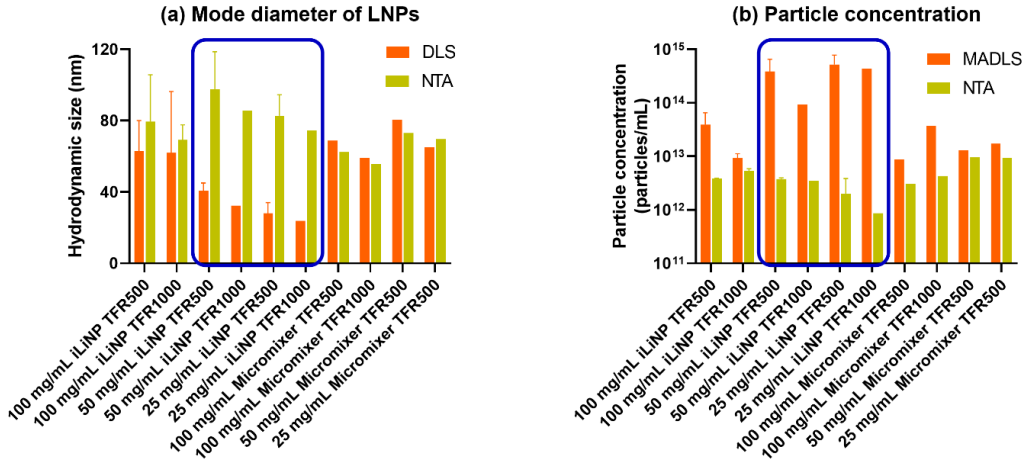

Figure 3.5 (a) Mode diameter of lipid-based nanoparticles (Lb-NPs) measured by dynamic light scattering (DLS) and nano tracking analysis (NTA); (b) particle concentration measured by multi-angle dynamic light scattering (MADLS) and NTA. The error bars represent the standard deviation calculated from repeating each Lb-NP formation experiment twice (N = 1–2).

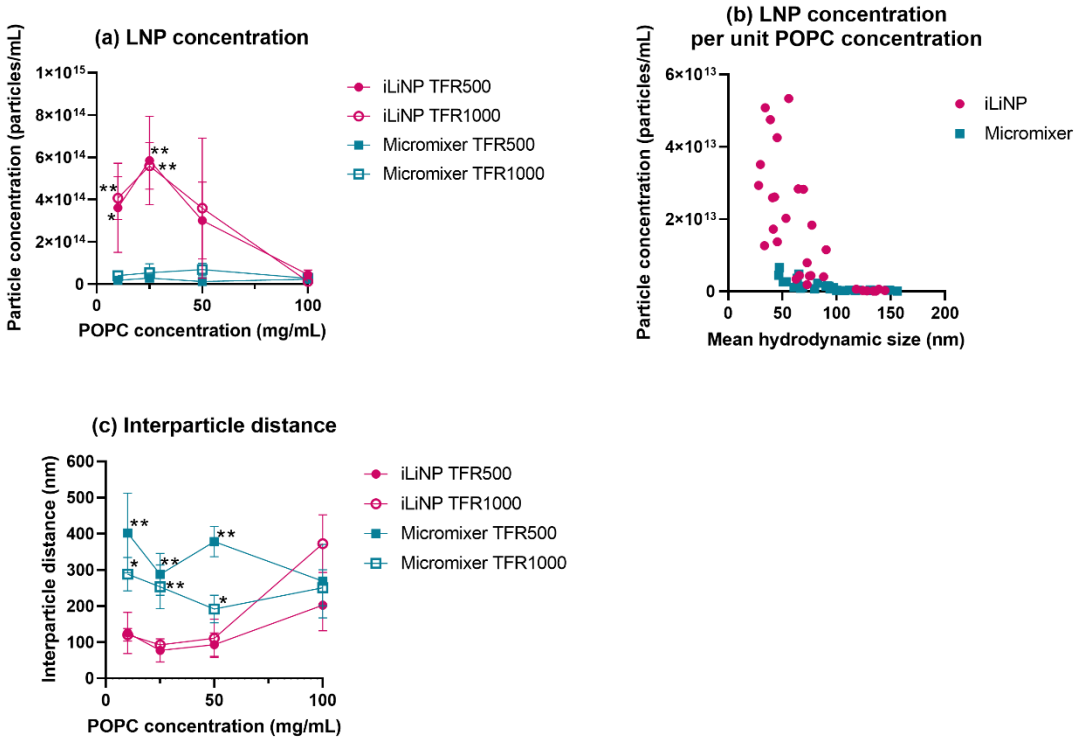

Figure 3.6 Transition of the (a) concentration (particles/mL) of lipid-based nanoparticles (Lb-NPs), (b) concentration of Lb-NPs per unit 1-palmitoyl-2-oleoyl-sn-glycero-3-phosphocholine (POPC) concentration, and (c) interparticle distance in the final product using solutions with different POPC concentrations. The error bars represent the standard deviation calculated from repeating each Lb-NP formation experiment at least three times. Significant difference (*; $P < 0.05$, **; $P < 0.01$) between iLiNP® and micromixer under the same TFR conditions was calculated by one-way ANOVA followed by Tukey's multiple comparison test.

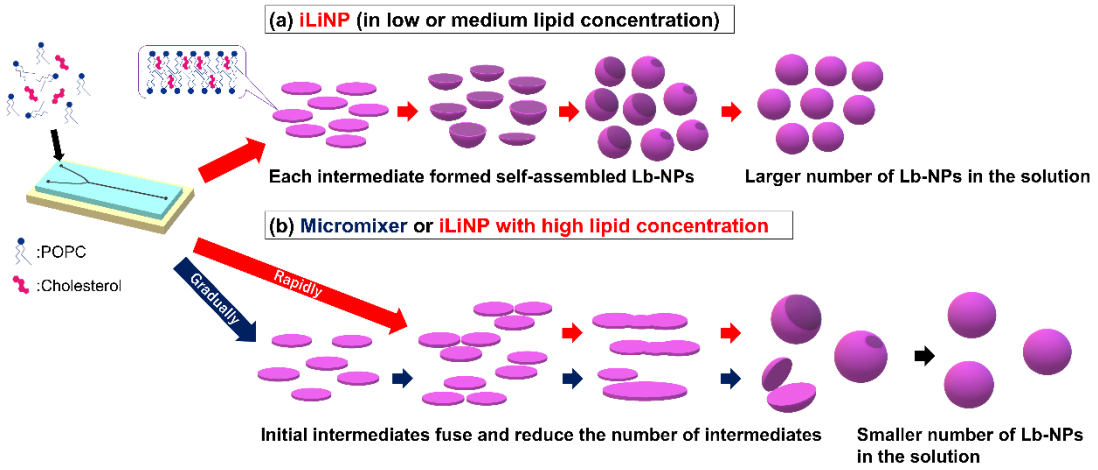

Figure 3.7 The proposed mechanism of lipid-based nanoparticle (Lb-NP) formation in each device and under each condition. (a) Each initial intermediate forms self-assembled Lb-NPs and results in a large number of Lb-NPs. This mechanism of Lb-NP formation is dominant when using iLiNP®. The most effective factor for reducing the size of Lb-NPs is the ethanol dilution rate. (b) The initial intermediates fuse with the existing initial intermediates in the vicinity and reduce the number of intermediates and Lb-NPs. This type of Lb-NP formation is dominant when using the micromixer device (blue arrow) and also when using the highest lipid concentration (e.g., 100 mg/mL POPC) as an ethanol phase with iLiNP® (red arrow). At the higher lipid concentration, the speed of growth of intermediates was regulated by the ethanol dilution rate and the area of the aqueous-ethanol interface. The contribution of the area of the aqueous-ethanol interface on Lb-NP size increased at the higher lipid concentration.

3.3.4. Effect of increasing the area of the aqueous-ethanol interface on the concentration and size of Lb-NPs produced using a three-inlet iLiNP® device

Based on the process of Lb-NP formation in the microchannel proposed (Figure 3.7), I assumed that both the rapid dilution of ethanol and the broad area of the aqueous-ethanol interface have a considerable effect on the size and concentration of Lb-NPs at high lipid concentrations. The micromixer device achieves slower ethanol dilution than iLiNP®, but the former has three inlets that increase the aqueous-ethanol interface. The large aqueous-ethanol interface of the micromixer device contributes to the prevention of the fusion of intermediates to the same extent as that of iLiNP® at a POPC concentration of 100 mg/mL. I fabricated a three-inlet iLiNP® device (Figure 3.8 (a)) to verify

the effect of the aqueous-ethanol interface area on the size and concentration of LNPs at a high lipid concentration.

The three-inlet iLiNP® device could produce 110–120 nm-sized Lb-NPs at a TFR of 1000 μL/min (Figure 3.8 (b)). The Lb-NP concentration and intraparticle distance between the Lb-NPs prepared using the three types of microfluidic devices are shown in Figure 3.8 (c–d). The Lb-NP concentration in the three-inlet iLiNP® device was more than four-fold higher than that in the two-inlet iLiNP® and micromixer devices at a TFR of 1000 μL/min (Figure 3.8 (c)). Unlike the two-inlet iLiNP®, the concentration of Lb-NPs prepared using the three-inlet iLiNP® was increased, and the interparticle distance between Lb-NPs prepared using the three-inlet iLiNP® decreased with the increasing TFR.

Compared with the two- and three-inlet iLiNP®, the micromixer device exhibited a smaller PDI (Figure 3.8 (e)); however, the Lb-NPs prepared using each device showed monodispersity (Figure 3.8 (f)). Although the broader aqueous-ethanol interface achieved using the micromixer device might slightly affect the dispersity of Lb-NPs, there was no significant difference among the three microfluidic devices.

This difference in the size and concentration of Lb-NPs between the two- and three-inlet iLiNP® devices was not observed at a TFR of 500 μL/min. The Lb-NP preparation using the three-inlet iLiNP® at a TFR of 1000 μL/min allowed the production of the smallest Lb-NPs among the three types of microfluidic devices. I assume that the increase in the aqueous-ethanol interface and rapid ethanol dilution using the three-inlet iLiNP® allows the production of small-sized Lb-NPs and more concentrated Lb-NP suspensions [24,25].

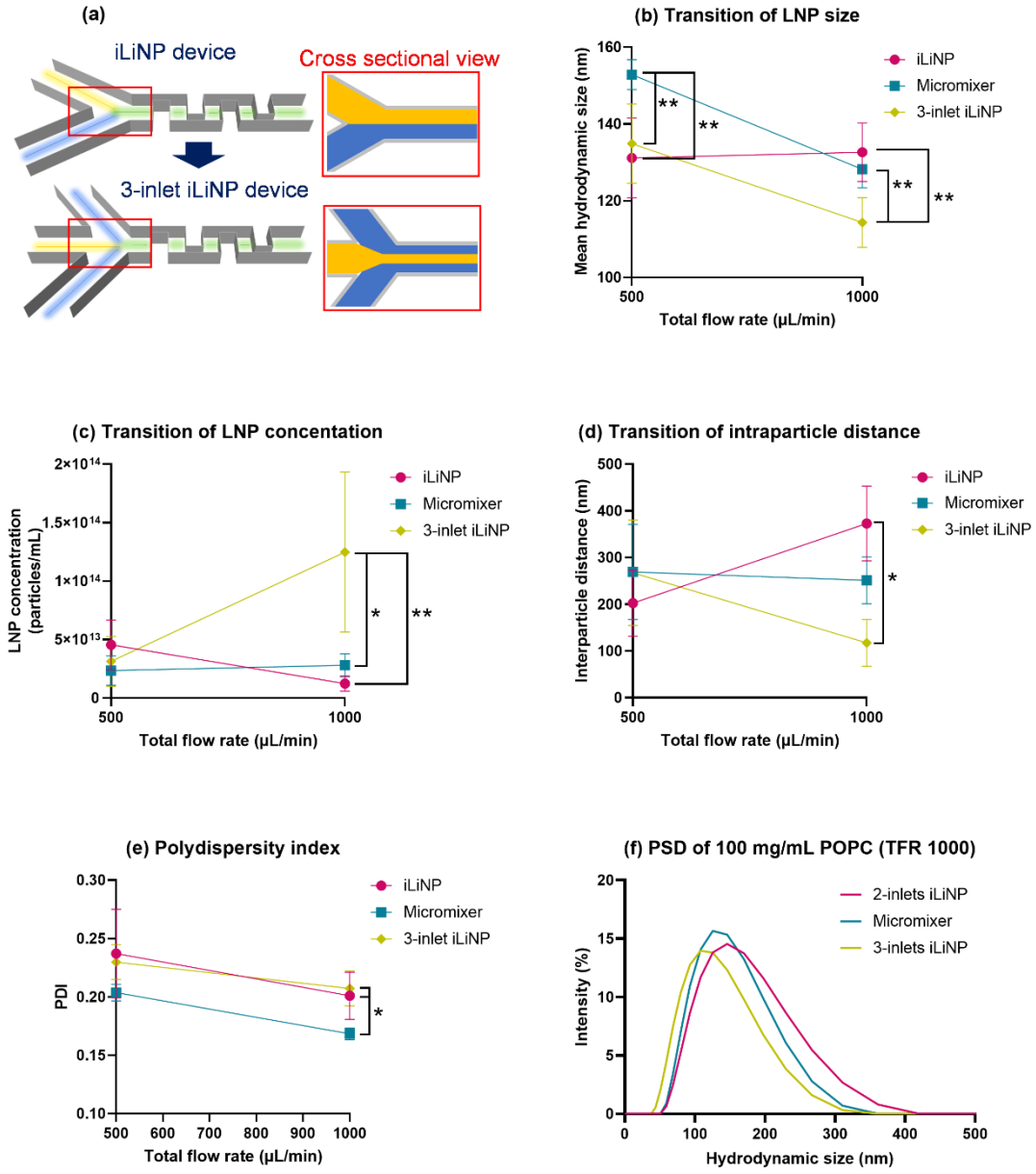

Figure 3.8 (a) Device design of iLiNP and 3-inlet iLiNP. Transition of (b) the lipid-based nanoparticle (LNP) size, (c) the concentration of LNPs, (d) the interparticle distance, and (e) polydispersity index, using 100 mg/mL 1-palmitoyl-2-oleoyl-sn-glycero-3-phosphocholine (POPC) in ethanol as the organic solvent phase. (f) Particle size distribution (PSD) prepared using each microfluidic device at 100 mg/mL POPC and a TFR of 1000 μL/min. The error bars represent the standard deviation calculated from repeating each LNP formation experiment at least three times. Significant difference (*; $P < 0.05$, **; $P < 0.01$) was calculated by one-way ANOVA followed by Tukey's multiple comparison test.

3.4. Conclusion

I demonstrated the effect of lipid concentration on Lb-NP size using four microfluidic devices. I explored the critical factors that affect the size tuning ability under high lipid concentrations. The preparation of uniform and submicron-sized Lb-NPs in highly concentrated lipid solutions was possible by introducing solutions at a high flow rate into microchannel devices using mixer structures, such as those in iLiNP® and micromixer devices. I found that the main factors controlling the particle size varied depending on the lipid concentration and device structure. At low lipid concentrations, ethanol dilution rate dominated the Lb-NP formation behavior. In contrast, the dilution performance of the two-inlet iLiNP® device and the micromixer device was insufficient in controlling the Lb-NP production at a POPC concentration of 100 mg/mL. Based on these findings, I modified iLiNP® to increase the aqueous-ethanol interface and demonstrated that the three-inlet iLiNP® could prevent the fusion of the initial intermediates and produced the smallest Lb-NPs among the three types of microfluidic devices.

I also confirmed that iLiNP® can produce a higher concentration of Lb-NPs per unit volume than the micromixer device. This result suggests that iLiNP® provides many advantages for the mass production of size-controlled Lb-NPs using microfluidic devices. The performance of dense Lb-NP suspensions is significant for practical application of the microfluidic technology in the production of Lb-NP-based nanomedicines and cosmetics. I consider iLiNP®-based microfluidic devices to be a suitable platform for mass production of Lb-NPs.

In conclusion, this chapter characterizes the factors that affect particle size controllability in the case of highly concentrated lipid solutions. As a result, unimodal Lb-NPs of submicron size were successfully prepared even under high concentration lipid conditions.

3.5. References

[1] R. Tenchov, R. Bird, A.E. Curtze, Q. Zhou, Lipid Nanoparticles-From Liposomes to mRNA Vaccine Delivery, a Landscape of Research Diversity and Advancement, Acs Nano. 15 (2021) 16982–17015.

[2] N.R.H. Stone, T. Bicanic, R. Salim, W. Hope, Liposomal Amphotericin B (AmBisome®): A Review of the Pharmacokinetics, Pharmacodynamics, Clinical Experience and Future Directions, Drugs. 76 (2016) 485–500.

[3] L.M. Ickenstein, P. Garidel, Lipid-based nanoparticle formulations for small molecules and RNA drugs, Expert Opin Drug Del. 16 (2019) 1205–1226.

[4] M.E.R. O'Brien, N. Wigler, M. Inbar, R. Rosso, E. Grischke, A. Santoro, R. Catane, D.G. Kieback, P. Tomczak, S.P. Ackland, F. Orlandi, L. Mellars, L. Alland, C. Tendler, Reduced cardiotoxicity and comparable efficacy in a phase III trial of pegylated liposomal doxorubicin HCl (CAELYX™/Doxil®) versus conventional doxorubicin for first-line treatment of metastatic breast cancer, Ann Oncol. 15 (2004) 440–449.

[5] X. Zhang, V. Goel, G.J. Robbie, Pharmacokinetics of Patisiran, the First Approved RNA Interference Therapy in Patients With Hereditary Transthyretin-Mediated Amyloidosis, J Clin Pharmacol. 60 (2019) 573–585.

[6] X. Zhang, V. Goel, H. Attarwala, M.T. Sweetser, V.A. Clausen, G.J. Robbie, Patisiran Pharmacokinetics, Pharmacodynamics, and Exposure-Response Analyses in the Phase 3 APOLLO Trial in Patients With Hereditary Transthyretin-Mediated (hATTR) Amyloidosis, J Clin Pharmacol. 60 (2020) 37–49.

[7] Y.N. Lamb, BNT162b2 mRNA COVID-19 Vaccine: First Approval, Drugs. 81 (2021) 495–501.

[8] L. Schoenmaker, D. Witzigmann, J.A. Kulkarni, R. Verbeke, G. Kersten, W. Jiskoot, D. Crommelin, mRNA-lipid nanoparticle COVID-19 vaccines: structure and stability, Int J Pharmaceut. 601 (2021) 120586.

[9] S.A. Roberts, N. Parikh, R.J. Blower, N. Agrawal, SPIN: rapid synthesis, purification, and concentration of small drug-loaded liposomes, J Liposome Res. 28 (2017) 1–30.

[10] S. Amrani, M. Tabrizian, Characterization of Nanoscale Loaded Liposomes Produced by 2D Hydrodynamic Flow Focusing, Acs Biomater Sci Eng. 4 (2018) 502–513.

[11] S. Shah, V. Dhawan, R. Holm, M.S. Nagarsenker, Y. Perrie, Liposomes: Advancements and innovation in the manufacturing process, Adv Drug Deliver Rev. 154–155 (2020) 102–122.

[12] M. Maeki, S. Uno, A. Niwa, Y. Okada, M. Tokeshi, Microfluidic technologies and devices for lipid nanoparticle-based RNA delivery, J Control Release. 344 (2022) 80–96.

[13] N. Kimura, M. Maeki, Y. Sato, Y. Note, A. Ishida, H. Tani, H. Harashima, M. Tokeshi, Development of the iLiNP Device: Fine Tuning the Lipid Nanoparticle Size within 10 nm for Drug Delivery, Acs Omega. 3 (2018) 5044–5051.

[14] M. Maeki, Y. Fujishima, Y. Sato, T. Yasui, N. Kaji, A. Ishida, H. Tani, Y. Baba, H. Harashima, M. Tokeshi, Understanding the formation mechanism of lipid nanoparticles in microfluidic devices with chaotic micromixers, Plos One. 12 (2017) e0187962.

[15] R.R. Hood, D.L. DeVoe, J. Atencia, W.N. Vreeland, D.M. Omiatek, A facile route to the synthesis of monodisperse nanoscale liposomes using 3D microfluidic hydrodynamic focusing in a concentric capillary array, Lab Chip. 14 (2014) 2403–2409.

[16] A. Jahn, S.M. Stavis, J.S. Hong, W.N. Vreeland, D.L. DeVoe, M. Gaitan, Microfluidic Mixing and the Formation of Nanoscale Lipid Vesicles, Acs Nano. 4 (2010) 2077–2087.

[17] M. Maeki, N. Kimura, Y. Sato, H. Harashima, M. Tokeshi, Advances in microfluidics for lipid nanoparticles and extracellular vesicles and applications in drug delivery systems, Adv Drug Deliver Rev. 128 (2018) 84–100.

[18] M. Maeki, Y. Okada, S. Uno, A. Niwa, A. Ishida, H. Tani, M. Tokeshi, Production of siRNA-Loaded Lipid Nanoparticles using a Microfluidic Device, J Vis Exp. No. 181 (2022) e62999.

[19] N. Kimura, M. Maeki, Y. Sato, A. Ishida, H. Tani, H. Harashima, M. Tokeshi, Development of a Microfluidic-Based Post-Treatment Process for Size-Controlled Lipid Nanoparticles and Application to siRNA Delivery, Acs Appl Mater Inter. 12 (2020) 34011–34020.

[20] A. Zizzari, M. Bianco, L. Carbone, E. Perrone, F. Amato, G. Maruccio, F. Rendina, V. Arima, Continuous-Flow Production of Injectable Liposomes via a Microfluidic Approach, Materials. 10 (2017) 1411.

[21] F. Yanar, A. Mosayyebi, C. Nastruzzi, D. Carugo, X. Zhang, Continuous-Flow Production of Liposomes with a Millireactor under Varying Fluidic Conditions, Pharm. 12 (2020) 1001.

[22] M. Michelon, D.R.B. Oliveira, G. de F. Furtado, L.G. de la Torre, R.L. Cunha, High-throughput continuous production of liposomes using hydrodynamic flow-focusing microfluidic devices, Colloids Surfaces B Biointerfaces. 156 (2017) 349–357.

[23] R.R. Hood, D.L. DeVoe, High-Throughput Continuous Flow Production of Nanoscale Liposomes by Microfluidic Vertical Flow Focusing, Small. 11 (2015) 5790–5799.

[24] T.A. Balbino, N.T. Aoki, A.A.M. Gasperini, C.L.P. Oliveira, A.R. Azzoni, L.P. Cavalcanti, L.G. de la Torre, Continuous flow production of cationic liposomes at high lipid concentration in microfluidic devices for gene delivery applications, Chem Eng J. 226 (2013) 423–433.

[25] H. Aghaei, A.R.S. Nazar, Continuous Production of the Nanoscale Liposome in a Double Flow-Focusing Microfluidic Device, Ind Eng Chem Res. 58 (2019) 23032–23045.

[26] C.B. Roces, E.C. Port, N.N. Daskalakis, J.A. Watts, J.W. Aylott, G.W. Halbert, Y. Perrie, Rapid scale-up and production of active-loaded PEGylated liposomes, Int J Pharmaceut. 586 (2020) 119566.

[27] M. Mijajlovic, D. Wright, V. Zivkovic, J.X. Bi, M.J. Biggs, Microfluidic hydrodynamic focusing based synthesis of POPC liposomes for model biological systems, Colloids Surfaces B Biointerfaces. 104 (2013) 276–281.

[28] R.R. López, P.G.F. de Rubinat, L.-M. Sanchez, T. Tsering, A. Alazzam, K.-F. Bergeron, C. Mounier, J.V. Burnier, I. Stiharu, V. Nerguizian, The effect of different organic solvents in liposome

properties produced in a periodic disturbance mixer: Transcutol®, a potential organic solvent replacement, Colloids Surfaces B Biointerfaces. (2020) 111447.

[29] J.C. McDonald, G.M. Whitesides, Poly(dimethylsiloxane) as a Material for Fabricating Microfluidic Devices, Accounts Chem Res. 35 (2002) 491–499.

[30] N. Kimura, M. Maeki, K. Sasaki, Y. Sato, A. Ishida, H. Tani, H. Harashima, M. Tokeshi, Three-dimensional, symmetrically assembled microfluidic device for lipid nanoparticle production, Rsc Adv. 11 (2021) 1430–1439.

[31] J. Bresseleers, M. Bagheri, C. Lebleu, S. Lecommandoux, O. Sandre, I.A.B. Pijpers, A.F. Mason, S. Meeuwissen, C.F. van Nostrum, W.E. Hennink, J.C.M. van Hest, Tuning Size and Morphology of mPEG-b-p(HPMA-Bz) Copolymer Self-Assemblies Using Microfluidics, Polymers-Basel. 12 (2020) 2572.

[32] T. Hao, R.E. Riman, Calculation of interparticle spacing in colloidal systems, J Colloid Interf Sci. 297 (2006) 374–377.

[33] J.M. Zook, W.N. Vreeland, Effects of temperature, acyl chain length, and flow-rate ratio on liposome formation and size in a microfluidic hydrodynamic focusing device, Soft Matter. 6 (2010) 1352–1360.

[34] J. Kotouček, F. Hubatka, J. Mašek, P. Kulich, K. Velínská, J. Bezděková, M. Fojtíková, E. Bartheldyová, A. Tomečková, J. Stráská, D. Hrebík, S. Macaulay, I. Kratochvílová, M. Raška, J. Turánek, Preparation of nanoliposomes by microfluidic mixing in herring-bone channel and the role of membrane fluidity in liposomes formation, Sci Rep-Uk. 10 (2020) 5595.

[35] C. Webb, S. Khadke, S.T. Schmidt, C.B. Roces, N. Forbes, G. Berrie, Y. Perrie, The Impact of Solvent Selection: Strategies to Guide the Manufacturing of Liposomes Using Microfluidics, Pharm. 11 (2019) 653.

[36] Z. Hamrang, N.J.W. Rattray, A. Pluen, Proteins behaving badly: emerging technologies in profiling biopharmaceutical aggregation, Trends Biotechnol. 31 (2013) 448–458.

[37] R.A. Dragovic, C. Gardiner, A.S. Brooks, D.S. Tannetta, D.J.P. Ferguson, P. Hole, B. Carr, C.W.G. Redman, A.L. Harris, P.J. Dobson, P. Harrison, I.L. Sargent, Sizing and phenotyping of cellular vesicles using Nanoparticle Tracking Analysis, Nanomed Nanotechnol Biology Medicine. 7 (2011) 780–788.

[38] P. Kramberger, M. Ciringer, A. Štrancar, M. Peterka, Evaluation of nanoparticle tracking analysis for total virus particle determination, Virol J. 9 (2012) 265.

[39] J. Austin, C. Minelli, D. Hamilton, M. Wywijas, H.J. Jones, Nanoparticle number concentration measurements by multi-angle dynamic light scattering, J Nanopart Res. 22 (2020) 108.

CHAPTER 4

Controlling Lamellarity and Physicochemical Properties of Liposomes Prepared using a Microfluidic Device

4.1 Introduction

Lipid-based nanoparticles (Lb-NPs) have been used in many clinical applications in the pharmaceutical and cosmetic fields for therapeutic purposes. Lb-NPs can successfully deliver both poorly water-soluble and water-soluble drugs and high molecular-weight modalities, such as oligonucleotides. Based on their internal structure, Lb-NPs can be subdivided into liposomes [1], lipid emulsions [2], lipid nanoparticles (LNPs) [1,3], solid lipid nanoparticles [1,4], and nanostructured lipid carriers [1]. Lb-NPs have the great advantages of high biocompatibility and biodegradability [5]. Based on these characteristics, LNPs have been utilized for the vaccines against COVID-19 [1,6–8], and liposomes are widely used in pharmaceutical products such as Doxil [1,6,9], AmBisome [6,10], and cosmetic products [11].

The most basic Lb-NPs are liposomes, which are enclosed vesicles consisting of one or more lipid bilayers. The size of such liposomes can be adjusted from nano- to micro-order, depending on the target organ/cells for delivery and the site of application. The physicochemical properties of liposomes, such as the encapsulation efficiency [12–16], drug release profile [12–16], morphology [17], stiffness [17], and photoprotection of drugs [18], significantly impact drug delivery to target organs and cellular uptake [14,19]. These physicochemical properties change depending on the liposome composition, size, and lamellar structure of the lipid bilayer.

Comparisons of the physicochemical properties and effects on drug activity between uni- and multi-lamellar liposomes have been reported [15–21]. Generally, liposomes are classified according to their preparation method. For example, liposomes prepared using a lipid thin-film hydration method tend to form multi-lamellar vesicles. Then, uni-lamellar vesicles can be obtained by extrusion or sonication of the multilamellar vesicles. Liposomes are also classified according to particle size. Specifically, micro-ordered liposomes form multilayer lamellar vesicles, while nano-ordered liposomes form single-layer lamellar vesicles. However, Scott et al. observed that even if liposomes of uniform particle size are obtained by extrusion through a 100 μm membrane filter, they still contain some multilamellar vesicles [22]. Thus, if the lamellar properties of liposomes are inferred from indirect physicochemical properties, the evaluations and results might include large uncertainties regarding the lamellar properties of these liposomes. In addition, micro-ordered liposomes have often been evaluated as representatives of multi-lamellar liposomes in terms of liposome size [15,16,19,20]. It is more desirable to evaluate multi- and uni-lamellar liposomes in a realistic size range that can be applied to drug delivery for intravascular administration by injection, such as intravenous (IV)

injection or infusion; however, such reports remain scarce.

Microfluidic technology is widely used to prepare nanoparticles composed of lipids and polymers [23]. Microfluidic technology offers precise particle size control, ease of operation, and continuous production, allowing seamless scale-up from laboratory (lab) to production scale [24]. Therefore, this preparation technique is one of the most promising nanoparticle preparation methods currently being investigated [25]. According to the literature, liposomes prepared using microfluidic devices have been characterized by microscopy and X-ray diffraction and were observed to form both uni- and multi-lamellar structures [26,27]. However, the effect of the microfluidic preparation conditions on the detailed lamellar structure of liposomes is still not fully understood.

I previously reported that microfluidic technology can be used to prepare uniform liposomes of different sizes and particle concentrations by simply changing the lipid concentration in the same formulation [28]. Based on these findings, I considered the possibility of obtaining liposomes with different lamellar structures by changing the process parameters and lipid concentrations. In particular, I reported that a large number of small-sized liposomes were prepared under the condition of using the low lipid concentration and the microfluidic device which equipped the baffle structure inside the channel (Kimura et. al. named this device “invasive lipid nanoparticle production (iLiNP)” [29]), whereas a small number of larger liposomes were prepared by using high lipid concentration solution [28]. These differences might affect not only the size and number of liposomes but also the internal lamellarity of liposomes, which have a potential to change the drug release and activity.

In this current study, paclitaxel (PTX) was used as a model compound, and PTX-loaded liposomes were prepared with homogeneous compositions. Specifically, the PTX-loaded liposomes were prepared under three lipid concentrations and two flow rate ratio (FRR) conditions using a microfluidic device (Figure 4.1 (a)). In this study, I focused on the preparation of liposomes with different lamellar properties and compared their physicochemical properties. Furthermore, I confirmed the effect of the liposome lamellar structure on the in vitro release kinetics and in vitro activity of PTX.

4.2 Experimental

4.2.1 Materials

1-Palmitoyl-2-oleoyl-sn-glycero-3-phosphocholine (POPC) was purchased from the NOF

AMERICA Corporation (White Plains, NY, US). Cholesterol, ethanol (≥ 99.5%, HPLC grade), Tween® 80 (TW80), and 1,6-diphenyl-1,3,5-hexatriene (DPH) were purchased from Sigma-Aldrich (St. Louis, MO, US). Monohydrate, phosphate-buffered saline (PBS) was purchased from FUJIFILM Wako Pure Chemical Corporation (Osaka, Japan). Paclitaxel (PTX) was purchased from Tokyo Chemical Industry (Tokyo, Japan).

4.2.2 Fabrication of microfluidic device with baffle structures

The microfluidic device was fabricated using standard photolithography [30]. The detailed protocol has been described in the literature [29,31]. Briefly, the master molds were made from SU-8 3050 (Nippon Kayaku, Tokyo, Japan) for the 100 μm thick layer on silicon wafers. Next, the SU-8 layer on the silicon wafer was exposed to UV light with a mask aligner after which replicated poly(dimethylsiloxane) (PDMS) pieces were bonded with a glass substrate by oxygen plasma treatment (CUTE-1MP/R, Femto Science, Gwangju, Korea). The channel structure and dimensions of the microfluidic device are illustrated in Figure 4.1 (a).

4.2.3 Preparation of PTX-loaded liposomes

PTX-loaded liposomes were prepared by mixing an aqueous phase and lipid/ethanol (organic) phase in the microfluidic device. An ethanol solution containing certain amounts of POPC, cholesterol, and PTX (POPC/cholesterol/PTX = 90/7/3 molar ratio) was used as the organic solvent phase, while MilliQ water was used as the aqueous phase.

These two solutions were placed in a liquid feeding pump (Mitos P-Pumps, Blacktrace Company, Royston, UK) and fed into the microfluidic device. The lipid solution was prepared with three concentrations (10, 50, and 100 mM) of the total components. The total flow rate (TFR) was maintained at 500 μL/min and the FRR was fixed at 3 or 9. The collected liposome suspensions were dialyzed with 10,000 MWCO dialysis membrane tubing (SnakeSkin™ Dialysis Tubing, Thermo Fisher Scientific, Waltham, MA) overnight against a PBS solution. The dialyzed liposome suspension was then filtered through a 0.45 μm filter (DISMIC®, ADVANTEC MFS, California, US) to remove the crystalized/unincorporated PTX. The size of the LNPs was measured by dynamic light scattering (DLS) using a Zetasizer Ultra instrument (Malvern Instruments, Worcestershire, UK).

4.2.4 Evaluation of the encapsulation efficiencies, drug loading, and recovery ratios of PTX-loaded liposomes

The PTX EE% was expressed as the mass of PTX encapsulated over the total PTX amount in the PTX-loaded LNP suspension filtered through a 0.45 μm filter. The PTX-loaded liposome suspension was filtered through a 0.45 μm filter, diluted with a mixture of acetonitrile and water (50:50), and subsequently measured by HPLC. The PTX-loaded liposome suspension filtered through a 0.45 μm filter was placed in a unit with a centrifugal filter (Amicon Ultra, MWCO 50 kDa, Merck, Darmstadt, Germany) and centrifuged for 10 min at 7500 rpm and 4 °C. The ultrafiltered solution was then collected and analyzed by HPLC using the method described above. The EE% was calculated as follows:

EE% = ((PTX concentration in PTX-loaded liposome solution filtered through 0.45 μm filter) – (PTX concentration in the ultracentrifuged solution)) / (PTX concentration in PTX-loaded liposome solution filtered through 0.45 μm filter) x 100

The drug loading (DL%) was expressed as the mass of the PTX loaded over the total weighted mass of the freeze-dried samples. The PTX-loaded liposomes filtered through a 0.45 μm filter were lyophilized by freeze dryers (EPSILON2-4LSCplus, Martin Christ, Germany) and the lyophilized powder was then weighed. The DL% was calculated as follows:

DL% = (PTX amount in PTX-loaded liposome solution filtered through 0.45 μm filter per unit volume) / ((Mass of PTX-loaded LNPs filtered through 0.45 μm filter after lyophilization per unit volume) – (Theoretical amount of PBS salt weight per unit volume)) x 100

The percentage recovery (Recovery%) was expressed as the ratio of the PTX amount loaded in the liposome and the total theoretical amount of PTX added. The percentage recovery was calculated as follows:

Recovery% = (PTX amount in PTX-loaded liposome solution filtered through 0.45 μm filter per unit volume) / (Theoretical PTX amount of PTX-loaded liposome solution before filtering through 0.45 μm filter per unit volume) x 100

For the HPLC analysis, an Agilent 1200 Series high-performance liquid chromatograph (Agilent Technologies, Palo Alto, CA) equipped with a YMC-Pack Pro C8 column (4.6 x 50 mm; 5 μm bead diameter) and a UV detector were used to quantify the drug content in the samples. Samples were eluted with a mixture of acetonitrile and water (50:50, v/v) for 5 min (retention time = 2.8 min) followed by acetonitrile and water (90:10, v/v) for 5 min. The elution flow rate, injection volume, and detection wavelength were set at 1.0 mL/min, 20 μL, and 227 nm, respectively.

4.2.5 Evaluation of the lamellar structure of liposomes using SAXS and TEM analysis

Small-angle X-ray scattering (SAXS) measurements were performed on the beamline BL15A2 at the Photon Factory (Ibaraki, Japan). A wavelength of 1.2 Å was employed and the X-ray detector (PILATUS 2M, DECTRIS, Switzerland) distance was set to 1.5 m. SAXS data were collected with 1 s exposure time and integrated 300 images.

The morphology and inner structure of the liposomes were observed by transmission electron microscopy (TEM, HITACHI H-7600) at an acceleration energy of 100 kV. Liposome suspensions were diluted with PBS at the appropriate concentration and added to carbon-coated copper grids (400 mesh) followed by staining with a 2% phosphotungstic acid solution. TEM images were collected using a CCD camera (XR16, AMT imaging).

4.2.6 *In vitro* release study

Each sample of PTX concentration was adjusted to 50 μg/mL of which 1 mL was placed in the 10,000 MWCO dialysis membrane tubing. The tubing was inserted in 100 mL of PBS containing 0.1% of TW80 and incubated at 37 °C under constant agitation. At timed intervals, 0.5 mL of release medium was sampled and replaced with 0.5 mL of fresh PBS containing 0.1% of TW80. The release medium was then analyzed by HPLC. At the endpoint, the samples remaining in the dialysis membrane tubing were also collected and analyzed by HPLC. The release ratio (Release%) was calculated as follows:

Release% = (PTX amount in the release medium sampled at each time point) / (PTX amount in the initial sample) x 100

4.2.7 Fluorescence polarization assay of liposomes

The membrane fluidity was evaluated by fluorescence polarization assay (FPA). At the liposome preparation process stage, 0.5 mol% DPH was added to each lipid mixture/ethanol sample to produce DPH-labeled PTX-loaded liposomes. Fluorescence polarization (P) values were obtained using a microplate reader (Infinite® 200 PRO, TECAN, Japan). The excitation/emission wavelengths were set to 360/430 nm, and the measurement temperature was maintained at 25 °C. After the FPA measurement, the degree of change in the fluorescence polarization value (ΔP) was calculated as follows:

ΔP = (P values of each liposome suspension) – (P values of 100 mM FRR3 liposome suspension)

4.2.8 Cell culture and *in vitro* assay

HeLa cells were cultured in cell-culture dishes (Corning) containing Dulbecco's Modified Eagle Medium (DMEM) supplemented with 10% Fetal Bovine Serum (FBS), penicillin (100 U/mL), and streptomycin (100 μg/mL) at 37 °C in 5% CO_2. Cells were seeded at a concentration of 4×10^3 cells per well in a 96-well microplate for 24 h prior to the liposome treatment for the cell viability assay. The cells were then treated with liposomes and incubated for 48 h at 37 °C in 5% CO_2. After the incubation, the cell viability was measured using a Cell Counting Kit-8 (Dojindo, Kumamoto, Japan) according to the manufacturer's protocol.

4.2.9 Statistical analysis

The results are expressed as mean ± standard deviation. For multiple comparisons, I performed one-way ANOVA followed by Tukey’s multiple comparison test.

4.3 Results and discussion

4.3.1 Investigation of the physicochemical properties of the PTX-loaded liposomes

First, I investigated the physicochemical properties of the PTX-loaded liposomes. The particle size of the liposomes decreased with decreasing lipid concentration and increasing FRR (Figure 4.1 (b)). These trends were comparable to those of placebo liposomes and other publications [28,29]. The polydispersity index (PDI) of the liposomes was lower than 0.2 except at the lowest lipid concentration (Figure 4.1 (c)). Indeed, at a lipid concentration of 10 mM, the liposome sizes were smaller than 50 nm, which might have contributed to the higher PDI values compared to those of the larger liposomes. The FRR affected both the recovery (recovery%) and drug loading (DL%) percentages. Thus, the liposomes prepared at an FRR of 9 showed a higher recovery% than those prepared at an FRR of 3 (Figure 4.1 (d)). Notably, Zheng et al. reported the same trend using erythromycin as the model compound for the hydrophobic drug [32]. The DL% showed a similar trend to that of the recovery% (Figure 4.1 (e)). The PTX in the ethanol phase was precipitated once the ethanol phase made contact with the aqueous phase and the PTX concentration reached the supersaturated concentration. Hydrophobic PTX was incorporated into the lipid bilayer of liposomes at the interface of the aqueous and ethanol phases. A higher FRR induced more rapid ethanol dilution. Therefore, the faster liposome formation rate allowed for the incorporation of PTX into the lipid bilayer rather than the crystallization of PTX [32]. The EE% of PTX into the liposomes was almost 100%, indicating that almost all the PTX was loaded into the liposomes (Figure 4.1 (f)).

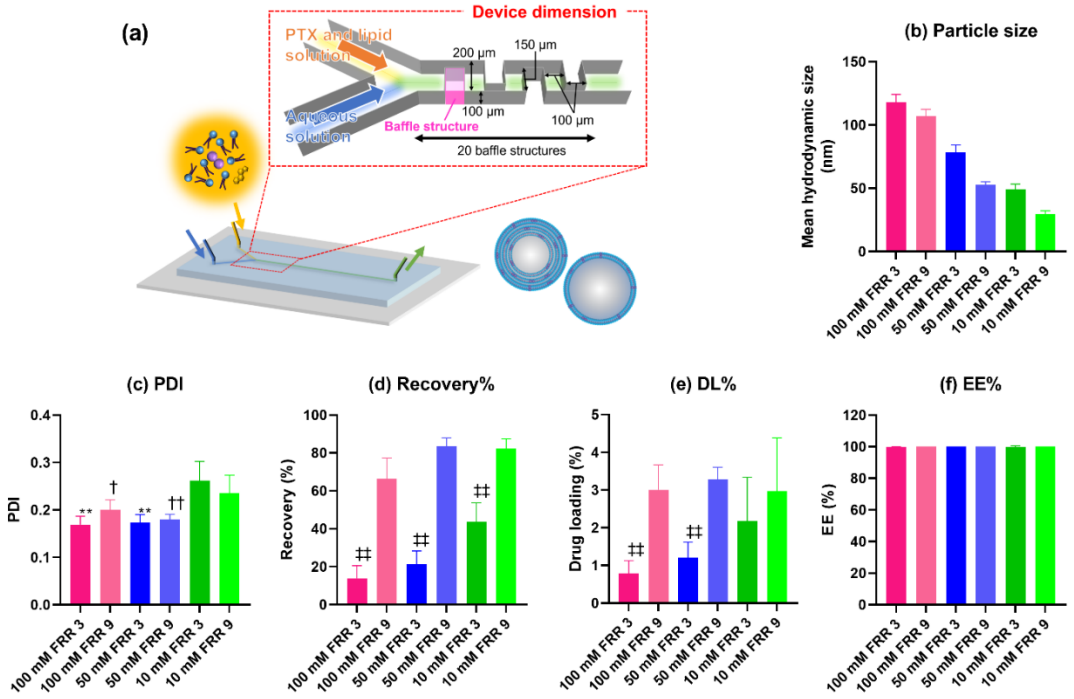

Figure 4.1 (a) Schematic illustration of the microfluidic device and the preparation method of the paclitaxel (PTX)-loaded liposomes: Composition of lipid, 1-palmitoyl-2-oleoyl-sn-glycero-3-phosphocholine (POPC)/cholesterol/PTX = 90/7/3 molar ratio; total flow rate (TFR) = 500 μL/min, and flow rate ratio (FRR) of the aqueous and ethanol phases = 3 or 9. Physicochemical properties of PTX-loaded Liposomes: (b) Particle size, (c) polydispersity index (PDI), (d) percentage recovery, (e) percentage drug loading (DL%), and (f) percentage encapsulation efficiency (EE%). The error bars represent the standard deviation calculated from repeating each experiment at least three times. Definition of symbols: **, $P < 0.01$ (vs 10 mM FRR = 3); †, $P < 0.05$; ††, $P < 0.01$ (vs 10 mM FRR = 9) for (c) and ‡‡, $P < 0.01$ (vs each lipid concentration of FRR = 9) for (d) and (e).

4.3.2 Evaluation of the lamellar structure of liposomes

Liposomes of different sizes and physicochemical properties were prepared with the same lipid compositions, as shown in Figure 4.1. The liposomes were then analyzed by small-angle X-ray scattering (SAXS) and transmission electron microscopy (TEM) techniques to elucidate their internal structure, especially their lamellarity. For the SAXS measurements, peaks derived from the lamellar structure were observed in the liposomes prepared at lipid concentrations of 100 mM and 50 mM

(Figure 4.2 (a) and (b), respectively). Comparing the two liposomes prepared with the latter lipid concentration, the liposomes prepared with an FRR of 9 presented peaks with a weaker peak intensity than those prepared with an FRR of 3. This indicated that the liposomes prepared with an FRR of 3 formed more multi-lamellar structures than those prepared with an FRR of 9.

In contrast, the two liposomes prepared with 100 mM lipid showed comparable peak intensities. These results suggested that high lipid concentrations (e.g., 100 mM) can form multi-lamellar liposomes, regardless of the FRR. At moderate lipid concentrations (e.g., 50 mM), the FRR may affect the lamellarity of the liposomes. At such concentrations, the lower FRR could induce the formation of multi-lamellar liposomes, whereas the higher FRR could form liposomes with less lamellae (Figure 4.2 (b)). In addition, from the results of Figure 4.1 (a), the liposomes that showed a stronger peak intensity in the SAXS results had a larger mean hydrodynamic size of more than 50 nm. Based on these results, for the same lipid composition and preparation method, the hydrodynamic size of the liposomes could be closely related to their lamellar structures. Moreover, these results proved that the liposomes prepared from a 10 mM lipid concentration consisted of uni-lamellar liposomes because they showed almost no peaks derived from the lamellar structure (Figure 4.2 (c)).

TEM analysis was also carried out to confirm the SAXS results. In the TEM images, the liposomes prepared with 100 mM and 50 mM lipid concentration showed multi-lamellar vesicles inside the liposomes (Figure 4.3 (b), (c), (e), and (f)). In contrast, the liposomes prepared at a lipid concentration of 10 mM showed only homogeneous particles, which indicated that these liposomes consisted mainly of uni-lamellar liposomes (Figure 4.3 (a) and (d)). These TEM images were consistent with the SAXS results, and I therefore concluded that the liposome lamellarity can be changed by adjusting the lipid concentration and flow conditions.

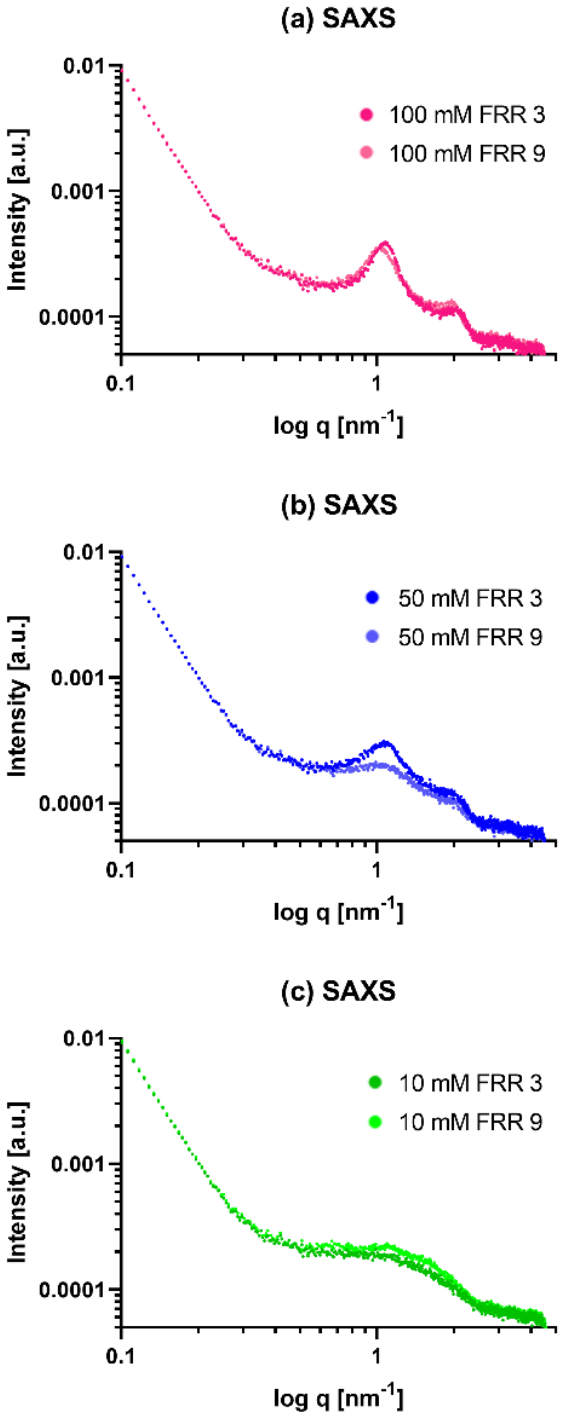

Figure 4.2 SAXS profiles of PTX-loaded liposomes prepared with (a) 100 mM, (b) 50 mM, and (c) 10 mM concentrations at FRR values of 3 and 9

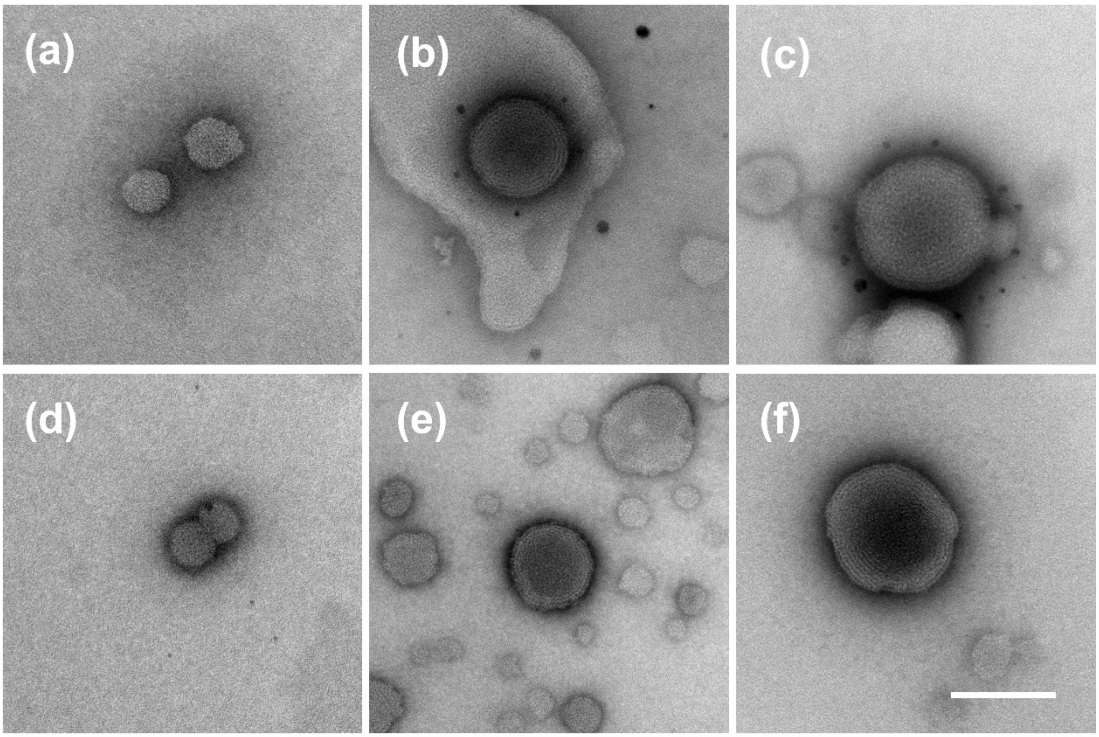

Figure 4.3 TEM images of the PTX-loaded liposomes: (a) 10 mM FRR = 3, (b) 50 mM FRR = 3, (c) 100 mM FRR = 3, (d) 10 mM FRR = 9, (e) 50 mM FRR = 9, and (f) 100 mM FRR = 9. (Scale bar: 100 nm)

4.3.3 Investigation of the release profiles of PTX from liposomes

I next investigated the release profiles of PTX from liposomes using dialysis [33] to evaluate the effect of the physicochemical properties on drug release behavior. The PTX release profile from liposomes produced from the lowest (10 mM) lipid concentration showed the fastest release kinetics compared to the liposomes prepared with the higher lipid concentration (50 mM and 100 mM) solutions (Figure 4.4 (a)). The liposomes with higher lamellarity released PTX more slowly because the presence of several lamellae inside the liposomes delayed the transport of PTX from the inter- to the outer layers and the release of PTX to the outer phases of the liposomes [16].

The residual PTX in the dialysis membrane bag also showed an extended-release trend. Indeed, a significantly higher amount of PTX was present at the end of the release test in the liposomes prepared with 100 mM lipid than in those prepared from the other two concentrations (Figure 4.4 (b)).

The total amount of PTX at the time point of 72 h decreased to 58–71% of the initial PTX

amount. I anticipated that the Tween 80 (TW80) present in the release medium would degrade the PTX during the release test, and indeed, the total amount of PTX decreased after 72 h of the release study. Abouelmagd et al. reported that PTX was decomposed by TW80, and the assay value became lower than 75% after 3 d of incubation at 37 °C [33]. Notably, their reported value was almost equivalent to my assay decreasing ratio after 72 h of incubation.

At lipid concentrations of 50 mM and 100 mM, the liposomes prepared using an FRR of 3 showed a slightly faster release rate after 24 h than those prepared with an FRR of 9. According to the SAXS and TEM results, liposomes prepared with an FRR of 3 had an equal number or more lamellar structures than those prepared using an FRR of 9. I therefore supposed that these differences in the release rate might be derived from physicochemical properties other than the lamellar structure. Hence, I proceeded to analyze these liposomes using a fluorescence polarization assay (FPA) to evaluate the fluidity of the lipid membrane. Liposomes with high lipid bilayer fluidity show low fluorescence polarization from 1,6-diphenyl-1,3,5-hexatriene (DPH) in the lipid bilayer. In contrast, liposomes with low lipid bilayer fluidity show high fluorescence polarization because the rigid lipid layer suppresses DPH rotational movement. Therefore, the degree of the change in the fluorescence polarization value (ΔP) is the index of the lipid membrane fluidity. In this study, the liposomes prepared with an FRR of 9 and lipid concentrations of 50 mM and 100 mM showed significantly higher ΔmP values than those prepared using an FRR of 3 (Figure 4.5). These results revealed that for each lipid concentration, the liposomes prepared using an FRR of 3 displayed a higher membrane fluidity than those prepared with an FRR of 9. These differences could be attributed to the different loading ratios of PTX. It has been reported that the cholesterol content influences the membrane fluidity and phase transition temperature of liposomes [34]. PTX, a hydrophobic drug, was therefore expected to be inserted into the lipid bilayers and to play a similar role to that of cholesterol. Some studies have also suggested that the membrane fluidity of liposomes affects the release rate of drugs loaded into the liposomes [35,36]. In summary, the drug release performance can be controlled by tuning the physicochemical properties and liposome inner structure by changing the lipid concentration and flow conditions.

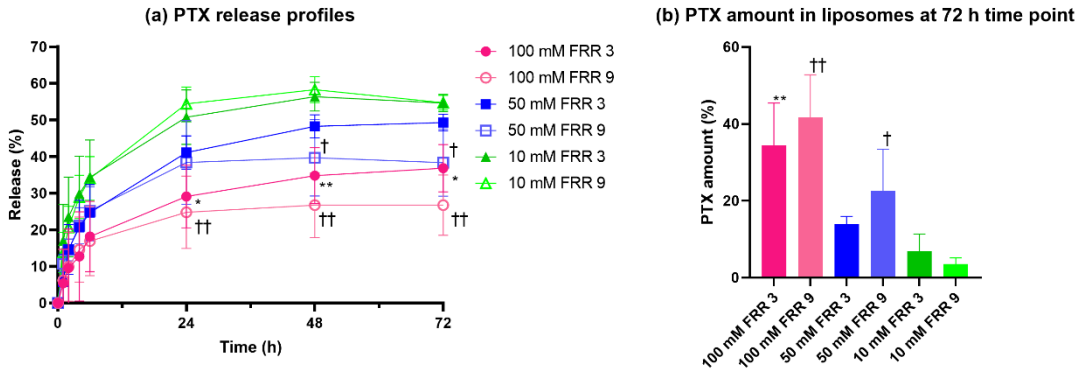

Figure 4.4 Release profiles of PTX from the liposomes. Error bars represent the standard deviation calculated from repeating each experiment at least three times. Symbol definitions: *, $P < 0.05$; **, $P < 0.01$ (vs 10 mM FRR = 3); †, $P < 0.05$; ††, $P < 0.01$ (vs 10 mM FRR = 9).

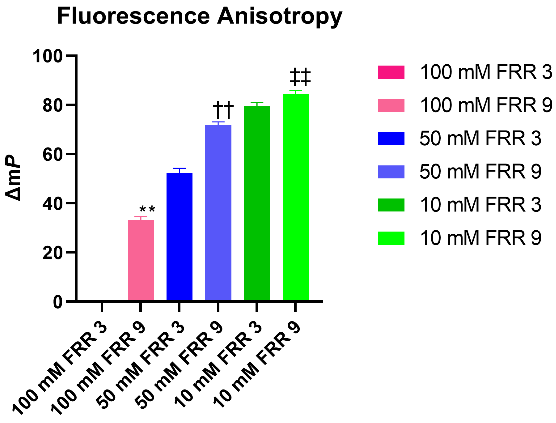

Figure 4.5 Fluorescence polarization assay of the liposomes. Error bars represent the standard deviation calculated from repeating each experiment at least three times. Symbol definitions: **, $P < 0.01$ (vs 100 mM FRR = 3); ††, $P < 0.01$ (vs 50 mM FRR = 3); ‡‡, $P < 0.01$ (vs 10 mM FRR = 3).

4.3.4 In vitro cytotoxicity assay

To confirm the effect of the PTX release profile on the PTX activity, I evaluated the cytotoxicity of the PTX-loaded liposomes in HeLa cells. As shown in Figure 4.6, the liposomes prepared with a

lipid concentration of 100 mM at FRR values of 3 and 9 showed significantly higher HeLa cell viability in the PTX concentration range of 0.1–10 ng/mL compared to the cell viability observed following treatment with the PTX solution. This was consistent with the results of the PTX release profiles. From these results, I concluded that multilamellar liposomes could regulate the release of PTX, and its activity in cultured cells could be moderate.

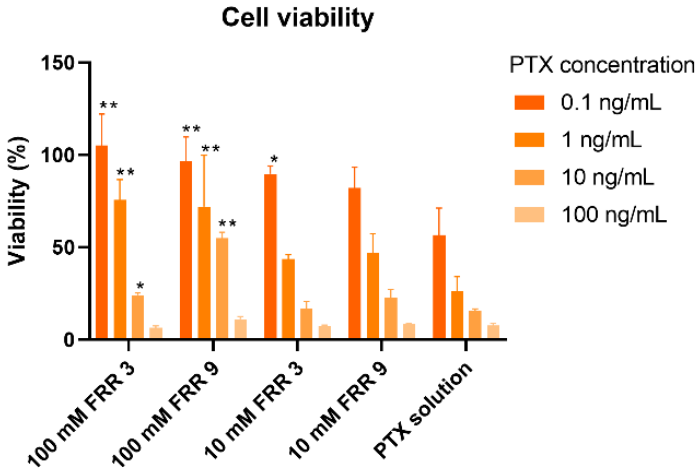

Figure 4.6 In vitro cytotoxicity assay of the PTX-loaded liposomes. Error bars represent the standard deviation calculated from repeating each experiment at least three times. Symbol definitions: *, $P < 0.05$; **, $P < 0.01$ (vs PTX solution).

4.4 Conclusion

I investigated the structural differences in PTX-loaded liposomes prepared using a microfluidic device. I observed that the lipid concentration and FRR affected the inner structure and physicochemical properties, such as the liposome size and DL%. More lamellar structures in the liposomes were associated with a more extended release of PTX from the liposomes. Furthermore, the differences in DL% affected the fluidity of the liposome membranes, leading to differences in the release kinetics of PTX from the liposomes 24 h after the in vitro PTX release study. These differences in the release kinetics of PTX were also reflected in the evaluation of the PTX activity in an in vitro cytotoxicity study. The extended release of drugs from liposomes may contribute to lower adverse side

effects in patients and less frequent dosing, owing to prolonged drug activity.

In this chapter, I established a method for preparing liposomes that exhibit different lamellar structures and drug release properties even with the same lipid composition. Few studies have focused on the lamellar nature of liposomes prepared by ethanol dilution using microfluidic technology. My findings will be valuable for more detailed design and quality control of liposome-based nanomedicines and cosmetics. I anticipate that these findings will make a substantial contribution to the precise formulation of liposomes using microfluidic devices in the pharmaceutical and cosmetic fields.

4.5 References

[1] R. Tenchov, R. Bird, A.E. Curtze, Q. Zhou, Lipid Nanoparticles-From Liposomes to mRNA Vaccine Delivery, a Landscape of Research Diversity and Advancement, Acs Nano. 15 (2021) 16982–17015.

[2] K. Hörmann, A. Zimmer, Drug delivery and drug targeting with parenteral lipid nanoemulsions — A review, J Control Release. 223 (2016) 85–98.

[3] P.R. Cullis, M.J. Hope, Lipid Nanoparticle Systems for Enabling Gene Therapies, Mol Ther. 25 (2017) 1467–1475.

[4] Y. Mirchandani, V.B. Patravale, S. Brijesh, Solid lipid nanoparticles for hydrophilic drugs, J Control Release. 335 (2021) 457–464.

[5] Y. Matsuura-Sawada, S. Uno, M. Maeki, K. Wada, M. Tokeshi, Microfluidic Platform Enabling Efficient On-Device Preparation of Lipid Nanoparticles for Formulation Screening, Acs Appl Eng Mater. 1 (2023) 278–286.

[6] L.M. Ickenstein, P. Garidel, Lipid-based nanoparticle formulations for small molecules and RNA drugs, Expert Opin Drug Del. 16 (2019) 1205–1226.

[7] Y.N. Lamb, BNT162b2 mRNA COVID-19 Vaccine: First Approval, Drugs. 81 (2021) 495–501.

[8] L. Schoenmaker, D. Witzigmann, J.A. Kulkarni, R. Verbeke, G. Kersten, W. Jiskoot, D. Crommelin, mRNA-lipid nanoparticle COVID-19 vaccines: structure and stability, Int J Pharmaceut. 601 (2021) 120586.

[9] M.E.R. O'Brien, N. Wigler, M. Inbar, R. Rosso, E. Grischke, A. Santoro, R. Catane, D.G. Kieback, P. Tomczak, S.P. Ackland, F. Orlandi, L. Mellars, L. Alland, C. Tendler, Reduced cardiotoxicity and comparable efficacy in a phase III trial of pegylated liposomal doxorubicin HCl (CAELYXTM/Doxil®) versus conventional doxorubicin for first-line treatment of metastatic breast cancer, Ann Oncol. 15 (2004) 440–449.

[10] N.R.H. Stone, T. Bicanic, R. Salim, W. Hope, Liposomal Amphotericin B (AmBisome®): A Review of the Pharmacokinetics, Pharmacodynamics, Clinical Experience and Future Directions, Drugs. 76 (2016) 485–500.

[11] A. Sharma, A. Kuhad, R. Bhandari, Novel nanotechnological approaches for treatment of skin-

aging, J Tissue Viability. 31 (2022) 374–386.

[12] J.J. Moon, H. Suh, A. Bershteyn, M.T. Stephan, H. Liu, B. Huang, M. Sohail, S. Luo, S.H. Um, H. Khant, J.T. Goodwin, J. Ramos, W. Chiu, D.J. Irvine, Interbilayer-Crosslinked Multilamellar Vesicles as Synthetic Vaccines for Potent Humoral and Cellular Immune Responses, Nat Mater. 10 (2011) 243–251.

[13] K.-I. Joo, L. Xiao, S. Liu, Y. Liu, C.-L. Lee, P.S. Conti, M.K. Wong, Z. Li, P. Wang, Crosslinked multilamellar liposomes for controlled delivery of anticancer drugs, Biomaterials. 34 (2013) 3098–3109.

[14] M. Al-Amin, F. Bellato, F. Mastrotto, M. Garofalo, A. Malfanti, S. Salmaso, P. Caliceti, Dexamethasone Loaded Liposomes by Thin-Film Hydration and Microfluidic Procedures: Formulation Challenges, Int J Mol Sci. 21 (2020) 1611.

[15] G.V. Betageri, D.L. Parsons, Drug encapsulation and release from multilamellar and unilamellar liposomes, Int J Pharmaceut. 81 (1992) 235–241.

[16] Saujanya.L. Gosangari, K.L. Watkin, Effect of preparation techniques on the properties of curcumin liposomes: Characterization of size, release and cytotoxicity on a squamous oral carcinoma cell line, Pharm Dev Technol. 17 (2010) 103–109.

[17] D. Vorselen, M. Marchetti, C. López-Iglesias, P.J. Peters, W.H. Roos, G.J.L. Wuite, Multilamellar nanovesicles show distinct mechanical properties depending on their degree of lamellarity, Nanoscale. 10 (2018) 5318–5324.

[18] A. Zgadzaj, J. Giebułtowicz, J. Gubernator, M. Podbielska, S. Sommer, M. Zaremba-Czogalla, G. Nałęcz-Jawecki, Multi- and unilamellar liposomal encapsulation of ciprofloxacin as ways to modify its phototoxicity and photodegradation, Eur J Pharm Sci. 129 (2019) 181–189.

[19] A.D. Sotto, P. Paolicelli, M. Nardoni, L. Abete, S. Garzoli, S.D. Giacomo, G. Mazzanti, M.A. Casadei, S. Petralito, SPC Liposomes as Possible Delivery Systems for Improving Bioavailability of the Natural Sesquiterpene β-Caryophyllene: Lamellarity and Drug-Loading as Key Features for a Rational Drug Delivery Design, Pharm. 10 (2018) 274.

[20] P. Kallinteri, S.G. Antimisiaris, D. Karnabatidis, C. Kalogeropoulou, I. Tsota, D. Siablis, Dexamethasone incorporating liposomes: an in vitro study of their applicability as a slow releasing delivery system of dexamethasone from covered metallic stents, Biomaterials. 23 (2002) 4819–4826.

[21] V. Gómez-Murcia, B.R.D. Couto, J.C. Gómez-Fernández, M.V. Milanés, M.L. Laorden, P. Almela, Liposome-Encapsulated Morphine Affords a Prolonged Analgesia While Facilitating Extinction of Reward and Aversive Memories, Front Pharmacol. 10 (2019) 1082.

[22] H.L. Scott, A. Skinkle, E.G. Kelley, M.N. Waxham, I. Levental, F.A. Heberle, On the mechanism of bilayer separation by extrusion; or, why your large unilamellar vesicles are not really unilamellar, Biophys J. 117 (2019) 1381–1386.

[23] L. Zhang, Q. Chen, Y. Ma, J. Sun, Microfluidic Methods for Fabrication and Engineering of Nanoparticle Drug Delivery Systems, Acs Appl Bio Mater. 3 (2020) 107–120.

[24] M. Maeki, S. Uno, A. Niwa, Y. Okada, M. Tokeshi, Microfluidic technologies and devices for lipid nanoparticle-based RNA delivery, J Control Release. 344 (2022) 80–96.

[25] C. Webb, S. Ip, N.V. Bathula, P. Popova, S.K.V. Soriano, H.H. Ly, B. Eryilmaz, V.A.N. Huu, R. Broadhead, M. Rabel, I. Villamagna, S. Abraham, V. Raeesi, A. Thomas, S. Clarke, E.C. Ramsay, Y. Perrie, A.K. Blakney, Current Status and Future Perspectives on MRNA Drug Manufacturing, Mol Pharmaceut. 19 (2022) 1047–1058.

[26] T.A. Balbino, N.T. Aoki, A.A.M. Gasperini, C.L.P. Oliveira, A.R. Azzoni, L.P. Cavalcanti, L.G. de la Torre, Continuous flow production of cationic liposomes at high lipid concentration in microfluidic devices for gene delivery applications, Chem Eng J. 226 (2013) 423–433.

[27] A. Ghazal, M. Gontsarik, J.P. Kutter, J.P. Lafleur, D. Ahmadvand, A. Labrador, S. Salentinig, A. Yaghmur, Microfluidic Platform for the Continuous Production and Characterization of Multilamellar Vesicles: A Synchrotron Small-Angle X-ray Scattering (SAXS) Study, J Phys Chem Lett. 8 (2017) 73–79.

[28] Y. Matsuura-Sawada, M. Maeki, T. Nishioka, A. Niwa, J. Yamauchi, M. Mizoguchi, K. Wada, M. Tokeshi, Microfluidic Device-Enabled Mass Production of Lipid-Based Nanoparticles for Applications in Nanomedicine and Cosmetics, Acs Appl Nano Mater. 5 (2022) 7867–7876.

[29] N. Kimura, M. Maeki, Y. Sato, Y. Note, A. Ishida, H. Tani, H. Harashima, M. Tokeshi, Development of the iLiNP Device: Fine Tuning the Lipid Nanoparticle Size within 10 nm for Drug Delivery, Acs Omega. 3 (2018) 5044–5051.

[30] J.C. McDonald, G.M. Whitesides, Poly(dimethylsiloxane) as a Material for Fabricating Microfluidic Devices, Accounts Chem Res. 35 (2002) 491–499.

[31] M. Maeki, Y. Okada, S. Uno, A. Niwa, A. Ishida, H. Tani, M. Tokeshi, Production of siRNA-Loaded Lipid Nanoparticles using a Microfluidic Device, J Vis Exp. No. 181 (2022) e62999.

[32] H. Zheng, H. Tao, J. Wan, K.Y. Lee, Z. Zheng, S.S.Y. Leung, Preparation of Drug-Loaded Liposomes with Multi-Inlet Vortex Mixers, Pharmaceutics. 14 (2022) 1223.

[33] S.A. Abouelmagd, B. Sun, A.C. Chang, Y.J. Ku, Y. Yeo, Release Kinetics Study of Poorly Water-Soluble Drugs from Nanoparticles: Are We Doing It Right?, Mol Pharmaceut. 12 (2015) 997–1003.

[34] S. Kaddah, N. Khreich, F. Kaddah, C. Charcosset, H. Greige-Gerges, Cholesterol modulates the liposome membrane fluidity and permeability for a hydrophilic molecule, Food Chem Toxicol. 113 (2018) 40–48.

[35] B. Maherani, E. Arab-Tehrany, A. Kheirolomoom, D. Geny, M. Linder, Calcein release behavior from liposomal bilayer; influence of physicochemical/mechanical/structural properties of lipids, Biochimie. 95 (2013) 2018–2033.

[36] T. Shimanouchi, H. Ishii, N. Yoshimoto, H. Umakoshi, R. Kuboi, Calcein permeation across phosphatidylcholine bilayer membrane: Effects of membrane fluidity, liposome size, and immobilization, Colloids Surfaces B Biointerfaces. 73 (2009) 156–160.

CHAPTER 5

Conclusion and Future Prospects

5.1 Conclusion and future perspectives

A method of preparing lipid-based nanoparticles (Lb-NPs) using microfluidic-device-assisted ethanol dilution was developed in the present research and described in this thesis.

Chapter 2 described the development of a novel microfluidic platform that enables the adjustment of lipid nanoparticle (LNP) composition and LNP preparation on a device in a single step for more efficient LNP formulation screening. The stable flow of three solutions simultaneously using this microfluidic platform was demonstrated even when the flow rates of the two ethanol phases were varied over a wide range of 50/50 to 10/90. This excellent flow rate stability contributed to the ability to precisely change the LNP composition and to prepare LNPs that exhibit trends in the physicochemical properties comparable to those of a conventional off-device preparation method. Ultimately, I proved the concept of on-device LNP formulation screening by investigating changes in the LNP composition and amount of surface modifier. The results clearly confirmed that my microfluidic platform concept worked well and could be among the best ways to prepare a large number of LNPs in the early development phases of pharmaceutical and cosmetic product development without requiring additional time and cost compared to conventional microfluidic-device-assisted LNP preparation.

Chapter 3 investigated the applicability of a highly concentrated lipid solution in the microfluidic-device-assisted preparation of Lb-NPs. To gain basic knowledge and experience in the application of highly concentrated lipid solutions, four types of microfluidic devices, three commercially available devices and one device developed in my laboratory (invasive lipid nanoparticle production (iLiNP)), and four lipid concentrations were examined. The results showed that microfluidic devices with mixer structures in the channel were capable of preparing smaller, monodisperse Lb-NPs using highly concentrated lipid solutions. To clarify the factors affecting the size reduction of Lb-NPs, I investigated the particle concentration and interparticle distance of Lb-NPs. I inferred that the key factors in the preparation of smaller and monodisperse Lb-NPs, even in highly concentrated solutions, were the dilution rate of the organic solvent phase and the interfacial area between the organic solvent and aqueous phases. The subsequent preparation of Lb-NPs using a three-inlet iLiNP device and a comparison of the physicochemical properties of Lb-NPs prepared using the iLiNP and micromixer devices demonstrated the correctness of my inferences and estimation of the key influencing factors in the Lb-NP formation process. Having identified the factors that affect particle size controllability when highly concentrated lipid solutions are used, I succeeded in preparing

submicron-sized unimodal Lb-NPs even under high lipid-concentration conditions.

Chapter 4 described the evaluation of the physicochemical properties of Lb-NPs, especially liposomes, prepared with lower and higher lipid concentrations using paclitaxel (PTX) as a model drug compound. The liposomes prepared using a highly concentrated lipid solution showed <120 nm particles and a better polydispersity index. The drug loading rate did not increase in a lipid-concentration-dependent manner, but the effect of flow rate ratio (FRR) on the drug loading rate was clearly observed. Small-angle X-ray scattering and transmission electron microscopy observation revealed that liposomes prepared using higher lipid concentrations had multilamellar structures, and the degree of lamellar structure was affected by the FRR at a lipid concentration of 50 mM. In addition, the internal lamellar structures of liposomes were found to affect the release profiles of PTX, and the liposomes prepared with a lipid concentration of 100 mM showed the slowest release profiles. Interestingly, liposomes with similar multilamellar structures showed different trends in the later part of the release profile. Therefore, I evaluated the fluidity of the lipid membrane of the liposomes; the results suggested that the fluidity of the lipid membrane may vary with the drug loading ratio and contribute to the differences in the later release profile of PTX. The liposomes prepared with a lipid concentration of 100 mM at an FRR of 9, which showed the slowest release profiles in all six samples, also showed relatively higher cell viability compared to PTX solutions in in vitro assay, confirming the extended release of PTX from multilamellar liposomes. I established a method for preparing liposomes with the same lipid composition but different lamellar structures and drug release properties simply by changing the lipid concentration. This finding is valuable for the precise control of the physicochemical properties of liposomes.

In this thesis, I summarized the findings and outcomes of my research on the preparation of Lb-NPs via microfluidic-device-assisted organic solvent dilution. To accelerate the application of microfluidic devices in the preparation of Lb-NPs in the cosmetic and pharmaceutical fields, I addressed two urgent concerns. The first is the lack of an appropriate microfluidic platform for preparing numerous types of LNPs for formulation screening, and the second is the lack of knowledge and experience in the scale-up and mass production of Lb-NPs, especially with the use of highly concentrated lipid solutions. The first concern was addressed by proposing and developing the novel microfluidic platform for adjusting the compositions of LNPs on the device. The second concern was addressed by examining the applicability of highly concentrated lipid solutions and identifying the influencing factors that can be varied to obtain smaller Lb-NPs. For a more practical evaluation, the

model-drug-encapsulated liposomes were prepared using highly concentrated lipid solutions, and their physicochemical properties, drug release profiles, and drug activities were evaluated in comparison with those of liposomes prepared using lower-lipid-concentration solutions. This evaluation revealed that the lipid concentration affects not only the size but also the lamellarity of the liposomes, which in turn affect the drug release profile and drug activity.

The optimization of the LNP compositions and physicochemical properties can be accelerated by utilizing a novel microfluidic platform for LNP formulation screening. I believe that a reduction by more than 50% of the time required to prepare LNPs for formulation optimization can be expected. By optimizing the composition and physicochemical properties of LNPs in conjunction with the optimization of the chemical structure and sequence of siRNAs and mRNAs, it is possible to design LNPs that are more effective and can be delivered efficiently to target organs and tissues, which will help maximize the value of the encapsulated active ingredient. Highly optimized LNPs can provide higher efficacy and reduced adverse effects for patients.

In addition, an understanding of the critical material attributes, process parameters, and quality attributes in the preparation of Lb-NP-based medicines will result in smoother and more seamless scale-up and proper quality control and management in practical production. These improvements will enable a stable supply of high-quality medicines, a critical mission for pharmaceutical companies.

Thus, maximizing the efficacy of Lb-NPs and the active ingredients encapsulated in them and a better understanding of the factors that affect the quality of Lb-NPs during manufacturing may help shorten development timelines, reduce the number of dropout candidates, and increase the success rates of drug development. With increasing drug development success rates and decreasing development costs, the number of nanomedicines in clinical use is expected to increase.

Finally, I hope that the fruits of my research will further spread these wonderful lipid-based nanomedicines and thus bring more value and benefits to patients. In addition, I hope that these Lb-NPs and knowledge of their preparation methods and technologies will be widely used in fields beyond pharmaceuticals, such as cosmetics and foods.

List of Publications

I. Reviewed Papers

[1] **Yuka Matsuura-Sawada**, Masatoshi Maeki, Takaaki Nishioka, Ayuka Niwa, Jun Yamauchi, Masashi Mizoguchi, Koichi Wada, Manabu Tokeshi, “Microfluidic Device-Enabled Mass Production of Lipid-Based Nanoparticles for Applications in Nanomedicine and Cosmetics”, *ACS Applied Nano Materials*, 5, 7867–7876 (2022). DOI: 10.1021/acsanm.2c00886.

[2] **Yuka Matsuura-Sawada**, Shuya Uno, Masatoshi Maeki, Koichi Wada, Manabu Tokeshi, “Microfluidic Platform Enabling Efficient On-Device Preparation of Lipid Nanoparticles for Formulation Screening”, *ACS Applied Engineering Materials*, 1, 278–286, (2023). DOI: 10.1021/acsaenm.2c00062.

[3] **Yuka Matsuura-Sawada**, Masatoshi Maeki, Shuya Uno, Koichi Wada, Manabu Tokeshi, “Controlling Lamellarity and Physicochemical Properties of Liposomes Prepared Using a Microfluidic Device”, *Biomaterials Science*, in press. DOI: 10.1039/D2BM01703B.

II. Reviewed International Conference Papers

[1] **Yuka Matsuura**, Masatoshi Maeki, Takaaki Nishioka, Jun Yamauchi, Masashi Mizoguchi, Koichi Wada, Manabu Tokeshi, “Inference of the Formation Process of Lipid Nanoparticles from the Viewpoint of Interparticle Distance”, *Proceedings of 25th International Conference on Miniaturized Systems for Chemistry and Life Sciences (μTAS 2021)*, 1125-1126 (2021).

[2] **Yuka Matsuura-Sawada**, Shuya Uno, Masatoshi Maeki, Koichi Wada, Manabu Tokeshi, “Development of Novel Microfluidic Platform for On-Chip Formulation Screening of Lipid Nanoparticles”, *Proceedings of 26th International Conference on Miniaturized Systems for Chemistry and Life Sciences (μTAS 2022)*, 869-870 (2022).

Acknowledgement

This thesis is the result of the author's research in the Laboratory of Microsystem Chemistry, Graduate School of Engineering, Hokkaido University.

First of all, I would like to express my sincerest respect and gratitude to my supervisor Professor Manabu Tokeshi of the Division of Applied Chemistry, Faculty of Engineering, Hokkaido University for his guidance and wisdom, meaningful advice, and continuous support. He warmly accepted me as a Ph.D. student even though I had no connection with him, and he always encouraged me.

I would like to acknowledge Associate Professor Masatoshi Maeki and Assistant Professor Akihiko Ishida for valuable discussions, advice, and assistance. Very special thanks go out to Associate Professor Maeki for providing me with his meaningful discussions and proper advice from the viewpoint of a professional researcher.

I would like to acknowledge Professor Toshifumi Satoh, Professor Shin Mukai, and Associate Professor Hirofumi Tani of the Faculty of Engineering, Hokkaido University, and Professor Kosei Ueno of the Faculty of Science, Hokkaido University for accepting the responsibilities as my official co-supervisors.

I also want to acknowledge Professor Hideyoshi Harashima of the Faculty of Pharmaceutical Sciences, Hokkaido University. He kindly introduced Professor Manabu Tokeshi and recommended me to jump into the Ph.D. course. Unfortunately, I could not research in collaboration with him and his research team and laboratory, but I hoped we would make and continue a good relationship.

I must acknowledge Dr. Sven Schreder and Dr. Koichi Wada for giving me an opportunity to research in Hokkaido University and for providing me with the facility, instruments, and reagents to use for my Ph.D. research. They also gave me kind support and encouragement as head of my function, Pharmaceutical development, Boehringer Ingelheim International GmbH, and Pharmaceutical development in Japan and Kobe pharma research institute, Nippon Boehringer Ingelheim. Owing to their kind support, my research could proceed. I also would like to acknowledge Dr. Masashi Mizoguchi and Dr. Roman Messerschmid who always supported my Ph.D. activity and kindly understood my situation.

I would like to thank all of my lab mates, especially Keine Nishiyama, Niko Kimura, Yuto Okada, Kazuki Shimizu, Shuya Uno, and Ayuka Niwa. Keine Nishiyama and Niko Kimura were

always willing to give me valuable advice whenever I asked them. Yuto Okada, Kazuki Shimizu, Shuya Uno, and Ayuka Niwa kindly supported my experiments both when I visited and could not visit the university and laboratory.

I would also like to thank my colleagues in Nippon Boehringer Ingelheim, especially Mayumi Ishida, Kazutoshi Yokoyama, Jun Yamauchi, Takaaki Nishioka, Saki Ichimura, Shio Harada, Mai Itagaki, Risa Aihara, Kyoko Hasegawa, Junichi Takano, Yumi Oka, Katsuyoshi Fujimoto, and David Johnson. Takaaki Nishioka and Jun Yamauchi gave me a lot of advice and encouragement. Mayumi Ishida, Kazutoshi Yokoyama, Saki Ichimura, and Shio Harada considered my situation and indirectly supported my Ph.D. work. Kyoko Hasegawa, Junichi Takano, Yumi Oka, and Katsuyoshi Fujimoto allowed me to use their instruments and gave me a lot of help. Mai Itagaki and Risa Aihara gently supported me mentally and worked hard together with me, but not in the same university as the Ph.D. candidates. David Johnson kindly support English proofing of my Ph.D. thesis.

I would like to acknowledge Hirofumi Takeuchi of Endowed Course, Gifu Pharmaceutical University. He brought me my basis of research skills, scientific knowledge, and also my interest in research. I was able to start my career thanks to the meaningful education I received from him and in his laboratory.

I also appreciate my family and my family in-law for giving me kind and supportive words. Finally, I would like to express my big thanks and love to the moon and back to my husband Yuki Sawada. He has supported me mentally and physically day in and day out for almost three years and more. I’m so much obliged to him.